



**TECHNISCHE UNIVERSITÄT MÜNCHEN**  
Fakultät für Medizin

Lehrstuhl für Stoffwechselerkrankungen

**„Novel regulators of energy metabolism:  
From alternatively activated macrophages to the role of the scaffold  
protein p62 in BAT thermogenesis”**

Katrin Christine Fischer

Vollständiger Abdruck der von der Fakultät für Medizin der Technischen Universität München zur Erlangung des akademischen Grades eines Doktors der Naturwissenschaften genehmigten Dissertation.

Vorsitzender: Prof. Dr. Percy A. Knolle  
Prüfer der Dissertation: 1. Prof. Dr. Matthias Tschöp  
2. Prof. Dr. Martin Klingenspor  
3. Prof. Dr. Tim Schulz (schriftliche Beurteilung)  
Prof. Dr. Wolfgang Wurst (mündliche Prüfung)

Die Dissertation wurde am 02.05.2017 bei der Technischen Universität München eingereicht und durch die Fakultät der Medizin am 20.03.2018 angenommen.

## Index of Contents

Index of Contents.....	i
Abbreviations.....	iv
Index of Figures.....	viii
Index of Tables.....	ix
<b>1. Introduction.....</b>	<b>1</b>
1.1 White, beige and brown adipose tissue – function and physiological relevance.....	2
1.1.1 Brown adipose tissue in mice.....	4
1.1.2 Brown adipose tissue in humans.....	5
1.2 Sympathetic neuronal control of brown adipose tissue thermogenesis.....	5
1.2.1 $\beta_3$ -adrenergic signaling pathway.....	6
1.2.2 The uncoupling protein UCP1.....	7
1.3 Crosstalk between metabolism and macrophages.....	8
1.3.1 Adipose tissue macrophages and their role during obesity.....	9
1.3.2 Innate immune regulation of thermogenesis.....	10
1.4 Scaffold protein p62/Sequestosome 1.....	11
1.4.1 Structure and function of p62.....	12
1.4.2 P62 and its relevance for obesity.....	13
<b>2. Scope of this thesis.....</b>	<b>16</b>
<b>3. Material and Methods.....</b>	<b>17</b>
3.1 Animal experiments.....	19
3.1.1 General experimental approaches for <i>in vivo</i> studies.....	19
3.1.2 Housing and diets.....	19
3.1.3 Mice.....	19
3.1.4 Genotyping.....	20
3.1.5 Analysis of mouse metabolic phenotypes.....	22
3.1.6 Intraperitoneal glucose tolerance test.....	22
3.1.7 Indirect calorimetry.....	22
3.1.8 IL-4 pharmacology studies.....	23
3.1.9 Positron emission tomography and magnetic resonance imaging.....	23
3.1.10 Infrared thermography.....	24
3.1.11 Bomb calorimetry.....	24
3.2 Molecular biological analysis.....	24
3.2.1 Tissue dissection.....	24
3.2.2 RNA isolation from tissue and cells.....	24
3.2.3 Reverse Transcription.....	25
3.2.4 Quantitative real-time polymerase chain reaction.....	25

---

3.2.5 Low Density Array.....	25
3.2.6 Protein isolation and Western blot analysis .....	25
3.2.7 Nuclear and cytosolic protein extraction from BAT tissue.....	26
3.2.8 Cytochrome C Oxidase activity measurement .....	26
3.2.9 Immunohistochemistry for UCP1.....	26
3.2.10 Luciferase reporter assay.....	27
3.2.11 Catecholamine measurement .....	27
3.3 Cell culture .....	28
3.3.1 Isolation of primary murine white and brown adipocytes .....	28
3.3.2 Isolation of bone marrow-derived macrophages .....	29
3.3.3 Depletion of macrophages from primary iWAT cells .....	29
3.3.4 Oil Red O staining.....	29
3.3.5 Flow cytometry .....	30
3.3.6 Bioenergetic analysis .....	30
3.4. Statistics .....	30
3.5. Contributions from Collaborations .....	31
<b>4. Results .....</b>	<b>32</b>
4.1 Role of alternatively activated macrophages in BAT thermogenesis .....	32
4.1.1 Effect of macrophage depletion on adipocyte function .....	32
4.1.2 Effect of alternatively activated macrophages on thermogenesis in primary adipocytes .....	36
4.1.2.1 IL-4 stimulation of Raw264.7 cell line .....	36
4.1.2.2 IL-4 stimulation of bone marrow-derived macrophages.....	37
4.1.3 Effect of alternatively activated macrophages on lipolysis in primary adipocytes .....	39
4.1.4 Catecholamine production in alternatively activated macrophages .....	39
4.2.5 Effect of cold exposure on macrophage content in C57Bl/6J mice.....	41
4.1.6 Effect of IL-4 on energy expenditure and BAT thermogenesis <i>in vivo</i> .....	42
4.1.6.1 Temperature challenge in IL-4-treated WT and IL4ra <sup>-/-</sup> mice .....	42
4.1.6.2 Tyrosine hydroxylase expression in adipose tissue macrophages .....	44
4.2 Characterization of mice lacking AA 69-251 of p62 (p62 <sup>Δ69-251</sup> ) .....	46
4.2.1 Genotype confirmation of p62 <sup>Δ69-251</sup> mouse .....	46
4.2.2 Metabolic phenotype of p62 <sup>Δ69-251</sup> mice .....	47
4.2.3 Energy expenditure of obese p62 <sup>Δ69-251</sup> mice.....	49
4.2.4 Brown adipose tissue function of obese p62 <sup>Δ69-251</sup> mice.....	50
4.2.5 Brown adipose tissue function of lean p62 <sup>Δ69-251</sup> mice.....	51
4.2.6 Metabolic phenotype of p62 <sup>Δ69-251</sup> mice kept at thermoneutrality .....	53
4.2.7 Regulation of nuclear-cytosolic transport of p-ATF2 in p62 <sup>Δ69-251</sup> mice .....	55
<b>5. Discussion .....</b>	<b>59</b>
5.1 Role of alternatively activated macrophages on BAT thermogenesis .....	59
5.2 Role of the scaffold protein p62 on BAT thermogenesis.....	65
<b>6. Outlook and Perspectives .....</b>	<b>71</b>

Abstract ..... 73

Zusammenfassung ..... 75

References ..... 77

Acknowledgments..... 89

Curriculum Vitae ..... 90

List of publications ..... 91

Eidesstattliche Erklärung..... 92

**Abbreviations**

AA	Amino acid
Adipoq	Adiponectin
Adrb3	Adrenoreceptor beta 3
ANCOVA	Analysis of covariance
ANOVA	Analysis of variance
aPKC	Atypical protein kinase C
ATF2	Activating transcription factor 2
Arg1	Arginase 1
Atg8	Autophagy-related protein 8
ATMs	Adipose tissue macrophages
ATP	Adenosine triphosphate
AUC	Area under the curve
BAT	Brown adipose tissue
BMDMs	Bone marrow-derived macrophages
BMI	Body mass index
BMR	Basal metabolic rate
Bmp8b	Bone morphogenetic protein 8b
brite	Brown-in-white
cAMP	Cyclic adenosine monophosphate
C/EBPs	CCAAT-enhancer-binding proteins
ChIP	Chromatin immunoprecipitation
Cidea	Cell death-inducing DFFA-like effector A
Cited1	Cbp/p300-interacting transactivator with Glu/Asp-rich c-terminal domain 1
CK2	Casein kinase 2
CM	Conditioned media
COX	Cytochrome c oxidase
Cox4i1	Cytochrome c oxidase Subunit 4
CRE	cAMP responsive element
CREB	cAMP response element binding
Cycs	Cytochrome C
DAPI	4',6-diamidino-2-phenylindole
DIO	Diet-induced obesity
Dio2	Deiodinase iodothyronine type II
DNA	Deoxyribonucleic acid
EE	Energy expenditure
ELISA	Enzyme-linked immunosorbent assay
Emr1	Adhesion G protein-coupled receptor E1
ERK	Extracellular-signal regulated kinase
Eva1	Myelin protein zero like 2

---

FA	Fatty acid
Fabp4	Fatty acid binding protein 4
Fasn	Fatty acid synthase
FACS	Fluorescence-activated cell sorting
FDG	Fluorodeoxyglucose
FFA	Free fatty acids
FGF21	Fibroblast growth factor 21
FM	Fat mass
h	Hours
H3	Histon 3
HET	Heterozygous
HFD	High fat diet
HPLC	High performance liquid chromatography
Hprt	Hypoxanthine Phosphoribosyltransferase
HSL	Hormone sensitive lipase
iBAT	Interscapular brown adipose tissue
IFN	Interferon
IL	Interleukin
Il4ra	Interleukin 4 receptor subunit alpha
ILC2	Type 2 innate lymphoid cell
ipGTT	Intraperitoneal glucose tolerance test
iWAT	Inguinal white adipose tissue
KEAP1	Kelch like ECH associated protein 1
KIR	KEAP1-interacting region
KO	Knockout
LC3	Microtubule-associated protein 1A/1B-light chain 3
Lhx8	LIM homeobox 8
LIR	LC3-interacting region
LM	Lean mass
LPS	Lipopolysaccharide
M-CSF	Macrophage colony-stimulating factor
MACS	Magnetic activated cell sorting
MAPK	Mitogen-activated protein kinase
MEK3	Mitogen-activated protein kinase 3
Metrn1	Meteorin-like
Mgl2	C-type lectin domain family 10 member A
min	Minutes
MKK6	Mitogen-activated protein kinase 6
Mrc1	Mannose receptor C type 1
mRNA	Messenger ribonucleic acid
MRT	Magnetic resonance tomography

---

mTORC1	Mammalian target of rapamycin complex 1
Myf5	Myogenic factor 5
NAFLD	Non-alcoholic fatty-liver disease
NE	Norepinephrine
NEAT	Non-exercise activity thermogenesis
NET	Norepinephrine transporter
NFκB	Nuclear factor kappa light chain enhancer of activated B-cells
NO	Nitric oxide
Nos	Nitric oxide synthase
NRF2	Nuclear factor erythroid 2-related factor 2
OCR	Oxygen consumption rate
PB1	Phox and Bemp1-1
PCR	Polymerase chain reaction
Pdk4	Pyruvate dehydrogenase kinase 4
PET-CT	Positron emission tomography computed tomography
Pgc-1	Peroxisome proliferator-activated receptor gamma coactivator 1
PKA	Protein kinase A
PMF	Proton motive force
Ppard	Peroxisome proliferator activated receptor delta
Pparg	Peroxisome proliferator activated receptor gamma
Ppib	Peptidylprolyl isomerase B
PPRE	Peroxisome proliferator response element
Prdm16	PR domain zinc finger protein 16
qRT-PCR	Quantitative real-time polymerase chain reaction
RER	Respiratory exchange ratio
Retnla	Resistin like beta
RIP	Receptor-interacting protein
RNA	Ribonucleic acid
ROS	Reactive oxygen species
s	Seconds
SNS	Sympathetic nervous system
Sqstm1	Sequestosome 1
SVF	Stromal vascular fraction
T3	Triiodothyronine
TAG	Triacylglycerine
TB	TRAF6-binding
Tbx1	T-box 1
TDEE	Total daily energy expenditure
TEF	Thermic effect of food
TH	Tyrosine hydroxylase
Tmem26	Transmembrane protein 26

---

Tnf	Tumor necrosis factor
TRAF6	TNF receptor associated factor 6
Ub	Ubiquitinated
UBA	Ubiquitin-associated domain
UCP1	Uncoupling protein 1
WAT	White adipose tissue
WHO	World Health Organisation
WT	Wild-type
Zic1	Zinc finger of the cerebellum
ZZ	Zinc finger motif



## Index of Figures

Figure 1: Norepinephrine induction of nonshivering thermogenesis. ....	6
Figure 2: Adipose tissue inflammation.....	9
Figure 3: Domain organization and interacting partners of the scaffold protein p62.....	12
Figure 4: Macrophage depletion in iWAT primary cells. ....	33
Figure 5: Effect of macrophage depletion on adipocyte differentiation.....	34
Figure 6: Effect of macrophage depletion on key metabolic pathways in primary inguinal white adipocytes. ....	34
Figure 7: Effect of macrophage depletion on mitochondrial function and beigeing/browning.....	36
Figure 8: Effect of alternatively activated macrophages from Raw264.7 cells on thermogenesis in primary BAT cells. ....	37
Figure 9: Effect of alternatively activated macrophages from C57Bl/6J mice on thermogenesis in primary white adipocytes. ....	38
Figure 10: Effect of alternatively activated macrophages from BALB/c mice on thermogenesis in primary inguinal white and brown adipocytes. ....	38
Figure 11: Effect of alternatively activated macrophages on lipolysis in primary adipocytes. ....	39
Figure 12: Catecholamine production in bone marrow-derived macrophages. ....	40
Figure 13: Effect of 6h cold exposure on macrophage content and catecholamine turnover in brown fat.....	41
Figure 14: Effect of IL-4 on energy expenditure and thermogenesis in C57Bl/6J and <i>I14ra</i> <sup>-/-</sup> mice. ....	43
Figure 15: Effect of IL-4 on lipolysis and catecholamine turnover in C57Bl/6J mice.....	44
Figure 16: Tyrosine hydroxylase and Mac-2 co-staining of cold-exposed adipose tissue.....	45
Figure 17: Structural domain organization of p62 wt and p62 <sup>Δ69-251</sup> .....	46
Figure 18: Genotype of p62 <sup>Δ69-251</sup> mice.....	47
Figure 19: Metabolic phenotype of p62 <sup>Δ69-251</sup> mice on chow diet. ....	48
Figure 20: Side-by-side metabolic phenotype of p62 <sup>Δ69-251</sup> , global p62 <sup>-/-</sup> and adipocyte-specific <i>aP2</i> <sup>cre+; p62<sup>flox/flox</sup></sup> mice on chow and 58% HFD diet.....	49
Figure 21: Energy expenditure of obese p62 <sup>Δ69-251</sup> mice on chow diet.....	50
Figure 22: Brown adipose tissue function of obese p62 <sup>Δ69-251</sup> mice on chow diet.....	50
Figure 23: Brown adipose tissue function of lean p62 <sup>Δ69-251</sup> mice on chow diet.....	52
Figure 24: Metabolic phenotype of p62 <sup>Δ69-251</sup> mice at thermoneutrality (on chow diet). ....	54
Figure 25: Effect of p62 ablation on nuclear and cytosolic distribution of p-ATF2 and p-p38.....	56
Figure 26: Effect of MKK6 on nuclear CRE activity in p62 WT and the truncated p62 <sup>Δ69-251</sup> .....	57

---

**Index of Tables**

Table 1: List of chemicals and reagents. ....	17
Table 2: List of antibodies. ....	18
Table 3: List of taqman probes for LDA qPCR analysis (murine targets). ....	18
Table 4: List of primer sequences for qPCR analysis (murine targets). ....	18
Table 5: PCR program for genotyping of p62 <sup>-/-</sup> mice. ....	20
Table 6: PCR program for genotyping of CRE recombinase. ....	21
Table 7: PCR program for genotyping of p62 <sup>Δ69-251</sup> mice. ....	22

## 1. Introduction

Obesity and its comorbidities, such as type 2 diabetes, represent one of today's most visible health problems (2000). The global obesity epidemic has dramatically increased over the last decades, and based on recent estimations by the World Health Organization (WHO) more than 1.9 billion adults are overweight, 600 million obese (WHO, Obesity and overweight fact sheet 2014). Obesity and diabetes is one of the top preventable causes of premature death and disability (Bauer et al., 2014) and more than 1.5 million annual deaths are directly attributed to diabetes worldwide (WHO, Diabetes fact sheet, 2016). Several life-threatening comorbidities are further directly attributed to excess body weight, such as certain types of cancer (Berger, 2014), Parkinson's disease (Chen et al., 2014), Alzheimer's disease (Naderali et al., 2009), non-alcoholic fatty-liver disease (NAFLD) (Koppe, 2014), dyslipidemia (Bays et al., 2013), atherosclerosis (Roche and Silversides, 2013), type 2 diabetes (Wilding, 2014), hypertension and a variety of cardiovascular diseases (Guo and Garvey, 2016). In obese people with a body mass index (BMI) above 40, the risk to die from cancer is around 1.5 times greater than in people with a BMI of 18.5-24.9 (Calle et al., 2003). In addition, obese individuals therefore have not only a greater prevalence to develop cancer, they also have a poorer prognosis after being diagnosed with cancer (Calle and Thun, 2004). Based on these numerous detrimental effects associated with excess body weight, and the observation that lifestyle changes in the form of dieting or exercise do not yield sustainable weight loss (Rodgers et al., 2012, Dansinger et al., 2005), the development of pharmacological options to decrease body weight is a major challenge with global priority.

Obesity ensues when caloric intake chronically exceeds energy expenditure. Following the first law of thermodynamics, an equilibrium between energy intake and expenditure is thus mandatory to prevent excess body weight gain (Lustig, 2006). Since energy can neither be created nor destroyed, just transformed from one form into the other (Vieland, 2014), weight loss can be achieved by either decreasing caloric intake or by increasing energy expenditure (or ideally both together). The total daily energy expenditure (TDEE) of homeothermic individuals can be divided into several sections. These sections typically include the basal metabolic rate (BMR), the thermic effect of food (TEF), non-exercise activity thermogenesis (NEAT) and the energy spent for physical activity and thermogenesis (Hall et al., 2012, Speakman, 2013). Notably, these sections are not independent from each other i.e. the energy spent during physical activity also accounts for maintaining body temperature, and depending on the species, the contributions of these sections to the overall TDEE varies substantially (Garland et al., 2011). In this regard, small mammals and hibernators especially spend a considerable amount of energy for maintaining their body temperature (Ortmann and Heldmaier, 2000). Therefore brown adipose tissue (BAT), which is able to dissipate heat through uncoupling oxidative phosphorylation from adenosine triphosphate (ATP) synthesis

via action of the uncoupling protein1 (UCP1) (Cannon and Nedergaard, 2004) plays a substantial role in the regulation of body temperature in mammals. Whereas the UCP1-dependent increase in energy expenditure (nonshivering thermogenesis) plays a profound role in small mammals, hibernators and even infants (Cannon and Nedergaard, 2004), its role in adult humans has long been underappreciated. However, recent observations that adult humans also possess pharmacologically relevant amounts of BAT and that the BAT is decreased in obese relative to lean individuals, as well as the observation that BAT increases upon cold exposure has resulted in a rekindled interest in targeting BAT for the treatment of obesity (Cypess et al., 2009, van Marken Lichtenbelt et al., 2009, Virtanen et al., 2009). Thus, in addition to the classical approaches comprising increasing energy expenditure through physical activity and reductions in food intake, successful strategies to combat obesity may benefit from pharmacotherapies selectively targeting the BAT (Saito, 2013). The development of such pharmacotherapies, however, requires a precise understanding of the function and regulation of BAT thermogenesis.

### **1.1 White, beige and brown adipose tissue – function and physiological relevance**

In mammals, there are two types of classical adipose tissue, white adipose tissue (WAT) and BAT and they both differ substantially in their morphology and function (Cinti, 2012). WAT plays a major role in nutrient homeostasis based on its ability to store and mobilize lipids, depending on the body's energetic demand (Konige et al., 2014). However, beyond its role in energy storage and mobilization, WAT is also recognized as an endocrine organ and as such secretes factors, including leptin, adiponectin or adipsin into the circulation to control metabolism (Trayhurn and Beattie, 2001). In contrast to WAT, which stores excess energy in form of triglycerides, BAT utilizes lipids to increase energy expenditure through a process called nonshivering thermogenesis. Beyond these two classical types of adipose tissue, there is also an intermediate form of adipose tissue called beige or brite ("brown-in-white") adipose tissue which carries certain characteristics of both white and brown adipocytes (Cinti, 2002, Wu et al., 2013). Brown and beige/brite adipocytes can develop from transdifferentiation of white adipocytes upon appropriate stimuli, such as cold ("browning/beiging/britening") (Harms and Seale, 2013).

While white adipocytes consist of one single large (unilocular) lipid droplet surrounded by a specific protein, perilipin (Greenberg et al., 1991), brown adipocytes are composed of a high abundance of small (multilocular) lipid droplets (Cinti, 2012). Furthermore, BAT is densely capillarized and displays a high mitochondrial density, thus giving brown adipocytes their characteristic brownish color (Cinti, 2012). Capillarization of BAT ensures sufficient supply of oxygen and hormones, such as norepinephrine (NE) to guarantee sympathetic innervation, as demonstrated by increased blood flow upon activation of BAT thermogenesis (Foster and

Frydman, 1979). Beige/brite adipocytes display a multilocular morphology, and show functional properties similar to that of brown adipocytes, but are predominantly located in the WAT (Harms and Seale, 2013). In order to dissipate chemical energy in the form of heat, brown and beige/brite adipocytes express UCP1, which uncouples oxidative phosphorylation from ATP production (Cohen and Spiegelman, 2015).

Based on the above-mentioned morphological criteria differentiating these adipose depots, their precise distinction is often complicated as some fat depots contain interspersed white, brown and/or beige/brite adipocytes (Kajimura et al., 2015). Thus, classification can be facilitated when investigating the transcriptional control of white, brown and beige/brite fat development.

Adipocytes originate from preadipocytes, which themselves derive from precursor cells (Tang and Lane, 2012). Lineage-tracing studies revealed that myocytes and brown adipocytes, but not white adipocytes, derive from myogenic regulatory factor (Myf5)-expressing precursor cells (Timmons et al., 2007). The dominant regulator of brown adipocyte commitment, PRD1-BF-1-RIZ1 homologous domain-containing protein-16 (Prdm16), serves as a molecular switch to decide whether Myf5-expressing progenitor cells become myotubes or brown adipocytes (Seale et al., 2007, Seale et al., 2008). Although beige/brite adipocytes exhibit a similar morphology to brown adipocytes, they do not originate from Myf5-expressing precursor cells, clarifying their distinction as a unique cell type (Seale et al., 2008).

A current controversy in the field is whether beige/brite adipocytes derive from transdifferentiation of existing mature white adipocytes or whether they exhibit an exclusive precursor signature and can be generated *de novo* (Himms-Hagen et al., 2000, Cinti, 2009, Wang et al., 2013b). On the one hand, it has been shown that beige/brite adipocytes can adjust their capability to store or burn lipids, with main emphasis on one or the other process, depending on the environmental temperature (Rosenwald et al., 2013). On the other hand, pulse-chase studies in which all pre-existing mature adipocytes were labeled indicate that beige/brite adipocytes can develop from *de novo* differentiation of precursor cells (Wang et al., 2013b). While the origin of beige/brite adipocytes remains controversial, white, brown and beige/brite adipocytes exhibit unique gene signatures. Adipogenic differentiation and preadipocyte commitment into mature adipocytes involves some shared transcription factors between each type of adipocytes, which includes among others peroxisome proliferator-activated receptor gamma (PPAR $\gamma$ ) and CCAAT/enhancer-binding proteins (C/EBPs) (Farmer, 2006, Gesta et al., 2007). Transcription factors that specifically refer to brown and beige/brite adipocyte differentiation are Prdm16 and the peroxisome proliferator-activated receptor gamma-coactivator-1 alpha (Pgc-1 $\alpha$ ). The zinc finger protein Prdm16 binds and regulates C/EBP $\beta$ , PPAR $\gamma$ , PPAR $\alpha$  and Pgc-1 $\alpha$  (Seale et al., 2008, Kajimura et al., 2009, Hondares et al., 2011) whereas Pgc-1 $\alpha$  stimulates mitochondrial biogenesis, which is crucial

for adaptation to cold exposure (Wu et al., 1999, Puigserver et al., 1998). To distinguish between brown and beige/brite adipose tissue, several markers that are selectively enriched in either tissue were identified, such as *Zic1*, *Lhx8*, *Eva1*, *Pdk4* for brown fat or *CD137*, *Tbx1*, *Tmem26*, *Cited1* for beige/brite fat (Petrovic et al., 2010, Jespersen et al., 2013, Wu et al., 2012, Sharp et al., 2012). While beige/brite adipocytes display lower basal expression of *Ucp1* than classical brown adipocytes,  $\beta$ -adrenergic stimulation can induce an increase in *Ucp1* expression comparable to activated brown adipocytes (Wu et al., 2012). Several external stimuli, such as NE or the bone morphogenetic protein 7 (BMP7) are capable of inducing brown adipocyte differentiation (Tseng et al., 2008) and further numerous circulating hormones, such as triiodothyronine (T3), fibroblast growth factor 21 (FGF21) or natriuretic peptides have been implicated in BAT activation (Villarroya and Vidal-Puig, 2013, Silva and Larsen, 1983).

### 1.1.1 Brown adipose tissue in mice

Historically, BAT is believed to have evolved as a natural defense mechanism against hypothermia in homoeothermic mammals (Cannon and Nedergaard, 2004). The physiological importance of BAT was originally observed in seasonal mammals, which required BAT thermogenesis to maintain their body temperature during hibernation and torpor to enable arousal and re-warming from their decreased metabolic state (Oelkrug et al., 2015).

Murine neonates, in particular, possess significant amounts of active BAT in order to survive the cold stress of birth (Kozak and Koza, 2010). In addition, adult mice that are housed below their thermoneutral zone at room temperature show chronically activated BAT, which maintains their body temperature (Cannon and Nedergaard, 2004). In mice, the largest brown adipose depot is the interscapular BAT (iBAT), which consists of two symmetric depots above the shoulder blades (Walden et al., 2012). Several smaller depots of BAT have been identified around the kidneys (perirenal BAT), cervical spine (cervical BAT), heart (mediastinic BAT) and in an intermuscular depot beneath the scapulae (axillary BAT) (Frontini and Cinti, 2010, Walden et al., 2012). Because of its size, accessibility and clear innervation, the iBAT represents the main depot used to examine BAT thermogenic capacity in mice. In addition to the classical brown adipose depots, inducible and recruitable beige/brite adipocytes are primarily distributed in the inguinal white adipose tissue (iWAT) upon  $\beta$ -adrenergic stimulation (Sanchez-Gurmaches and Guertin, 2014).

### 1.1.2 Brown adipose tissue in humans

Similarly to mice, human newborns and infants exhibit relevant amounts of BAT, such as interscapular and perirenal BAT depots (Lidell et al., 2013). BAT has a functional significance in newborns. The sudden change of environmental temperature during birth (from intrauterine to external milieu) requires BAT-mediated heat production for survival (Cypess and Kahn, 2010). With growth, social culture adaptation and associated clothing, the necessity of protection against cold decreases, along with the need for active BAT. Thus, the previous scientific consensus was that the presence of BAT was restricted to newborns and infants. However, in 2009 relevant amounts of BAT were detected in adult humans by positron emission tomography (PET) scanning (Cypess et al., 2009, van Marken Lichtenbelt et al., 2009, Virtanen et al., 2009). PET computed tomography (PET-CT) imaging, primarily applied for cancer research, enables the detection of radioactive  $^{18}\text{F}$ -labelled [ $^{18}\text{F}$ ]-2-deoxy-glucose (2-deoxy-2-[fluorine-18]fluoro-D-glucose) uptake within living organisms, to track metabolically active sites. PET-CT studies in healthy human subjects revealed that mild cold stress induces a substantial increase in uptake of [ $^{18}\text{F}$ ]-2-deoxy-glucose in the supraclavicular area, the retroperitoneum, and along the aorta (Cypess et al., 2009, van Marken Lichtenbelt et al., 2009, Virtanen et al., 2009). Biopsy analysis of these brown adipose depots confirmed their identity, as UCP1 mRNA and protein levels are elevated upon cold exposure (Virtanen et al., 2009). These findings have rekindled scientific interest in the BAT and its therapeutic potential. When selecting an appropriate model organism to study BAT thermogenesis, some limitations arise when comparing laboratory mice to humans. Since humans live mostly at thermoneutrality due to clothing and social circumstances, their amount of BAT is relatively small (estimated 0.02% of body weight) as compared to the BAT mass of mice (estimated 0.4-1% of body weight) (Geisler, 2011). In addition, the distribution as well as the gene signature of the different BAT depots, is different between mice and humans. Although first studies found a molecular signature of the supraclavicular BAT similar to that of beige/brite adipocytes (Lidell et al., 2013), later studies demonstrated that both types of classical brown and beige/brite adipocytes co-exist in the above-mentioned BAT depots of adult humans (Jespersen et al., 2013). Nevertheless, with the discovery of active BAT depots in adult humans, investigations into BAT thermogenesis, with an emphasis on elucidating its role in energy expenditure, could yield potential therapeutic targets for the treatment of obesity.

### 1.2 Sympathetic neuronal control of brown adipose tissue thermogenesis

Nonshivering thermogenesis is almost exclusively under control of the sympathetic nervous system (SNS). BAT thermogenesis is triggered by the release of NE from the SNS, elicited through cold sensation, to stimulate  $\beta_3$ -adrenergic receptors on adipocytes that activate an

intracellular signaling cascade leading to the activation of UCP1 (described in detail below). In 1965, Wirsén first described catecholaminergic varicosity among blood vessels in brown adipocytes (Wirsén, 2011). Electron microscopy subsequently revealed parenchymal and vasculature innervation in BAT (Bargmann et al., 1968). Surgical denervation demonstrated the essential role of the SNS and NE in thermogenic regulation, since denervated BAT does not increase thermogenesis in response to NE (Hamilton et al., 1989).

### 1.2.1 $\beta_3$ -adrenergic signaling pathway

In mature brown adipocytes, the process of nonshivering thermogenesis is induced by NE binding to  $\beta_3$ -adrenergic receptors, a member of the G protein-coupled receptor family. Although NE can interact with all three types of adrenergic receptors ( $\beta$ ,  $\alpha_1$  and  $\alpha_2$ ), the  $\beta_3$ -adrenergic receptor plays the most significant role in activation of the thermogenic signaling pathways in brown adipocytes, as shown by studies utilizing a selective  $\beta_3$ -agonist CL316,243 (Himms-Hagen et al., 1994). A unique feature of  $\beta_3$ -adrenergic receptors is the lack of amino acid (AA) residues traditionally involved in receptor desensitization, therefore these receptors are not easily desensitized (Emorine et al., 1989, Nahmias et al., 1991). In contrast,  $\alpha_2$ -adrenergic receptors are coupled to  $G_i$  proteins, whose activation leads to inhibition of the adenylyl cyclase, thus preventing activation of the thermogenic pathway. Norepinephrine's capability to either bind to  $\beta_3$  or  $\alpha_2$ -adrenergic receptors enables the cell to balance between stimulation and inhibition of nonshivering thermogenesis depending on prevailing metabolic requirements (Cannon and Nedergaard, 2004).

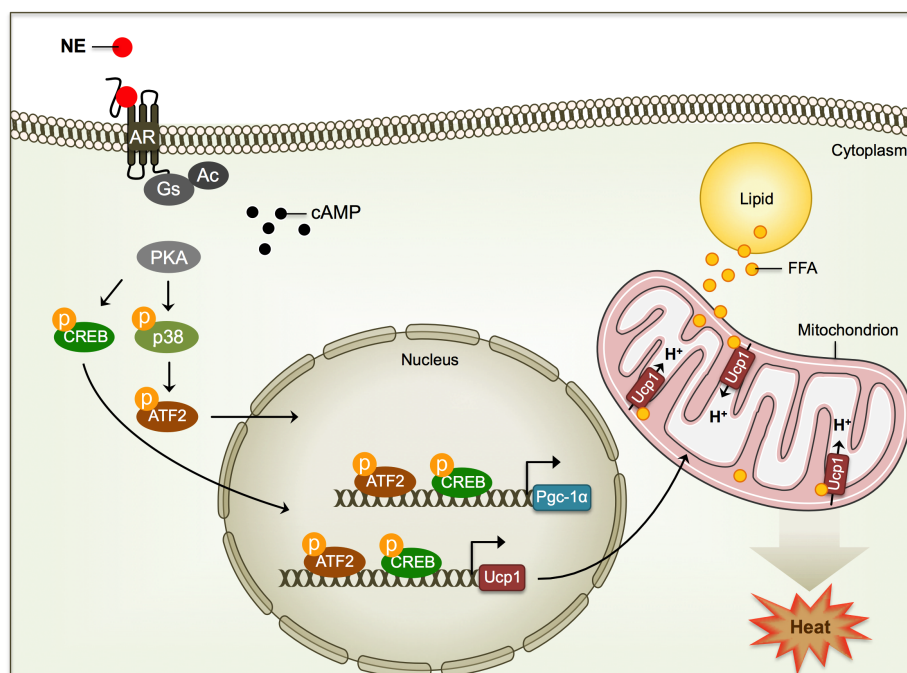


**Figure 1: Norepinephrine induction of nonshivering thermogenesis.**



Norepinephrine binds to the  $\beta$ -adrenergic receptor (AR), leading to activation of the adenylyl cyclase (AC) and increased levels of cAMP. Thus activated PKA phosphorylates CREB (p-CREB) and p38 (p-p38), which further activates ATF2 (p-ATF2). P-CREB and p-ATF2 enter the nucleus, bind to the DNA and activate *Pgc-1 $\alpha$*  and *Ucp1* gene expression. UCP1 then translocates to the inner mitochondrial membrane and uncouples respiration, which generates heat by usage of free fatty acids (FFA) that have released from lipid droplets through lipolysis.

Norepinephrine-induced activation of the  $\beta_3$ -adrenergic receptor mediates  $G_s$  protein signaling, thus activating the adenylyl cyclase to induce cyclic AMP (cAMP) formation (Fig. 1) (Zhao et al., 1997). Consequently, increased intracellular levels of the secondary messenger cAMP lead to activation of the protein kinase A (PKA), which phosphorylates a series of target enzymes. Of note, activation of PKA is essential for thermogenic and lipolytic processes, as its inhibition blocks all effects mediated by  $\beta_3$ -stimulation (Cao et al., 2001, Fredriksson et al., 2001). Lipolysis is defined as the hydrolysis of triacylglycerol (TAG), stored in lipid vesicles, to generate fatty acids (FA) and glycerol. This process is composed of two steps: activation of the hormone-sensitive lipase (HSL) and phosphorylation (deactivation) of perilipin. Perilipin covers lipid droplets and functions as a protective barrier that restricts the access of lipases, such as HSL, in order to prevent lipolysis (Martinez-Botas et al., 2000). PKA-induced phosphorylated perilipin dissociates from the lipid droplets and rendering the droplets accessible to HSL, thereby activating lipolysis (Morimoto et al., 2001). Liberated free fatty acids (FFAs) are channeled towards the mitochondria as essential substrate for UCP1-dependend thermogenesis, whereas glycerol is released into the circulation.

PKA also activates (via phosphorylation) the cAMP-responsive element (CRE)-binding protein (CREB) and the mitogen-activated protein kinase (MAPK) p38. The latter in turn activates the activating transcription factor 2 (ATF2) (Fig. 1) (Cao et al., 2004). Phosphorylated CREB and ATF2 are targeted to the nucleus and regulate *Pgc-1 $\alpha$*  and *Ucp1* expression by direct binding to the CRE element of their enhancer region (Cao et al., 2004). UCP1 protein then translocates to the inner mitochondrial membrane where BAT nonshivering thermogenesis occurs. FFAs that have been ferried to the mitochondria via carnitine shuttle then undergo  $\beta$ -oxidation and are further catabolized in the citric acid cycle, and finally transfer the released electrons through the respiratory chain. Thus, protons are pumped from the mitochondrial matrix to the inner mitochondrial membrane, where a membrane potential, the proton motive force (PMF), is generated (Divakaruni and Brand, 2011). UCP1 requires FFAs as substrate and the energy from the PMF in order to create a futile cycle, which dissipates chemical energy in the form of heat.

### 1.2.2 The uncoupling protein UCP1

UCP1, an integral 32 kDa protein of the inner mitochondrial membrane, is a member of the mitochondrial carrier protein family. UCP1 uncouples aerobic respiration by dissipating the

chemical energy that is generated in the form of the PMF by creating a futile cycle of protons to generate heat instead of ATP. In the presence of long-chain fatty acids, UCP1 increases the permeability of the inner mitochondrial membrane for protons, which enables the flow of protons down the electrochemical gradient into the mitochondrial matrix (Nicholls and Locke, 1984). Besides UCP1 activation by FFAs, UCP1 can be inhibited by purine nucleoside di- and triphosphates (Locke et al., 1982). Currently, three competing models strive to unify how UCP1 catalyzes proton conductance (Divakaruni and Brand, 2011). In the first model, FFAs function as cofactors essential for proton transport, embedding their carboxyl group into the core of UCP1 to provide a functional group that facilitates proton transport (Klingenberg and Huang, 1999, Klingenberg and Winkler, 1985). The second model proposes, that FA anions are protonated in the acidic intermembrane space, therefore allowing the neutral molecule to enter the inner mitochondrial matrix (Garlid et al., 1998). Proton dissociation from the FFAs is then mediated by the alkaline milieu of the matrix. The third model describes a competitive mechanism, where FFAs are not directly required for proton transport but rather induce an allosteric change by competing with nucleotides (Shabalina et al., 2004).

The precise mechanism, however, remains elusive, since it has not been clarified whether FFAs act as cofactors, proton shuttles, or allosteric regulators to increase the membrane proton conductance via UCP1.

### **1.3 Crosstalk between metabolism and macrophages**

Macrophages, an integral component of innate immunity, function to perform phagocytic clearance of dying cells during development and throughout life, and to protect the host from pathogens. The majority of macrophages originate from bone marrow-derived monocytes (BMDMs), which upon stimulation with the macrophage colony-stimulating factor (M-CSF) develop into macrophages (Martinez and Gordon, 2014). Unlike models first suggested in 1968, where tissue resident macrophages originate from circulating adult blood monocytes (van Furth and Cohn, 1968), it has been shown in the last few years that tissue resident macrophages develop independently of circulating monocytes. Of note, tissue resident macrophages originate during embryonic development and persist into adulthood independently of blood monocytes (Ginhoux et al., 2010, Schulz et al., 2012, Hashimoto et al., 2013).

The adipose organ not only stores lipids, it also operates as an endocrine and immunologically active organ. During the progression of obesity, the lipid overflow in WAT leads to enhanced production and secretion of pro-inflammatory cytokines, which leak into the circulation and contribute to the development of glucose intolerance and insulin resistance (Lauterbach and Wunderlich, 2017, Schenk et al., 2008). The increased cell damage associated with excessive lipid accumulation leads to enhanced recruitment of

immune cells, most prominently macrophages, that warrant a continuous turnover of adipocytes by promoting the disposal of cellular debris following adipocyte apoptosis (Weisberg et al., 2003, Xu et al., 2003). Obesity-associated metabolic inflammation demonstrates the important and diverse role of macrophages to regulate and maintain healthy tissue homeostasis.

### 1.3.1 Adipose tissue macrophages and their role during obesity

The percentage of macrophages relative to all cells in adipose tissue is estimated to range from under 10% in lean mice and humans to up to 40% in obese mice and humans, suggesting that macrophages play a major role in maintenance of adipose tissue homeostasis (Weisberg et al., 2003). Different nomenclatures have been used to define macrophage populations, but herein we refer to anti-inflammatory or alternatively activated macrophages as M2-type and pro-inflammatory or classically activated macrophages as M1-type (Olefsky and Glass, 2010).

Adipose tissue macrophages (ATMs) are usually small and interspersed among adipocytes in lean individuals, but during the progression of obesity, ATMs aggregate to form crown-like structures around adipocytes (Fig. 2) (Weisberg et al., 2003, Lumeng et al., 2008, Kosteli et al., 2010, Ferrante, 2013). General macrophage infiltration markers, that do not distinguish between M1 or M2 phenotype reveal the surface proteins CD11b and F4/80 (Gordon et al., 2014). Notably, alternatively activated macrophages primarily occur within lean adipose depots, whereas during obesity the majority of macrophages within the adipose tissue consist of classically activated macrophages (Fig. 2) (Odegaard et al., 2007, Lumeng et al., 2008).

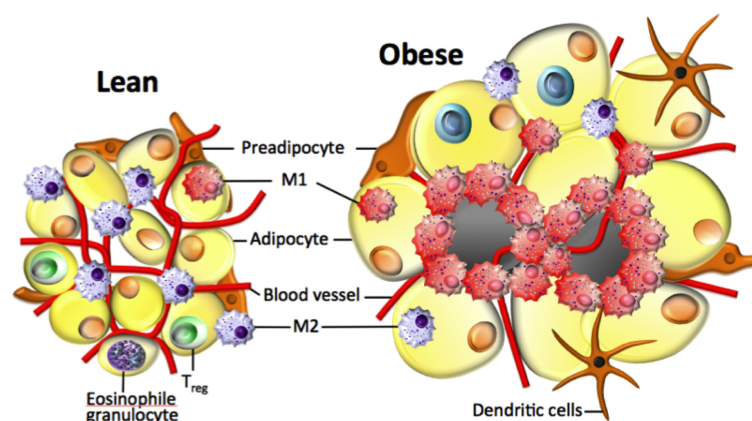


#### Figure 2: Adipose tissue inflammation

Distribution of immune cells in adipose tissue during lean and obese state. In the lean state, predominantly anti-inflammatory M2-type macrophages and regulatory t-cells (T<sub>reg</sub>) populate the adipose tissue to maintain metabolic homeostasis (left). In contrast, pro-inflammatory M1-type macrophages are mainly found in obese adipose tissue (right).

Adipose tissue macrophages are capable of switching their phenotype in response to environmental conditions, as M2-type ATMs can switch to the M1 phenotype with the progression of obesity (Lumeng et al., 2007a). Whether ATMs polarize towards M1 or M2 phenotype strongly depends on different cytokines and interleukins. Alternatively activated macrophages are triggered by stimulation with the type 2 cytokines interleukins IL-4 and IL-13, which signal through the IL-4 receptor alpha (Il4ra) to induce the expression of a variety of markers that are characteristic for M2 macrophage activation, such as macrophage galactose N-acetyl-galactosamine specific lectin 2 (Mgl2), arginase 1 (Arg1), mannose receptor C type 1 (Mrc1) (Van Dyken and Locksley, 2013, Mantovani et al., 2004, Murray et al., 2014, Martinez et al., 2008). IL-4 is highly expressed in lean individuals and induces expression of PPAR $\gamma$  and promotes insulin sensitivity by secretion of anti-inflammatory cytokines, such as IL-10 (Huang et al., 1999, Olefsky and Glass, 2010). In contrast, recruitment and differentiation into M1-type macrophages is induced by inflammatory mediators, such as lipopolysaccharide (LPS) and interferon- $\gamma$  (IFN- $\gamma$ ), thus causing secretion of pro-inflammatory cytokines, such as tumor necrosis factor alpha (TNF- $\alpha$ ), IL-1 $\beta$  and production of toxic intermediates, such as nitric oxide (NO) (Lumeng et al., 2007b, Martinez et al., 2008).

Although a clear definition of M1 and M2 macrophage polarity exists, this is an oversimplification because macrophages display a heterogeneous cell population *in vivo*, capable to also develop into different phenotypes beyond the pro- and anti-inflammatory state (Morris et al., 2011, Martinez et al., 2006).

### 1.3.2 Innate immune regulation of thermogenesis

Beyond their role in adipose tissue inflammation, alternatively activated macrophages were recently shown to play an important role in BAT thermogenesis by producing catecholamines that act locally within the BAT to promote nonshivering thermogenesis through induction of  $\beta_3$ -adrenergic signaling (Nguyen et al., 2011). Chawla and colleagues demonstrated that the number of M2-type macrophages in BAT increases upon cold exposure, as indicated by elevated expression of numerous M2-specific markers, which induced expression of UCP1 as well as tyrosine hydroxylase (TH), the rate-limiting enzyme in catecholamine synthesis (Nguyen et al., 2011). Further, chronic administration of recombinant IL-4 induced enhanced oxygen consumption, accompanied by increased expression of TH in wild-type (WT) mice but not in mice lacking the Il4ra either constitutively or specifically in myeloid cells (Nguyen et al., 2011). Likewise, lack of TH in myeloid cells further impairs energy expenditure (Qiu et al., 2014). Moreover, alternatively activated macrophages promote beiging/browning of white adipocytes and control beige fat biogenesis (Qiu et al., 2014). Genetic disruption of IL-4 and IL-13 prevents cold-induced beiging/browning of white adipocytes (Qiu et al., 2014).

In addition to catecholamine production by alternatively activated macrophages, another type of immune cells, Type 2 innate lymphoid cells (ILC2s), have recently been reported to elicit activation of M2-type macrophages via *Il4ra* signaling and therefore may play a role in regulation of beige/brite adipose tissue biogenesis (Brestoff et al., 2015, Lee et al., 2015). IL-33, a nuclear cytokine that mediates type 2 immune responses and activates ILC2s, triggers commitment of adipocyte precursors to beige/brite adipocyte lineage (Lee et al., 2015). During the perinatal period, IL-33, the ligand for the receptor ST2 and ST2 itself are both required for normal splicing of *Ucp1* mRNA to obtain functional UCP1 protein in BAT (Odegaard et al., 2016).

Supporting this role of M2 macrophages in adaptive thermogenesis, Meteorin-like (*Metnl*), a circulating hormone induced in adipose tissue upon cold exposure, was recently shown to promote nonshivering thermogenesis through enhanced recruitment of M2-type macrophages (Rao et al., 2014). A similar requirement for M2 macrophages has been observed for adiponectin-enhanced beige/browning of subcutaneous WAT during prolonged cold exposure (Hui et al., 2015). Finally ablation of the receptor interacting protein 140 (RIP140), a positive regulatory molecule for pro-inflammatory M1 macrophages, improves insulin sensitivity and triggers WAT beige/browning by increasing numbers of M2-type macrophages (Liu et al., 2015).

Numerous studies now demonstrate the existence of an alternative pathway, independent of the classical view of sympathetic regulation, to control adaptive thermogenesis by local production of catecholamines within the adipose tissue mediated by alternatively activated macrophages.

#### **1.4 Scaffold protein p62/Sequestosome 1**

Metabolic homeostasis requires cooperation of multiple signals and cellular activities. Scaffold proteins are crucial regulators of many cell-signaling cascades. The function of scaffolding proteins is to assemble two or more proteins, while maintaining a relatively stable configuration (Garbett and Bretscher, 2014). In most cases, a stable complex is formed by these protein-protein interactions that facilitates interactions and functions between different proteins, although some scaffold proteins exhibit dynamic properties (Garbett and Bretscher, 2014). The protein p62 (also known as Sequestosome 1/*Sqstm1*) is a scaffold protein that is capable of recruiting and oligomerizing multiple signaling molecules to function as signaling center which mediates a variety of cell signaling pathways, such as osteoclastogenesis, inflammation, cancer and obesity (Moscat et al., 2007).

### 1.4.1 Structure and function of p62

P62 consists of 442 AA that give rise to six distinct functional domains: Protein-binding (Phox and Bem1p-1) domain (PB1), zinc finger motif (ZZ), TRAF6-binding (TB) domain, LC3-interacting region (LIR), Keap1-interacting region (KIR) and ubiquitin-associated domain (UBA). Proteins recruited to these domains enable p62 to implement kinase-activated and ubiquitin-mediated cell signaling pathways.

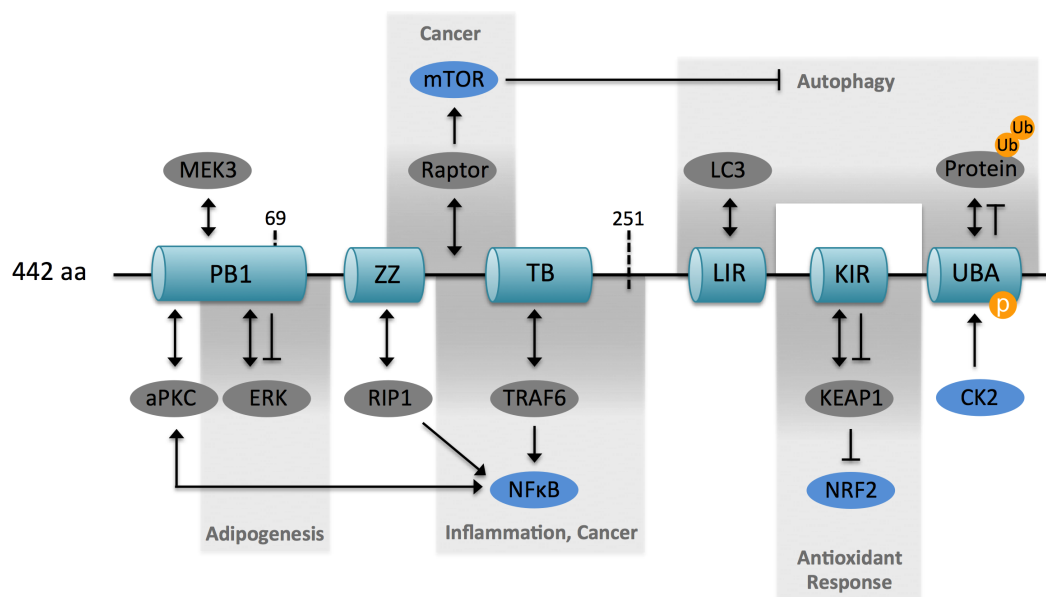


**Figure 3: Domain organization and interacting partners of the scaffold protein p62**

The 442 amino acid (AA) protein p62 consists of a protein-binding (Phox and Bem1p-1) domain (PB1), a zinc finger motif (ZZ), a TRAF6-binding (TB) domain, a LC3-interacting region (LIR), a KEAP1-interacting region (KIR) and an ubiquitin-associated domain (UBA). Some of these domains are able to interact with some of the following proteins: mitogen-activated protein kinase 3 (MEK3); raptor, mechanistic target of rapamycin (mTOR); microtubule-associated protein 1A/1B-light chain (LC3); ubiquitinated (Ub) proteins; atypical protein kinase C (aPKC); extracellular signal-regulated kinase (ERK); receptor-interacting protein 1 (RIP1); TNF receptor associated factor 6 (TRAF6); nuclear factor kappa-light-chain-enhancer of activated B-cells (NFκB); Kelch-like ECH-associated protein 1 (KEAP1); nuclear factor erythroid 2-related factor (NRF2); casein kinase 2 (CK2)

The N-terminal PB1 domain of p62 binds the homotypic region of the atypical protein kinase C (aPKC), thus mediating activation of the transcription factor nuclear factor kappa-light-chain-enhancer of activated B-cells (NFκB) (Sanz et al., 2000, Duran et al., 2004). Further interaction of p62 with the receptor-interacting protein 1 (RIP1) via the ZZ domain and the TNF receptor associated factor 6 (TRAF6) via the TB domain, enables NFκB activation to mediate inflammatory responses (Sanz et al., 2000). TRAF6 has been identified as an E3 ubiquitin ligase that catalyzes the synthesis of polyubiquitin chains required for IKK activation (Chen et al., 2006). Ablation of TRAF6 shows impaired NFκB activation upon IL-1 stimulation followed by development of an osteopetrotic phenotype (Duran et al., 2004, Kobayashi et al., 2001). Besides the requirement of p62 for osteoclastogenesis and inflammation, its PB1 domain orchestrates interactions with the mitogen-activated protein kinase MEK3 and the extracellular signal-regulated kinase (ERK). Whereas, p62 preferentially interacts with ERK1 by mediating repression of adiposity, p62-deficient mice reveal enhanced adipogenesis with

increased ERK levels (Rodriguez et al., 2006). However, double-knockout of p62 and ERK1 reverses adipogenesis and lowers energy expenditure (Lee et al., 2010).

Notably, it has been shown that p62 enhances activity of MAPK p38 (Sudo et al., 2000) while knockdown of p62 impairs p38 phosphorylation (Kawai et al., 2008). Although two p38 interaction domains, one comprising AA 173-182 and the other AA 335-244 of p62, have been identified recently, only the N-terminal (173-183) domain is known to have direct interaction between p62 and p38 as revealed by surface plasmon resonance (Kawai et al., 2008).

The scaffold protein p62 also interacts with raptor to activate the mammalian target of rapamycin complex 1 (mTORC1), which on the one hand plays a critical role in cancer cell proliferation and on the other hand is proposed to be a positive modulator of adiposity, as ablation of raptor reverses adipogenesis (Duran et al., 2011, Polak et al., 2008). Inhibition of mTOR signaling by nutrient removal or addition of rapamycin activates autophagy (Sabatini, 2006). Autophagy plays an important role in quality control of proteins by elimination of invading pathogens and degradation of misfolded or aggregated proteins to ensure constant protein turnover (Glick et al., 2010). The observation that p62 accumulates in autophagy-deficient mice indicates its function in inclusion body formation and draws a connection between p62 and autophagy (Komatsu et al., 2007). P62 can bind to the autophagy regulator autophagy-related protein 8 (Atg8) and the microtubule-associated protein 1A/1B-light chain (LC3) through the LIR domain (Moscat and Diaz-Meco, 2009). At its C-terminus, p62 harbors a UBA domain that enables assembly of ubiquitinated proteins to mediate their disposal (Moscat et al., 2007). The remaining KIR domain facilitates p62 to interact with KEAP1, which functions as an adapter protein for degrading nuclear factor erythroid 2-related factor (NRF2), a master regulator of oxidative stress (Komatsu et al., 2010, Filomeni et al., 2015).

Many of the different functions of p62 seem to be interconnected, such as the observation that reduced NF $\kappa$ B activation, triggered by lack of p62, reduces levels of reactive oxygen species (ROS) scavengers, thus leading to enhanced ROS and more apoptosis (Moscat and Diaz-Meco, 2009). This might explain the lower carcinogenic potential observed in p62-deficient mice (Duran et al., 2008). The scaffold protein p62 is a multi-faceted adaptor protein involved in a cascade of cell signaling processes, however the scope of this work focuses on p62 and its specific role in the regulation of energy homeostasis.

#### **1.4.2 P62 and its relevance for obesity**

Moscat and colleagues provided the first evidence for a potential role of p62 in the control of metabolic homeostasis by showing that mice globally lacking p62 develop mature onset insulin resistance and obesity (Rodriguez et al., 2006). At an age of three months and older, these mice become severely obese, which seems to be primarily a result of enhanced fat

content (Rodriguez et al., 2006). Following the characterization of several different p62 tissue-specific knockout (KO) mice, the adipose tissue was identified as the tissue that caused the obesity phenotype in mice lacking p62 globally (Muller et al., 2013). Therefore, both global and adipose-specific ablation of p62 elicited severe obesity and insulin resistance (Muller et al., 2013, Rodriguez et al., 2006). In the obese state, mice lacking p62 globally had a higher calorie intake than healthy control mice. However when normalized to total body weight, this difference vanished (Rodriguez et al., 2006). Pair feeding studies further demonstrated that altered food intake was not the contributor to the adiposity observed upon p62 ablation (Rodriguez et al., 2006), since under these experimental conditions the mice that were lacking p62 still gained more fat mass. In agreement, mice lacking p62 specifically in adipose tissue gained weight independently of caloric intake, as no change in food intake was observed compared to WT mice (Muller et al., 2013). Instead, p62-deficient mice exhibit reduced energy expenditure as well as impaired function in BAT thermogenesis (Rodriguez et al., 2006, Muller et al., 2013). Mice lacking p62 in the adipose tissue reveal a reduced body temperature upon stimulation of the  $\beta$ -adrenergic pathway, along with decreased expression of key regulatory genes of BAT thermogenesis (Muller et al., 2013). Furthermore, mitochondrial structure and oxidative capacity is impaired in the BAT of fat-specific p62-deficient mice, indicating an additional mitochondrial dysfunction in these mice (Muller et al., 2013). Characterization of p62-deficient primary adipocytes reveals that p62 controls mitochondrial function and its responsiveness to  $\beta$ -adrenergic stimulation in a cell autonomous manner (Muller et al., 2013).

These results indicate that loss of p62 provokes characteristics of the metabolic syndrome, such as obesity, glucose intolerance and insulin resistance. However, glucose intolerance and insulin resistance of p62-deficient mice is secondary to the obesity and displays no intrinsic defect, because lean mice lacking p62 reveal normal glucose and insulin homeostasis (Rodriguez et al., 2006). Notably, even before the onset of obesity, young mice lacking p62 revealed increased expression of the adipogenic regulator PPAR $\gamma$  in WAT (Rodriguez et al., 2006). In addition, lack of p62 leads to enhanced ERK activity in both lean and obese p62-deficient mice, suggesting that p62 is required to maintain low basal ERK activity low to prevent the development of adipogenesis and its related progression to obesity (Rodriguez et al., 2006). Notably, genetic inactivation of ERK1 is sufficient to reverse the obese phenotype observed in p62-deficient mice (Lee et al., 2010). Simultaneous deletion of p62 and ERK1 restores the impaired energy expenditure of p62-deficient mice (Lee et al., 2010).

Collectively, p62 plays a major role in regulation of energy homeostasis. While some indications point towards an ERK-related function promoting mature onset obesity (Rodriguez et al., 2006, Lee et al., 2010), other findings suggest that p62 might regulate BAT



---

thermogenesis via the p38 MAPK pathway. However, identification of a functional domain of p62 that is capable of interacting with p38 (Kawai et al., 2008), as well as the finding that  $\beta$ -adrenergic stimulation of p62-deficient primary brown adipocytes impairs activation of p38 and its downstream target ATF2 (Muller et al., 2013), indicates that the MAPK pathway is a potential regulator of energy metabolism via p62. Nonetheless, the precise mechanism how p62 controls BAT thermogenesis remains elusive and detailed studies to unravel p62's mechanistic underpinnings and its possible involvement in the MAPK pathway are required.

## 2. Scope of this thesis

The scope of this current work was to characterize specific regulators of energy metabolism – in particular their contribution to BAT thermogenesis. The specific aims of this PhD thesis were:

**(1) To corroborate the role of macrophages in mitochondrial function and thermogenesis.**

The overarching objective of this first part of the thesis was to elucidate the precise role of alternatively activated macrophages in the control of adipocyte function and nonshivering thermogenesis. In detail, the objectives were to examine the effects of macrophage depletion and of macrophage polarization towards M2 phenotype by IL-4 on energy metabolism. Catecholamine production and tyrosine hydroxylase expression were determined in adipose depots upon activation of M2-type macrophages and/or cold exposure to investigate the capability of macrophages to produce and secrete catecholamines. In sum, the data obtained from these studies suggest that alternatively activated macrophages do not contribute to BAT thermogenesis, instead the findings support the acknowledged dominant role of the SNS in thermogenic regulation.

**(2) To identify the molecular mechanism underlying energy metabolism control by p62.**

One critical downstream component of sympathetic-controlled activation of BAT thermogenesis is the scaffold protein p62 that regulates energy metabolism via modulation of mitochondrial function and BAT thermogenesis.

The objective of this second part of the thesis was to unravel the molecular underpinnings of energy metabolism control by p62. Since the protein p62 affects BAT thermogenesis by interfering in the MAPK pathway, this part of the thesis investigated the specific region (AA 69-251) of p62 that contains the p38-binding domain of p62. To identify the functional domain of p62 responsible for impaired BAT thermogenesis, mice that globally lack AA 69-251 of p62 (p62<sup>Δ69-251</sup>) were metabolically characterized. *Ex vivo* and *in vitro* analysis of adipose tissue and primary adipocytes derived from iWAT or BAT of p62<sup>Δ69-251</sup> mice showed alterations in the MAPK signaling pathway, thus affecting activation of UCP1. Another objective was to elucidate the role of this p62 domain for the nuclear transport of phosphorylated ATF2 (p-ATF2) that could impact UCP1 activity. Together, the data from these studies identified the region of p62 that is controlling BAT thermogenesis. Furthermore, nuclear transport of p-ATF2 is not possible upon loss of AA 69-251 of p62, thus preventing activation of UCP1.

### 3. Material and Methods

**Table 1: List of chemicals and reagents**

<b>Chemical</b>	<b>Provider</b>
2-Deoxyglucose	Sigma Aldrich
Antimycin	Sigma Aldrich
Ascorbate	Sigma Aldrich
CaCl <sub>2</sub>	Carl Roth
Calyculin A	CST
Carbonyl cyanide-p-trifluoromethoxyphenylhydrazone	Sigma Aldrich
Collagenase II	Life Technologies
Collagenase IV	Life Technologies
Cytochrome C	Sigma Aldrich
Dapi	Sigma Aldrich
Dexamethasone	Sigma Aldrich
Dispase II	Sigma Aldrich
DMEM, high glucose (#41965)	Thermo Fisher Scientific
DMEM/F12 (1:1)+Glutamax (#10565018)	Thermo Fisher Scientific
dNTP	NEB
DTT	Sigma Aldrich
EDTA	Lonza
Fatty-acid free BSA	Sigma Aldrich
FBS	Gibco
Ficoll	GE healthcare
Glucose	Carl Roth
Glutathione	Sigma Aldrich
Hematoxylin	Applichem
Hydrogen peroxide	Carl Roth
Indomethacine	Sigma Aldrich
Insulin solution, human	Sigma Aldrich
Isobutylmethylxanthine	Sigma Aldrich
Isoproterenol hydrochloride	Sigma Aldrich
Lipofectamine 2000	Thermo Fisher Scientific
MgCl <sub>2</sub>	Sigma Aldrich
N-dodecyl-β-D-maltoside	Sigma Aldrich
NaOH	Carl Roth
Nile Red	Sigma Aldrich
Oil Red O	Sigma Aldrich
Oligomycin	Sigma Aldrich
Paraformaldehyde	Carl Roth
PBS	Gibco
Penicilin/Streptomycin	Thermo Fisher Scientific
PMSF	Carl Roth
Potassium phosphate	Carl Roth
Protease/phosphatase inhibitor	Thermo Fisher Scientific
Pyruvate	Sigma Aldrich
Recombinant murine IL-4	Peprtech
Ripa buffer	Sigma Aldrich
Rosiglitazone	Cayman
Rotenone	Sigma Aldrich
Saline	B. Braun
Sodium Azide	Sigma Aldrich
T3	Sigma Aldrich

**Table 2: List of antibodies**

Antibody	Ref	Provider
Anti-Mouse CD45 FITC	11-0451	Affymetrix eBioscience
Anti-Mouse F4/80 Antigen APC	17-4801	Affymetrix eBioscience
Anti-Tyrosine Hydroxylase	MAB318	Merck Millipore
Gapdh (G-9)	sc-365062	Santa Cruz
Goat anti-mouse IgG-HRP	sc-2005	Santa Cruz
Goat anti-rabbit IgG-HRP	sc-2030	Santa Cruz
Histone H3 Nuclear Loading Control and ChIP Grade HSL	ab1791	Abcam
MKK6 (D31D1)	#4107	Cell Signaling
p38 MAPK	#8550	Cell Signaling
p44/42 MAPK (Erk1/2) Antibody	#9212	Cell Signaling
Phospho-ATF-2 (Thr69/71)	#9102	Cell Signaling
Phospho-ATF-2 (Thr69/71)	#9225	Cell Signaling
Phospho-HSL (Ser660)	#4126	Cell Signaling
Phospho-p38 MAPK (Thr180/Tyr182) (D3F9)	#4511	Cell Signaling
Phospho-p44/42 MAPK (Erk1/2) (Thr202/Tyr204)	#9101	Cell Signaling
Sqstm1/p62	ab101266	Abcam
UCP1 (for IHC)	ab10983	Abcam
UCP1 (for Western blot)	ab23841	Abcam

**Table 3: List of taqman probes for LDA qPCR analysis (murine targets)**

Gene name	Abbr.	RefSeq
Adrenoceptor Alpha 2A	Adra2a	Mm00845383_s1
Adrenoceptor Beta 3	Adrb3	Mm02601819_g1
Arginase 1	Arg1	Mm00475988_m1
Bone Morphogenetic Protein 8b	Bmp8b	Mm00432115_g1
C-Type Lectin Domain Family 10 Member A	Mgl2	Mm00460844_m1
Cell Death-Inducing DFFA-Like Effector A	Cidea	Mm00432554_m1
Deiodinase, Iodothyronine, Type II	Dio2	Mm00515664_m1
Hypoxanthine Phosphoribosyltransferase	Hprt	Mm01545399_m1
Interleukin 6	Il6	Mm00446190_m1
Mannose Receptor, C Type 1	Mrc1	Mm00485148_m1
Nitric Oxide Synthase 2	Nos2	Mm00440502_m1
Nitric Oxide Synthase 3	Nos3	Mm00435217_m1
Peptidylprolyl Isomerase B	Ppib	Mm00478295_m1
Peroxisome Proliferator Activated Receptor Delta	Ppard	Mm00803184_m1
Peroxisome Proliferator Activated Receptor Gamma	Pparg	Mm01184322_m1
Peroxisome Proliferator Activated Receptor Gamma Coactivator 1	Pgc-1 $\alpha$	Mm01208835_m1
PPARG Coactivator 1 Beta	Pgc-1 $\beta$	Mm00504720_m1
Tumor Necrosis Factor	Tnf	Mm00443258_m1
Uncoupling Protein 1	Ucp1	Mm01244861_m1

**Table 4: List of primer sequences for qPCR analysis (murine targets)**

Abbreviation	Forward primer (5'-3')	Reverse primer (5'-3')
Adipoq	GGTCCTAAGGGTGAGACAGG	AGTCCCGGAATGTTGCAGTA
Adrb3	TGCTAGCATCGAGACCTTGT	GCATGTTGGAGGCAAAGGAA
Arg1	CTGAGCTTTGATGTCGACGG	TCCTCTGCTGTCTTCCCAAG
Cidea	AATGGACACCGGGTAGTAAGT	CAGCCTGTATAGGTCGAAGGT
Cox4i1	CTAGAGGGACAGGGACACAC	TGGTTCATCTCTGCGAAGGT
Cycs	GTTTCAGAAGTGTGCCAGTG	GTCTGCCCTTTCTCCCTTCT
Emr1	GAAGCATCCGAGACACACAC	TTGTGGTTCTGAACAGCACG
Fabp4	CAGCGTAAATGGGGATTTGG	CCGCCATCTAGGGTTATGAT
Fasn	AGAGATCCCGAGACGCTTCT	GCTTGGTCCTTTGAAGTCGAAGA
Hprt	AAGCTTGCTGGTGAAAAGGA	TTGCGCTCATCTTAGGCTTT
Il1b	ACTCATTGTGGCTGTGGAGA	TTGTTTCATCTCGGAGCCTGT

<i>Il4ra</i>	TCCAGACAACCTCACACTCC	TCAGCCTGGGTTCCCTGTAG
<i>Mgl2</i>	TGGAGAGCACAGTGGAGAAG	CGGCAGTACTTGTGAGCTTC
<i>Mrc1</i>	TGGATGGATGGGAGCAAAGT	GCTGCTGTTATGTCTCTGGC
<i>Nos2</i>	CCCCGCTACTACTCCATCAG	CCACTGACACTTCGCACAAA
<i>p62 WT</i>	CCAGTGATGAGGAGCTGACA	CCGTTGCAACCATCACAGAT
<i>p62<sup>Δ69-251</sup></i>	CACTACCGCGGCATTGAG	AGGTTTGCTGACTTCCGAAG
<i>Pgc-1α</i>	AGCCGTGACCACTGACAACGAG	GCTGCATGGTTCTGAGTGCTAAG
<i>Pparg</i>	TCGCTGATGCACTGCCTATG	GAGAGGTCCACAGAGCTGATT
<i>Ppib</i>	GCATCTATGGTGAGCGCTTC	CTCCACCTTCCGTACCACAT
<i>Prdm16</i>	CCGCTGTGATGAGTGTGATG	GGACGATCATGTGTTGCTCC
<i>Retnla</i>	CCCAGGATGCCAACTTTGAA	AGTAGCAGTCATCCCAGCAG
<i>Ucp1</i>	GGCCTCTACGACTCAGTCCA	TAAGCCGGCTGAGATCTTGT

*Adipoq* (Adiponectin), *Adrb3* (Adrenoreceptor Beta 3), *Arg1* (Arginase 1), *Cidea* (Cell Death-Inducing DFFA-Like Effector A), *Cox4i1* (Cytochrome C Oxidase Subunit 4), *Cyts* (Cytochrome C), *Emr1* (Adhesion G protein-coupled receptor E1), *Fabp4* (Fatty Acid Binding Protein 4), *Fasn* (Fatty Acid Synthase), *Hprt* (Hypoxanthine Phosphoribosyltransferase), *Il1b* (Interleukin 1 Beta), *Il4ra* (Interleukin 4 Receptor Subunit Alpha), *Mgl2* (C-Type Lectin Domain Family 10 Member A), *Mrc1* (Mannose Receptor, C Type 1), *Nos2* (Nitric Oxide Synthase 2), *p62 WT* (Sequestosome 1, WT (AA69-251)), *p62<sup>Δ69-251</sup>* (Sequestosome 1, p62<sup>Δ69-251</sup>), *Pgc-1α* (Peroxisome Proliferator-Activated Receptor Gamma Coactivator 1), *Pparg* (Peroxisome Proliferator Activated Receptor Gamma), *Ppib* (Peptidylprolyl Isomerase B), *Prdm16* (PR Domain Zinc Finger Protein 16), *Retnla* (Resistin Like Beta), *Ucp1* (Uncoupling Protein 1)

### 3.1 Animal experiments

#### 3.1.1 General experimental approaches for *in vivo* studies

For the *in vivo* studies, mice were randomized into the treatment groups based upon body weight and body composition (fat and lean tissue mass) and group sizes of 7-8 mice were preferentially used, which was determined from previous experiments where we determined this to be optimal for *in vivo* evaluation. All experiments were conducted with male animals.

#### 3.1.2 Housing and diets

All mice were housed in individual ventilated cages at an ambient temperature 23°C with constant humidity and a 12-hour light/12-hour dark cycle. For thermoneutrality studies, mice were kept in a separate animal housing room with an ambient temperature of 30°C. Housing of mice at other temperatures (30°C, 20°C, 10°C or 5°C) was conducted in temperature-controllable metabolic chambers. Mice had free access to water and were fed with either regular chow diet (Altromin GmbH) or a high fat diet (58% kcal fat; Research Diets Inc.). For the *in vivo* studies, mice were randomized into the treatment groups based upon body weight and body composition (fat and lean tissue mass).

#### 3.1.3 Mice

All animal procedures were approved by the local authorities of the Regierungspräsidium Tübingen or the regional animal welfare committee of the state of Bavaria.

*Il4ra<sup>-/-</sup>* mice (C57Bl6/J background) were kindly provided by Prof. Dr. Brombacher (Mohrs et al., 1999).

Mice that globally lack p62 (p62<sup>-/-</sup> mice) were kindly provided by Prof. Dr. J. Moscat. Mice genetically deficient for p62 were generated through deletion of exon 1 of p62 (Duran et al., 2004). The Cre-lox system was used to generate tissue specific knock out of p62 in the adipose tissue. Therefore the coding exon 1 of the p62 was deleted by mating p62 floxed mice with mice expressing Cre recombinase under the control of a promoter for adipocyte protein 2 (aP2) (Ap2 p62<sup>-/-</sup> mice) (Muller et al., 2013).

Mice that lack AA 69-251 of p62 (p62<sup>Δ69-251</sup>) were generated and provided by Prof. Dr. A. Gessner. To obtain partial deletion of p62, the coding exons 2, 3 and 4 of the p62 gene were replaced by a neomycin resistance cassette in embryonic stem cells (Bürgis, 2006, Hillmann, 2011).

### 3.1.4 Genotyping

For genotyping, DNA was extracted from ear punches with a genomic DNA extraction Kit from Favorgen. 1 µl of this DNA was used as template for the genotyping PCR.

#### 1. Genotyping PCR protocol for p62<sup>-/-</sup> mice:

Two separate PCRs were performed with either a WT (*Primer 1+2*) or KO (*Primer 1+3*) primer pair. Primers were produced by Sigma.

*Primer 1:* GGGGGCTACTACCGGGGACATTA

*Primer 2:* CGACCCCACTGCCTACTCTTTTC

*Primer 3:* CTTGGGTGGAGAGGCTATTC

The PCR reaction mix contained 0.15 µl GoTaq Flexi DNA polymerase (Promega), 5X buffer, 2.5 µl Betaine (Sigma), 2 mM MgCl<sub>2</sub>, 0.8 µM of each primer and 400 µM dNTP in 11.5 µl volume (in H<sub>2</sub>O). 11.5 µl of the PCR reaction mix was added to the DNA template and PCR was conducted as described in Table 5.

**Table 5: PCR program for genotyping of p62<sup>-/-</sup> mice**

Step	Temperature (°C)	Duration	Cycles
Initiation	94	4 min	x 35
Denaturation	94	30 sec	
Primer annealing	53	30 sec	
Elongation	72	45 sec	
Final elongation	72	10 min	

PCR products were separated in a 1.5% agarose gel (Agarose Biozym was dissolved in TAE buffer containing 5µl/200ml PeqGreen dye (Peqlab)). WT mice revealed a PCR product of 300bp whereas a 1400bp product was detected in p62<sup>-/-</sup> mice and heterozygous mice showed both products.

## 2. Genotyping PCR protocol for Ap2 p62<sup>-/-</sup> mice:

*Primer 1:* CTAGGCCACAGAATTGAAAGATC

*Primer 2:* GTAGGTGGAAATTCTAGCATCAT

*Primer 3:* GCGGTCTGGCAGTAAAACTATC

*Primer 4:* GTGAAACAGCATTGCTGTCACTT

First Ap2 p62<sup>-/-</sup> mice were tested for p62 gene deletion as described in PCR protocol for p62<sup>-/-</sup> mice, followed by CRE recombinase PCR. 2 µl of DNA and 23µl of reaction mix were used for CRE PCR. The reaction mix contained 0.3 µl GoTaq Flexi DNA polymerase (Promega), 5X buffer, 5 µl Betaine (Sigma), 1 mM MgCl<sub>2</sub>, 0.5 µM of each primer (*Primer 1-4*) and 200 µM dNTP in 23 µl volume (in H<sub>2</sub>O). CRE PCR was conducted as described in Table 6. A 100 bp PCR product was detected in CRE-positive mice, however CRE-negative mice reveal a control fragment at a size of 324 bp.

**Table 6: PCR program for genotyping of CRE recombinase**

Step	Temperature (°C)	Duration	Cycles
Initiation	94	3 min	x 36
Denaturation	94	45 sec	
Primer annealing	60	45 sec	
Elongation	72	1 min	
Final elongation	72	2 min	

## 3. Genotyping PCR protocol for p62<sup>Δ69-251</sup> mice:

p62<sup>Δ69-251</sup> mice were genotyped by two separate, WT (*Primer 1+2*) and KO (*Primer 3+4*), PCRs.

*Primer 1:* AATCCGGGGCTTCCTTCCTG

*Primer 2:* GCCCTTCCCCTCGCACACG

*Primer 3:* TCAGGAAATTGACATTGGGATCTT

*Primer 4:* AACAACTTAGATGGAGCCTGAATG

The PCR reaction mix contained 0.25 µl GoTaq Flexi DNA polymerase (Promega), 5X buffer, 2.5 µl Betaine (Sigma), 2 mM MgCl<sub>2</sub>, 0.8 µM of each primer and 400 µM dNTP in 11.5 µl

volume (in H<sub>2</sub>O). 11.5 µl of the PCR reaction mix was added to the DNA template and PCR was conducted as described in Table 7. WT mice revealed a PCR product of 347 bp whereas a 700 bp product was detected in p62<sup>Δ69-251</sup> mice.

**Table 7: PCR program for genotyping of p62<sup>Δ69-251</sup> mice**

Step	Temperature (°C)	Duration	Cycles
Initiation	94	5 min	x 35
Denaturation	94	1 min	
Primer annealing	60	1.5 min	
Elongation	72	2 min	
Final elongation	72	5 min	

### 3.1.5 Analysis of mouse metabolic phenotypes

For phenotyping studies, WT and KO mice, obtained from heterozygous (HET) breeding, were mated in homozygous WT/WT and KO/KO breeding pairs. For metabolic phenotyping 3-months-old mice were single- or double-housed and body weight and food intake was measured once a week until they reached an age of 30-weeks. Food intake was registered in single-housed mice by manually weighing food-hopper contents. Body composition (fat and lean mass) was measured using nuclear magnetic resonance technology (EchoMRI). Therefore each mouse was restrained in a tube for 60 seconds during the measurement.

### 3.1.6 Intraperitoneal glucose tolerance test

The mice were fasted for 6 hours in the morning, with free access to water, and body weight of the mice was recorded. Blood glucose was sampled from the tail vein and analyzed with a glucometer (FreeStyle Lite). Basal blood glucose was recorded and subsequently glucose concentrations were measured at 15, 30, 60 and 120 min after intraperitoneal (i.p.) injection of glucose (1.75 g/kg BW, dissolved in saline). The injection volume depends on the individual body weight and 5 µl per g body weight of glucose were injected. For analysis the average of repeated measurements were calculated and the area under the curve (AUC) was calculated from the individual glucose excursion curves.

### 3.1.7 Indirect calorimetry

Energy expenditure was measured using climate-controlled cabinets, which allows to simultaneously measure various metabolic parameters, such as food/water intake, substrate utilization and locomotor activity (TSE PhenoMaster, TSE Systems, Bad Homburg, Germany).

Body composition was analyzed using a magnetic resonance whole-body composition analyzer (EchoMRI) before and after indirect calorimetry. Mice were single-housed,



acclimatized for 24 hours prior to the measurement and genotypes or different groups were alternately arranged within the cabinets to guarantee equal exposure to potential technical issues of the system. The health status of the mice was daily monitored. Data for energy expenditure were analyzed using analysis of covariance (ANCOVA) with body weight as co-variant as previously described (Tschop et al., 2011).

### 3.1.8 IL-4 pharmacology studies

To assess the effect of IL-4 on energy expenditure, mice were treated daily for 12 consecutive days via intraperitoneal administration of either vehicle (0.9% saline, Braun, Melsungen, Germany) or recombinant murine IL-4 (50 µg/kg; Peprotech, Rocky Hill, NJ). Mice were acclimatized to the metabolic chambers for 24 hours prior to start of the measurement. Prior to study Day 9, mice were kept at thermoneutrality (30°C) and then switched for 24 hours to 20°C followed by 24 hours at 10°C and 24 hours at 4°C. Mice were then sacrificed for subsequent tissue analysis and catecholamine quantification. Time between the last injection of IL-4 and sacrifice was 24 h.

### 3.1.9 Positron emission tomography and magnetic resonance imaging

PET-CT imaging of p62<sup>A69-251</sup> mice was performed in the Werner Siemens Imaging Center of the University Tübingen in collaboration with Dr. M. Kneilling.

Awake animals were injected intraperitoneally with  $11.7 \pm 0.3$  MBq <sup>18</sup>F-FDG in sterile saline. <sup>18</sup>F-FDG was prepared according to (Hamacher et al., 1986). Animals were kept awake and allowed to freely move in their home cages during <sup>18</sup>F-FDG uptake for 30 min. Directly ensuing, mice were euthanized with CO<sub>2</sub>. Static PET acquisitions (10 min) were performed using a dedicated micro-PET scanner (DPET, Siemens Preclinical Solutions, Knoxville, USA). The spatial resolution was 1.4 mm (center of field of view), the axial field of view was 12.7 cm (Bao et al., 2009). All PET-scans were acquired with an energy window of 350 – 650 keV and a coincidence timing window of 3.432 ns. All major corrections were applied to the PET scans (e.g., normalization, decay & deadtime correction), but no attenuation correction was used as only mice on thin plastic beds were scanned. PET-images were reconstructed using the three-dimensional ordered-subset-expectation-maximization (OSEM3D) algorithm with a 128 x 128 matrix and a final pixel size of 0.79 x 0.79 x 0.80 mm<sup>3</sup>.

Animals were transferred on-bed to a 7 Tesla small animal MRI scanner (Clinscan or BioSpec with ParaVision 6.01, Bruker Biospin, Ettlingen, Germany) to ensure identical mouse positioning on-bed for PET and MRI acquisitions. T<sub>2</sub>-weighted anatomical MR-images were acquired using the following 3D-spoiled turbo spin echo sequence: matrix size: 256 x 256, FOV: 35 x 57 mm<sup>2</sup>, repetition time = 800 msec, echo time = 30.8 msec, slice thickness = 0.25 mm, flip angle 90°, echo train length 16.

### 3.1.10 Infrared thermography

Thermal imaging was applied to determine the skin surface temperature of mice. To avoid effects of fur removal on the thermal conductance, 7-day old pups were short-term seated in a 6-well dish for temperature record via a thermal imaging camera Optris, OPTPI400 (Ekomeß, Heilbronn, Germany). To ensure that pups of each genotype were equally long-exposed to the environmental temperature, they were alternately placed into the dish. A video of 6x WT and 6x KO mice was recorded and the hottest spot within a defined region over each mouse was determined in a temperature time diagram. The average over 2 min (27 pictures per sec) was calculated to determine surface temperature.

### 3.1.11 Bomb calorimetry

In collaboration with Prof. Dr. M. Klingenspor, the energy content of food and dried feces was calculated using a bomb calorimeter.

Feces samples, from single or double housed mice that were kept on chow diet at 30°C, were collected (for 5 days) and dried in a drying oven (50°C) for bomb calorimetric combustion. Food intake was measured during this 5 days period to convert food uptake to assimilated energy. Chow control diet was combusted to calculate energy content of the absorbed food. Dried feces were homogenized using a TissueLyser and 1 g of feces was pelletized. Each pellet was completely burned under high oxygen pressure (30 bar) using a 6300 Oxygen Bomb Calorimeter (Parr Instrument Technology, IL, USA).

Energy intake ( $E_{in}$ ) and energy excretion ( $E_{out}$ ) were calculated based on caloric intake and feces production. Assimilated energy is defined as the difference between the amount of consumed energy ( $E_{in}$ ) and the energy that is lost with feces ( $E_{out}$ ).

## 3.2 Molecular biological analysis

### 3.2.1 Tissue dissection

Tissues were dissected immediately after euthanasia of mice via carbon dioxide, frozen in dry ice and stored at -80°C until use. For immunohistochemistry tissues were fixed in 4% paraformaldehyde for further analysis.

### 3.2.2 RNA isolation from tissue and cells

Total RNA from tissue was extracted using RNeasy Lipid Mini Kit (Qiagen) according to manufacturer's instructions. Total RNA was isolated from cell lysates using RNeasy Mini Kit (Qiagen).

### 3.2.3 Reverse Transcription

cDNA synthesis was performed with QuantiTect Reverse Transcription Kit (Qiagen, Hilden, Germany) according to manufacturer's instructions.

### 3.2.4 Quantitative real-time polymerase chain reaction

Gene expression of cell samples ( $n = 3$  per group) was profiled with quantitative PCR-based (qPCR) techniques using SYBR green or TaqMan Single Probes (Thermo Fisher Scientific, Erlangen, Germany). The relative expression of the selected genes was measured using the 7900HT Fast Real-Time PCR System (Thermo Fisher Scientific, Erlangen, Germany). The relative expression levels of each gene were normalized to the housekeeping gene peptidylprolyl isomerase B (*Ppib*) or Hypoxanthine Phosphoribosyltransferase (*Hprt*). Primer sequences and accession number of Taqman probes are available (Table 3,4).

### 3.2.5 Low Density Array

TaqMan Low Density Array (Thermo Fisher Scientific, Erlangen, Germany) was performed according to instructions. Accession codes of Taqman probes are available (Table 3).

### 3.2.6 Protein isolation and Western blot analysis

Fat tissues were lysed in ice-cold RIPA buffer (Sigma Aldrich) containing 1 mM PMSF (Carl Roth), 10 nM Calyculin A (Cell signaling) and protease/phosphatase inhibitor (Thermo Fisher Scientific) using a polytron. Lysates were chilled on ice for 20 min and centrifuged for 15 min, 10,000 g, at 4°C. The supernatant was collected and protein concentration using a bicinchoninic acid (BCA) protein quantification kit (Thermo Scientific). Samples were boiled in 4x Laemmli loading buffer (Thermo Scientific) containing 50mM dithiothreitol (DTT) for 10 min at 95°C. Proteins were separated on a Criterion gel (Bio-Rad) and transferred on to nitrocellulose membranes. Membranes were blocked in Roti block solution (Carl Roth) for 1 h at room temperature and incubated with primary antibody (Cell Signaling) overnight at 4°C. HRP-coupled secondary antibody (Santa Cruz) was utilized to detect protein signal via the LI-COR imaging system. Membranes were washed between and after the antibody incubation steps with TBS-T for 3 times, 10 min each. Membranes were stripped using 0.2M NaOH for 10 min. Antibodies were purchased from Cell signaling (Phospho-HSL (Ser660) #4126, HSL #4107), Santa Cruz (Gapdh G-9, #365062) and Abcam (UCP1, #23841).

For protein isolation from cells, cells were scraped in ice cold Ripa buffer containing 1 mM PMSF (Carl Roth), 10 nM Calyculin A (Cell signaling) and protease/phosphatase inhibitor (Thermo Fisher Scientific) and samples chilled on ice for 20 min. Lysates were centrifuged

for 15 min, 10,000 g, at 4°C, the protein supernatant was collected and protein concentration was determined as described above.

Gapdh was used as a loading control. Data were analyzed relative to total protein and/or Gapdh using ImageJ for protein quantification.

### 3.2.7 Nuclear and cytosolic protein extraction from BAT tissue

For nuclear and cytosolic protein extraction BAT tissue from 3-4-week-old WT and p62<sup>Δ69-251</sup> mice or 3 months old WT and p62<sup>-/-</sup> mice were dissected freshly and immediately further proceeded using the NE-PER Nuclear and Cytoplasmic Extraction Reagent (Thermo Fisher Scientific, Erlangen, Germany) according to instructions. Protein fractions were further processed as described in section 3.2.6.

### 3.2.8 Cytochrome C Oxidase activity measurement

Cytochrome C Oxidase (Cox) activity was measured by Dr. S. Keipert (Division of Mitochondria, Helmholtz Zentrum München, IDO). Cox activity of interscapular BAT was assessed polarographically using a Clark type electrode (RANK Brothers) and a Powerlab for data processing (ADInstruments). Tissue was weighted and homogenized mechanically in tissue buffer (100mM potassium phosphate, 2mM EDTA, 10mM glutathione, pH 7.2, at 37°C) using QIAGEN TissueLyser. Homogenates were treated with detergent (0.1% *n*-dodecyl-β-D-maltoside) and subjected to a temperature-controlled reaction chamber containing 130μM cytochrome *c* from horse heart (Sigma Aldrich, Munich, Germany) and 18mM ascorbate in measuring buffer (100mM potassium phosphate, 5mM EDTA, pH 7.2, at 37°C).

### 3.2.9 Immunohistochemistry for UCP1

Immunohistochemistry for UCP1 was performed by L. Müller (Division of Molecular Pharmacology, Helmholtz Zentrum München, IDO). iWAT samples were dissected and subsequently fixed and stored in 4% paraformaldehyde. After dehydration, tissues were embedded in paraffin and cut in 5μm sections to perform immunohistochemistry using rabbit anti-UCP1 antibody (Abcam, Cambridge, MA). Therefore, samples were deparaffinized and microwaved in citrate buffer (pH 6) for antigen retrieval. To quench endogenous peroxidases samples were incubated with 3% hydrogen peroxide in methanol and then blocked with Avidin D, Biotin (Vectastain ABC Kit) (Vector Laboratories, Burlingame, CA) and normal goat serum (10%). UCP1 antibody (1:400) was added and incubated over night, before applying secondary rabbit antibody 1:300 (Vector Laboratories, Burlingame, CA). Vectastain ABC reagent was used followed by application of SIGMAFAST 3,3'-Diaminobenzidine (Sigma Aldrich, Munich, Germany) for signal development, and subsequent counterstaining with

hematoxylin and mounting. Finally, sections were analyzed using Microscope Scope A.1 (Zeiss).

### 3.2.10 Luciferase reporter assay

For luciferase reporter assay, the following plasmids were amplified using Qiagen plasmid Maxi Kit (Qiagen) according to manufacturer's instructions:

pCRE-Luc; pRL-TK; pcDNA3.MKK6dom+; pcDNA3.1-ATF2-HA; pcDNA3.1-C-DYK-p62wt; pcDNA3.1-C-DYK-p62 $\Delta$ 69-251; MigR1

Quality of each plasmid amplification was verified by control digestion with selected restriction enzyme and fragment size determination by gel electrophoretic separation.

For transfection, HEK cells were seeded one day prior to transfection to reach a confluence of 70-80% at the day of transfection. Plasmid DNA delivery was guaranteed by using Lipofectamine 2000 (ThermoFisher) as transfection reagent. Transfection was performed according to instructions of the Lipofectamine 2000 protocol using 0.25  $\mu$ g plasmid DNA (each construct) and 0.875  $\mu$ l Lipofectamine 2000 reagent in a total volume of 25  $\mu$ l Optimum medium (collagen-coated 96-well plate). Finally 12.5  $\mu$ l of DNA-Lipofectamine mix was added to HEK cells and incubated for 24 hours. ATF2 reporter assay was performed using the Dual-Glo Luciferase Assay (Promega), which allows normalization to transfection efficiency by simultaneous measurement of firefly and renilla luminescence. Therefore a renilla plasmid (pRL-TK) was routinely co-transfected to all samples except the non-transfected controls. To warrant equal DNA uptake of the cells, the DNA concentration was always adjusted to the highest content of plasmid DNA within an experiment with an empty vector (MigR1). Luciferase Assay was performed according to protocol and luminescence signal was measured using a PHERAstar plate reader.

### 3.2.11 Catecholamine measurement

Catecholamine analysis was examined in collaboration with J. Nagler and Prof. K.-W. Schramm (Molecular Exposomics, Helmholtz Zentrum München). For sample preparation: 100  $\mu$ l HClO<sub>4</sub> (0.3 M) and 4  $\mu$ l of internal standard (DHBA, 1 ng/  $\mu$ l) were added to the cell pellets. The mixture was ultra-sonicated under ice for 10 sec and transferred into an Amicon Ultra 0.5 mL (3 kDa) centrifugal filter unit (Merck Millipore, Darmstadt, Germany). The samples were then centrifuged at 13,000 rpm for 30 min at 1°C. The filtrate was transferred into a measurement vial and injected into the system.

The supernatant was thawed and 200  $\mu$ l were transferred into an Amicon Ultra 0.5 mL (3 kDa) centrifugal filter unit (Merck Millipore, Darmstadt, Germany). 4  $\mu$ l of internal standard (DHBA, 1 ng/ $\mu$ l) were added and the samples were centrifuged at 13,000 rpm for 30 min at 1°C. The filtrate was transferred into a measurement vial and injected into the system.

The BAT was thawed and 200  $\mu$ l of perchloric acid (0.3 M) and 4  $\mu$ l of internal standard (DHBA, 1 ng/ $\mu$ l) were added. The samples were homogenized by ultrasonication for 30 sec on ice. For this, they had to be in a 1.5-mL Eppendorf tube, as bigger tubes with their level lower end are not sufficient for the homogenization. Afterwards, the samples were centrifuged at 9,000 rpm for 10 min at 1°C. The residue was usually at the bottom of the tube, so that the supernatant could be directly transferred into a measurement vial and injected into the system. If the fat layer was on top, the solution had to be taken with a 1 mL syringe fitted with a cannula and filtered through a 0.2  $\mu$ m syringe filter (Whatman, Maidstone, United Kingdom) into the sample vial and was then injected into system.

Measurement of monoamines and metabolites: 20  $\mu$ l were injected into an Ultimate 3000 HPLC (high performance liquid chromatography) system from Thermo Fischer, consisting of an isocratic pump, an autosampler, and a coulometric Ultra Analytical Cell (6011 RS). The potential was set to 0.4 V with a data collection rate of 25 Hz. The separation of the compounds was carried out on a C<sub>18</sub>-column from Waters (Atlantis T3 100Å, 3  $\mu$ m, 4.6 mm X 150 mm), with a preceding security guard cartridge (Phenomenex, AJ0-4287). An isocratic elution with a commercially available mobile phase from RECIPE (1210, ClinRep® commercial HPLC) with 5.5% (v/v) added acetonitrile and a flow rate of 0.5 ml/min was used.

### 3.3 Cell culture

#### 3.3.1 Isolation of primary murine white and brown adipocytes

Preadipocytes, derived from the stromal vascular fraction of the adipose tissue, are *in vitro* differentiated to adipocytes and are herein called “primary cells”. The iWAT was obtained from 6-8 week-old male mice. Fat pads were minced and digested for 40 min at 37°C (1mg/ml Collagenase IV (Sigma Aldrich); 3U/ml Dispase II (Sigma Aldrich); 0,01mM CaCl<sub>2</sub> in PBS). Cell suspension was filtered through a 100 $\mu$ m cell strainer, centrifuged (500 x g for 10 min) and resuspended in growth medium DMEM/F12 (1:1) plus Glutamax (Thermo Fisher Scientific), 1% Pen/Strep and 10% FBS after each step. Homogenate was filtered through a 70  $\mu$ m cell strainer. Primary white adipocytes were plated onto collagen-coated dishes (Fisher Scientific) and grown to confluence (37°C, 10% CO<sub>2</sub>). At confluence, cells were exposed to the adipogenic cocktail containing dexamethasone (1  $\mu$ M), isobutylmethylxanthine (0.5 mM), rosiglitazone (1  $\mu$ M) and insulin (5  $\mu$ g/ml) in growth medium. After 48 h induction, cells were maintained in culture medium containing insulin (5  $\mu$ g/ml) and rosiglitazone (1  $\mu$ M). On day 4 of differentiation, cells were cultured in growth medium containing insulin (5  $\mu$ g/ml). To stimulate thermogenesis, cells were treated with 0.5  $\mu$ M isoproterenol (Sigma), dissolved in serum-free growth medium, for 6 hours on day 6 of adipocyte differentiation.

Primary brown adipocytes were isolated via the same procedure with the exception that 1mg/ml Collagenase II (Sigma) was used for digestion. For differentiation of primary brown adipocytes, the induction cocktail contains dexamethasone (5  $\mu$ M), isobutylmethylxanthine (0.5 mM), rosiglitazone (1  $\mu$ M), indomethacine (125  $\mu$ M), T3 (1 nM) and insulin (0.5  $\mu$ g/ml) in growth medium. 2 days post-induction of differentiation, cells were maintained in culture medium containing rosiglitazone (1  $\mu$ M), T3 (1 nM) and insulin (0.5  $\mu$ g/ml). On day 4 of differentiation, cells were cultured in growth medium containing T3 (1 nM) and insulin (0.5  $\mu$ g/ml).

### **3.3.2 Isolation of bone marrow-derived macrophages**

Bone marrow from the hind legs of 6-week-old C57Bl/6 or BALB/c mice was harvested, erythrocytes were lysed with ACK buffer (151 mM  $\text{NH}_4\text{Cl}$ , 10 mM  $\text{KHCO}_3$ , 0.2 mM EDTA in  $\text{H}_2\text{O}$ ) and the bone marrow was purified using Ficoll (GE Healthcare). Monocyte differentiation into macrophages was achieved by differentiation with DMEM medium containing 30% L929 supernatant, 20% FBS and 1% Pen/Strep for 5 d. BMDM polarization towards the M2 phenotype was accomplished by treatment with IL-4 (5, 10, 20 ng/ml, Peprotech) for 24 h.

### **3.3.3 Depletion of macrophages from primary iWAT cells**

Macrophages were separated from iWAT primary cells by magnetic immunoaffinity isolation using anti-CD11b antibodies conjugated to magnetic beads (MACS Cell Separation System; Miltenyi Biotec). Following iWAT isolation, CD11b-positive cells were separated using positive selection columns (LD columns; Miltenyi Biotec) according to manufacturer's instructions. For validation of cell separation, cell eluents were taken before and after depletion of CD11b-positive cells as well as from the retained cell fraction, bound to the conjugated beads. Successful depletion of macrophages was confirmed by flow cytometric and qPCR analysis.

### **3.3.4 Oil Red O staining**

Cells were fixed with 4% paraformaldehyde at differentiation Day 0, 3 or 6. Adipocytes were stained with Oil Red O (Sigma Aldrich, Munich, Germany) for 10 min and immediately washed with  $\text{H}_2\text{O}$ . Phase contrast microscopy was performed before and after Oil Red O staining with a Keyence BZ-9000 microscope. For lipid quantification, Oil Red O was retrieved from the cells by 100% isopropanol and absorbance was measured at 500 nm. Dapi signal was measured to correct for cell number.

### 3.3.5 Flow cytometry

Cell fractions of magnetic activated cell sorting (MACS) separation (CD11b<sup>+</sup>) were stained with APC-conjugated Emr1 (Anti-Mouse F4/80 Antigen APC, Affymetrix eBioscience, Frankfurt am Main, Germany) and FITC-conjugated CD45 (Anti-Mouse CD45 FITC, Affymetrix eBioscience, Frankfurt am Main, Germany), diluted 1:100 in fluorescence-activated cell sorting (FACS) buffer (BD Bioscience, Heidelberg, Germany) supplemented with 2 mM EDTA, 2% FBS and 0.1% sodium azide for 20 min at 4°C. Flow cytometry was performed on a FACS Aria III (BD Bioscience, Heidelberg, Germany), and results were analyzed using FACS Diva software (BD Bioscience, Heidelberg, Germany).

### 3.3.6 Bioenergetic analysis

Primary iWAT cells were isolated, macrophage-depleted and differentiated for 5 d on a collagen-coated XF96 well plate. On the day of the experiment (Day 5), cells were washed with DMEM XF Assay medium (Seahorse Bioscience), supplemented with 25 mM glucose, 10 mM pyruvate and 0.3% fatty-acid free BSA, and incubated in 180 µl of XF Assay medium in a non-CO<sub>2</sub> incubator at 37°C for 1 h. All port compounds were dissolved in pure DMEM XF Assay medium without supplements and 10-fold higher concentrated compounds were loaded into the ports of a XF Assay Cartridge. Oxygen consumption rate (OCR) was measured using an extracellular flux analyzer (XF96, Seahorse Bioscience). Basal OCR was recorded for 21 min followed by measurement of OCR after injection of isoproterenol (1 µM, 35 min), oligomycin (2 µg/ml, 21 min), carbonyl cyanide-p-trifluoromethoxyphenylhydrazone (FCCP) (1 µM, 21 min), rotenone (2.5 µM)/antimycin (2.5 µM)/2-Deoxyglucose (10 mM) (28 min). For normalization, the cell plate was subsequently co-stained with Dapi and Nile red and the fluorescence signal was detected to correct for cell number and differentiation.

### 3.4. Statistics

Statistical analyses were performed using statistical tools in GraphPad Prism. Differences between groups were assessed by 1-way or 2-way ANOVA followed by Bonferroni's *post-hoc* test or Student's 2-tailed t-test. All results are given as mean ± s.e.m. P<0.05 was considered statistically significant.



### 3.5. Contributions from Collaborations

In the 21<sup>st</sup> century, science has become progressively interdisciplinary, thus the expansion of global collaborations is a key driver to enhance research quality and efficiency. Collaborations enable scientists to gain knowledge through the diversity of experience, they allow access to hitherto inaccessible cutting-edge technologies and therefore can contribute to enhance the ambition and potential impact of research questions addressed.

Parts of the data in this thesis are the result of fruitful collaborations and thus contributors from numerous institutions must rightfully be acknowledged. Aiming to carefully detail out the contributions from collaboration partners and myself, I have, herein indexed every time external expertise added data presented. If not mentioned otherwise, experiments and analysis was conducted by myself (K. Fischer).

#### 1. Role of alternatively activated macrophages for BAT thermogenesis:

- Prof. Dr. Brombacher and Dr. Divanovic kindly provided *Ii4ra*<sup>-/-</sup> mice (ICGEB Cape Town and Cincinnati Children's Hospital)
- HPLC-based analysis of catecholamines was executed by J. Nagler in the group of Prof. Dr. Schramm (Helmholtz Zentrum München, MEX)

#### 2. Role of the scaffold protein p62 for BAT thermogenesis:

- Prof. Dr. Gessner kindly provided p62<sup>Δ69-251</sup> mice (Universität Regensburg)
- Prof. Dr. Moscat/ Prof. Dr. Diaz-Meco kindly provided p62<sup>-/-</sup> mice (Sanford Burnham Prebys)
- COX activity was measured by Dr. S. Keipert in the group of Dr. Jastroch (Helmholtz Zentrum München, IDO)
- Bomb calorimetric analysis was performed together with S. Mocek in the group of Prof. Dr. Klingenspor (TUM)
- PET-CT/MRT study was performed together with the group of Dr. Kneiling (Universität Tübingen)

## 4. Results

### Part I

#### 4.1 Role of alternatively activated macrophages in BAT thermogenesis

Beyond the traditional view of BAT thermogenic activation via the SNS, there has recently been postulated a SNS-independent alternative pathway controlling BAT thermogenesis. A paradigm shift was thus the report that alternatively activated macrophages locally produce catecholamines in the BAT to adjust thermogenesis (Nguyen et al., 2011). This indicates that the hematopoietic system might contribute relevant control over BAT thermogenesis, which, in turn, could turn out to be fundamental for potential new therapy options to treat obesity. Therefore, a detailed understanding of the molecular underpinnings of this biology is of utmost importance. In this thesis the role of alternatively activated macrophages in regulation of white, brown, brite adipocyte function *in vitro* and *in vivo* as well as their capability to produce catecholamines was in depth examined.

##### 4.1.1 Effect of macrophage depletion on adipocyte function

To evaluate a possible role of macrophages in thermogenic regulation *in vitro*, primary preadipocytes from iWAT were isolated and macrophages were depleted from the stromal vascular fraction (SVF) by magnetic activated cell sorting (MACS) of CD11b-positive cells, followed by culturing and differentiation of preadipocytes into mature adipocytes. Successful macrophage depletion was confirmed by fluorescence-activated cell sorting (FACS) analysis showing that CD45<sup>+</sup> F4/80<sup>+</sup> cells, present before the sorting (pre-sort), were not detected in the flow-through after MACS sorting (post-sort) (Fig. 4A). To elute retained macrophages, the column was removed from the magnet; flow-through was collected and subsequently analyzed by FACS, hence identifying the obtained cells as CD45<sup>+</sup> F4/80<sup>+</sup> macrophages (Fig. 4A). Macrophage depletion was further confirmed by lack of *Itgam* (alias *CD11b*) and *Emr1* mRNA levels during adipocyte differentiation (Fig. 4B,C), demonstrating that macrophages do not reconstitute over the time of differentiation. In line with that, low density array analysis showed absence of M1 and M2 inflammation markers, such as *Tnf*, *Arg1*, *Mgl2*, *Mrc1* and *Ii10* in macrophage-depleted cells relative to WT controls (Fig. 4D,E).

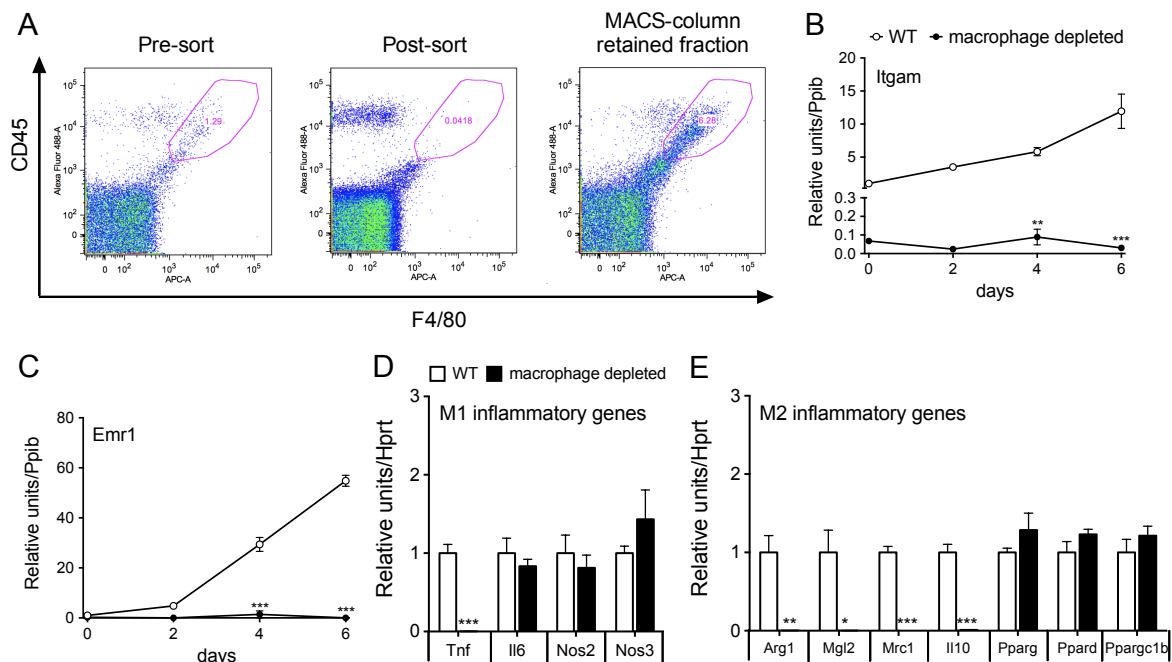


**Figure 4: Macrophage depletion in iWAT primary cells.**

Flow cytometric detection of macrophages in iWAT primary cells before and after MACS depletion of CD11b-positive cells. Macrophages were identified as CD45<sup>+</sup> F4/80<sup>+</sup> cells (A). Macrophage infiltration marker *Itgam* (B), *Emr1* (C), expression of genes related to M1 inflammation (*Tnf*, *Il6*, *Nos2*, *Nos3*) (D) and M2 inflammation (*Arg1*, *Mgl2*, *Mrc1*, *Il10*, *Pparg*, *Ppard*, *Ppargc1b*) (E) in WT or macrophage-depleted iWAT primary cells. Data are representative of three independently performed experiments, each performed in technical triplicates. Data represent mean  $\pm$  s.e.m ( $n = 3$ ). \* $P < 0.05$ ; \*\* $P < 0.01$ ; \*\*\* $P < 0.001$  based on 2-sided student's t test or 2-way ANOVA followed by Bonferroni post-hoc comparison of the individual time-points.

To test whether lipid accumulation was affected by the lack of macrophages, Oil Red O staining was assessed, showing no difference between WT and macrophage-depleted cells during differentiation, thus indicating that macrophages are dispensable for adipocyte differentiation (Fig. 5A,B). Consistent with this notion, expression profiles of markers indicative of adipocyte differentiation, such as *Fasn*, *Adipoq*, *Fabp4* and *Pparg* were not affected by the loss of macrophages (Fig. 5C-F). Likewise, no changes for gene programs indicative of fatty acid synthesis, fatty acid transport, cytokine signaling, lipoprotein metabolism, lipogenesis or lipolysis and carbohydrate metabolism were observed (Fig. 6).

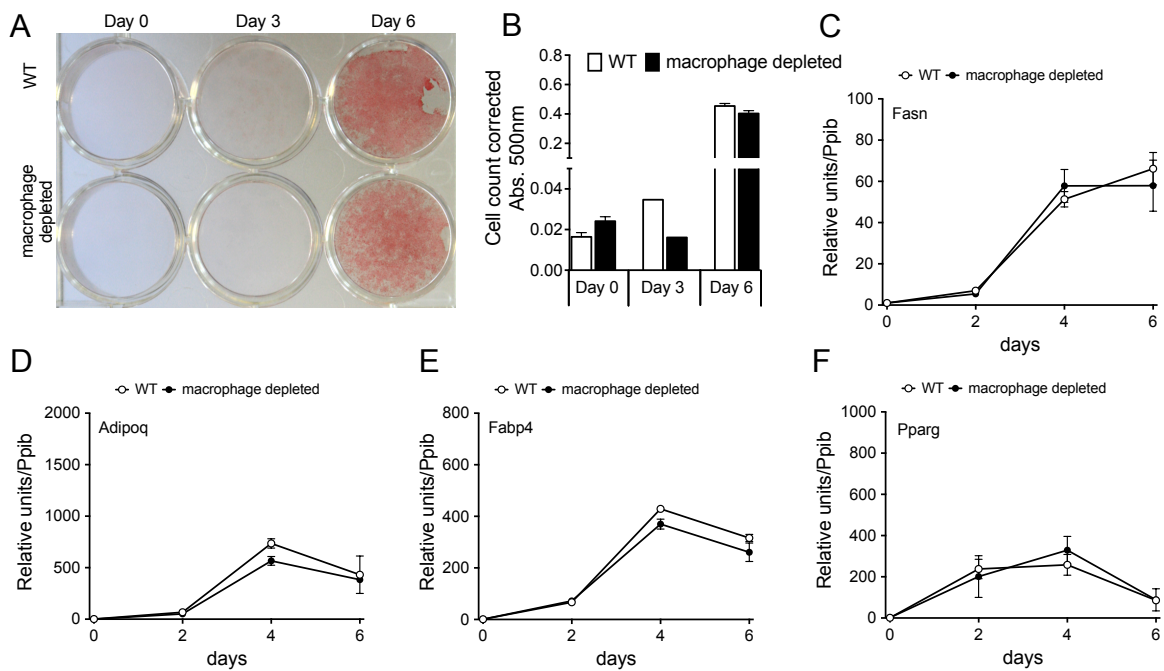


**Figure 5: Effect of macrophage depletion on adipocyte differentiation.**

Lipid accumulation measured by Oil Red O staining at different time points during adipocyte differentiation (A). Quantification of cell number corrected (Dapi staining) lipid accumulation (Oil Red O incorporation) after re-elution in isopropanol (B). Expression profile of markers indicative of white adipocyte differentiation (*Fasn*, *Adipoq*, *Fabp4*, *Pparg*) (C-F) in WT or macrophage-depleted iWAT primary cells. Data are representative of three independently performed experiments, each performed in technical triplicates. Data represent mean  $\pm$  s.e.m ( $n = 3$ ).

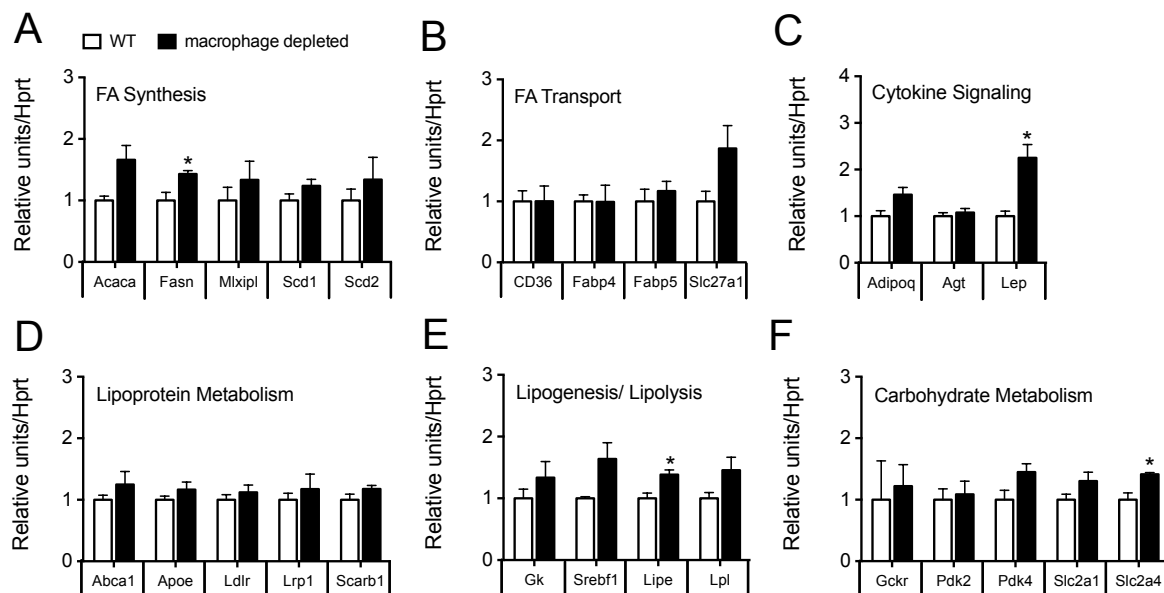


**Figure 6: Effect of macrophage depletion on key metabolic pathways in primary inguinal white adipocytes.**

Low Density Array analysis of WT and macrophage-depleted iWAT primary cells showed the expression profile of genes related to fatty acid synthesis (*Acaca*, *Fasn*, *Mlxipl*, *Scd1*, *Scd2*) (A), fatty acid transport (*CD36*, *Fabp4*, *Fabp5*, *Slc27a1*) (B), cytokine signaling (*Adipoq*, *Agt*, *Lep*) (C), lipoprotein metabolism (*Abca1*, *Apoe*, *Ldlr*, *Lrp1*, *Scarb1*) (D), lipogenesis (*Gk*, *Srebf1*), lipolysis (*Lipe*, *Lpl*) (E) and carbohydrate metabolism (*Gckr*, *Pdk2*, *Pdk4*, *Slc2a1*, *Slc2a4*) (F). Data are representative of three independently performed experiments, each performed in technical triplicates. Data represent means  $\pm$  s.e.m. Asterisks indicate: \*,  $p < 0.05$ ; \*\*,  $p < 0.01$  based on student's t test.

To further test if macrophages are implicated in the mitochondrial function of white adipocytes, expression of genes involved in electron transport were measured. No difference in *Cyts* and *Cox4i1* mRNA levels was detected during differentiation of WT and macrophage-depleted primary white adipocytes (Fig. 7A,B). Oxygen consumption was measured by Seahorse Technology to determine the effect of ATMs on cellular respiration. Of note, no changes in basal respiration, ATP-production, maximal respiration or non-mitochondrial respiration were observed in 5-day differentiated WT or macrophage-depleted iWAT primary cells, as assessed by treatment with isoproterenol (1  $\mu$ M), oligomycin (2  $\mu$ g/ml), carbonyl cyanide-4-(trifluoromethoxy)phenylhydrazone (FCCP) (1  $\mu$ M) or rotenone (2.5  $\mu$ M)/antimycin A (2.5  $\mu$ M)/2-deoxyglucose (10 mM) (Fig. 7C-E). Hence, it has been shown that mitochondrial function and cellular respiration of iWAT conducted normal after loss of macrophages.

Next it has been addressed whether depletion of macrophages impairs the capability of white adipocytes to beiging/browning. Key regulatory markers indicative of beiging/browning, such as *Ucp1*, *Pgc-1 $\alpha$*  and *Prdm16*, all increased over time during adipocyte differentiation but notably without any difference due to presence or absence of macrophages (Fig. 7F-H). Further, it was tested whether depletion of macrophages impairs the ability of isoproterenol to stimulate expression of *Ucp1* and *Pgc-1 $\alpha$*  in iWAT primary cells. Therefore, WT and macrophage-depleted iWAT primary cells were differentiated for 6 days and subsequently treated with 0.5  $\mu$ M isoproterenol for 6 hours. Consistent with the observation that no changes in *Ucp1*, *Pgc-1 $\alpha$*  gene expression were observed during differentiation, isoproterenol-induced stimulation of adipocytes did not affect mRNA levels of *Ucp1*, *Pgc-1 $\alpha$*  between WT and macrophage-free cells (Fig. 7I,J). Although the capability of both groups (WT and macrophage depleted) to accomplish beiging/browning was confirmed by increased levels of *Ucp1*, *Pgc-1 $\alpha$*  followed treatment with isoproterenol (Fig. 7I,J).

Unexpectedly, these data suggest that, at least, naïve adipose tissue macrophages do not contribute to differentiation, mitochondrial function and beiging/browning of white adipocytes.

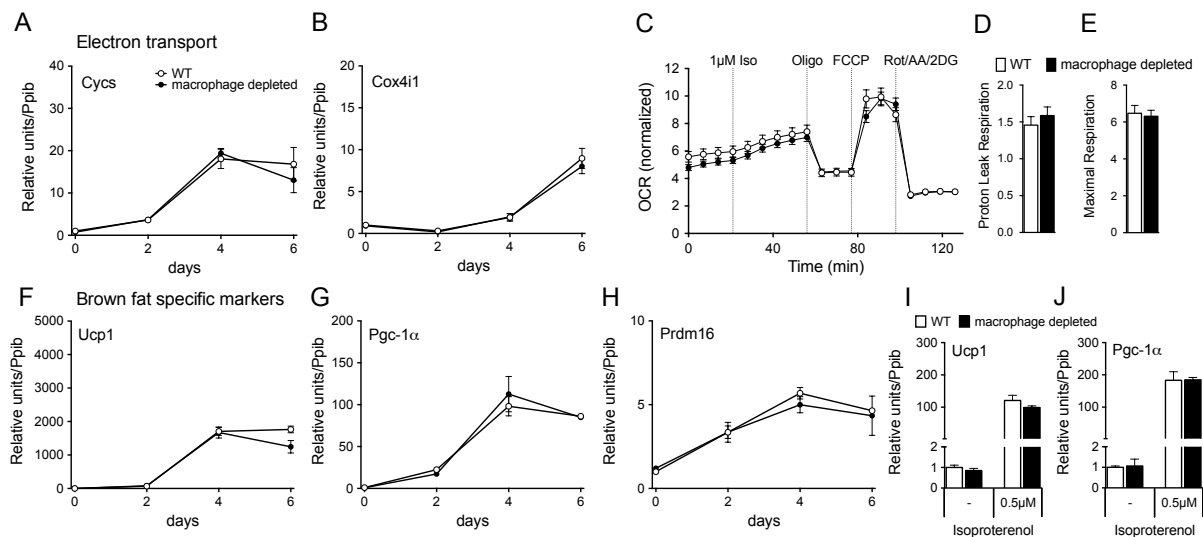


**Figure 7: Effect of macrophage depletion on mitochondrial function and beiging/browning.**

Expression levels of electron transport genes (*Cyts*, *Cox4i1*) in iWAT primary cells during adipocyte differentiation (A,B). Measurement of oxygen consumption rate (OCR), corrected for cell number (Dapi) of 6-d differentiated inguinal white adipocytes following treatment with isoproterenol (1 μM), oligomycin (2 μg/ml), FCCP (1 μM) and rotenone (2.5 μM)/antimycin A (2.5 μM)/2-Deoxyglucose (10 mM) (N). Proton Leak Respiration is calculated as the difference between ATP synthesis during blocked respiration (oligomycin) and non-mitochondrial respiration (O). Maximal Respiration is calculated as the difference between FCCP-induced respiration and non-mitochondrial respiration (P). Expression of brown fat-specific markers (*Ucp1*, *Pgc-1α*, *Prdm16*) (F-H) in iWAT primary cells during adipocyte differentiation. Expression levels of *Ucp1*, *Pgc1α* following stimulation with isoproterenol (0.5 μM) for 6 h in fully differentiated iWAT primary cells (I,J). Data in panel A,B, F-J are representative of three independently performed experiments, each performed in technical triplicates. Data in panel C-E are representative of two independently performed experiments, each performed with  $n = 23$  replicates per group. Data represent mean  $\pm$  s.e.m.

#### 4.1.2 Effect of alternatively activated macrophages on thermogenesis in primary adipocytes

To probe whether macrophages first need to undergo polarization in order to stimulate thermogenesis, two independent strategies were pursued. Therefore, either Raw264.7 cells or BMDMs were treated with recombinant IL-4 to activate the M2 phenotype and subsequently their impact on the thermogenic character of adipocytes was tested.

##### 4.1.2.1 IL-4 stimulation of Raw264.7 cell line

To first test whether M2-polarized Raw264.7 macrophages affect thermogenesis in BAT primary cells, M2-type macrophages were activated by treatment of Raw264.7 cells with different doses of murine, recombinant IL-4 (5 ng/ml, 10 ng/ml or 20 ng/ml) for 24 hours. After stimulation, polarization of the Raw264.7 cells was confirmed by increased expression of M2 macrophage markers *Arg1* and *Mrc1* in IL-4-treated cells as compared to vehicle control (Fig. 8A,B). Afterwards, primary adipocytes, isolated from the BAT of C57Bl/6J mice were differentiated for 6 days and treated with the supernatant of the 24-h stimulated Raw264.7 cells (conditioned media, CM) for 6 hours. Surprisingly, none of the different IL-4-dosed CM increased expression of *Ucp1* and *Pgc-1α* in primary brown adipocytes (Fig. 8C,D), disproving a role of alternatively activated Raw264.7 macrophages for activation of

BAT thermogenesis. Notably, isoproterenol treatment of BAT primary cells corroborated their functionality to become thermogenically active (Fig. 8C,D).

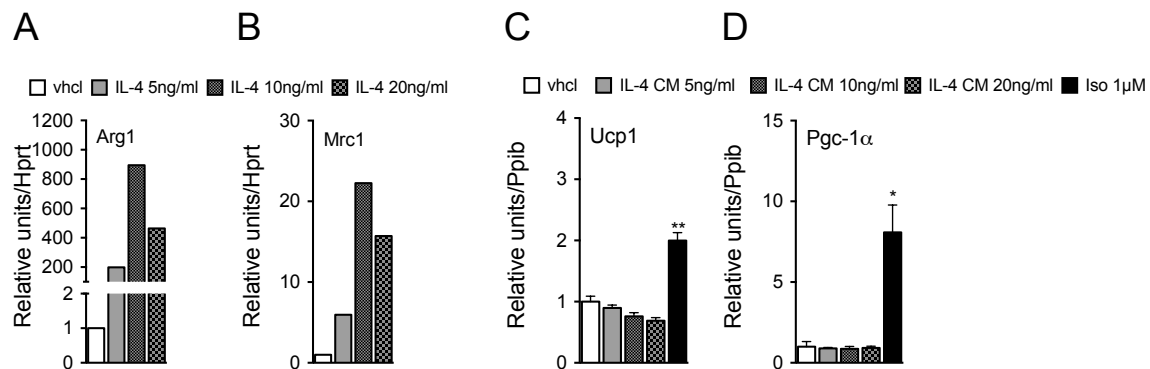


**Figure 8: Effect of alternatively activated macrophages from Raw264.7 cells on thermogenesis in primary BAT cells.**

Raw264.7 cells were polarized towards the M2 phenotype by 24-h stimulation with 5, 10 or 20 ng/ml recombinant IL-4. Primary brown adipocytes were isolated from  $n = 3$  6-8 week-old C57Bl/6J mice, pooled and individually differentiated for 6 days followed by 6-h treatment with conditioned media (CM) from the IL-4-treated Raw264.7 cells or isoproterenol (1  $\mu$ M) ( $n = 3$  technical replicates each treatment). Expression profile of M2 macrophage marker (*Arg1*, *Mrc1*) (A,B) in IL-4-treated Raw264.7 cells. Expression of thermogenic genes (*Ucp1*, *Pgc-1 $\alpha$* ) in CM or isoproterenol-treated BAT primary cells. Displayed results are representative of three independent experiments. Data represent mean  $\pm$  s.e.m. \* $P < 0.05$ ; \*\* $P < 0.01$  based on 1-way ANOVA followed by Bonferroni-multiple comparison test.

#### 4.1.2.2 IL-4 stimulation of bone marrow-derived macrophages

To further investigate the effect of alternatively activated macrophages on the thermogenic capacity of primary adipocytes in a biologically more relevant system than the Raw264.7 cell line, BMDMs were isolated from both C57Bl/6J and BALB/c mice and stimulated with different doses of IL-4 (5 ng/ml, 10 ng/ml or 20 ng/ml) for 24 hours. This thesis showed that 24-h treatment of BMDMs with IL-4, derived from different background strains, mediated increase of *Arg1*, *Mrc1* and *Mgl2* expression levels, confirming activation of M2 macrophages (Fig. 9A,B; Fig. 10A-C). Of note, stimulation of either iWAT or BAT primary cells, derived from BALB/c mice, with CM from IL-4-treated BMDMs did not affect expression of the thermogenesis marker *Ucp1* and *Pgc-1 $\alpha$*  compared to control (Fig. 10D-G). Markedly, this lack of effect on promoting beiging/browning of iWAT primary cells by IL-4-activated macrophages was observed independently of the background strain (C57Bl/6J or BALB/c) (Fig. 9C,D; Fig. 10.D,E). Thus catecholamines or other secreted factors released by IL-4-activated BMDMs do not affect beiging/browning and thermogenesis in primary adipocytes, which aligns with the observation using Raw264.7 cells.

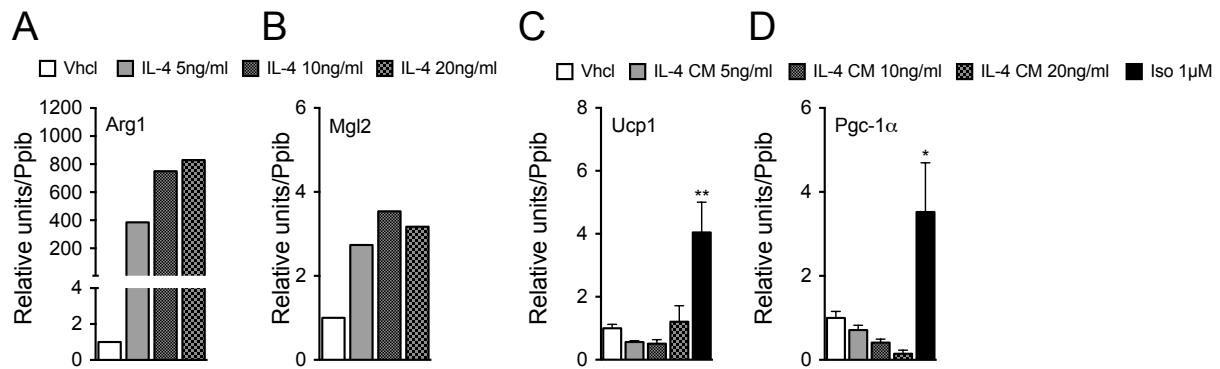


**Figure 9: Effect of alternatively activated macrophages from C57Bl/6J mice on thermogenesis in primary white adipocytes.**

Bone marrow-derived macrophages (BMDM) were isolated from C57Bl/6J mice and polarized towards the M2 phenotype by 24-h stimulation with 5, 10, or 20 ng/ml recombinant IL-4. Representative expression profile of M2 macrophage markers (*Arg1*, *Mgl2*) in activated BMDM cells (A-B). For primary cell experiments, adipocytes were harvested from  $n = 3-4$  mice, pooled and individually differentiated in triplicates (technical replicates) for 6 d followed by 6-h treatment with either conditioned media (CM) from IL-4 treated BMDM or isoproterenol ( $1 \mu\text{M}$ ). Gene expression of brown fat-specific markers (*Ucp1*, *Pgc-1a*) in IL-4 CM or isoproterenol-treated iWAT ( $n = 3$  technical replicates) (C,D) primary cells for 6 h. Displayed results display one performed experiment. Data represent mean  $\pm$  s.e.m. \* $P < 0.05$ ; \*\* $P < 0.01$ ; \*\*\* $P < 0.001$

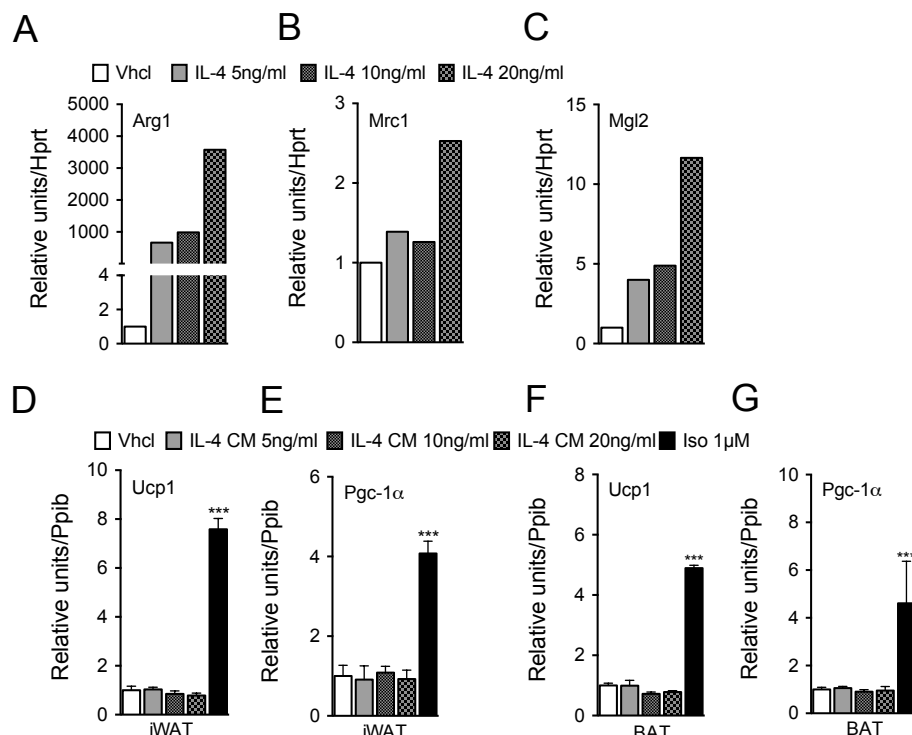


**Figure 10: Effect of alternatively activated macrophages from BALB/c mice on thermogenesis in primary inguinal white and brown adipocytes.**

Bone marrow-derived macrophages (BMDM) were isolated and polarized towards the M2 phenotype by 24-h stimulation with 5, 10, or 20 ng/ml recombinant IL-4. Representative expression profile of M2 macrophage markers (*Arg1*, *Mrc1*, *Mgl2*) in activated BMDM cells (A-C) (graph shows 1 out of 3 independently performed experiments). For primary cell experiments, adipocytes were harvested from  $n = 3-4$  mice, pooled and individually differentiated in triplicates (technical replicates) for 6 d followed by 6-h treatment with either conditioned media (CM) from IL-4 treated BMDM or isoproterenol ( $1 \mu\text{M}$ ). Gene expression of brown fat-specific markers (*Ucp1*, *Pgc-1a*) in IL-4 CM or isoproterenol-treated iWAT ( $n = 3$  technical replicates) (D,E) or BAT ( $n = 3$  technical replicates) (F,G) primary cells for 6 h. Displayed results are representative for three independently performed experiments, each performed with three technical replicates. Data represent mean  $\pm$  s.e.m. \* $P < 0.05$ ; \*\* $P < 0.01$ ; \*\*\* $P < 0.001$  based on 1-way ANOVA followed by Bonferroni-multiple comparison test.



### 4.1.3 Effect of alternatively activated macrophages on lipolysis in primary adipocytes

Based on the finding that alternatively activated macrophages effect lipolysis (Nguyen et al., 2011), one aim of this thesis was to evaluate whether phosphorylation of HSL, the key enzyme in the mobilization of FAs, is induced upon IL-4 stimulation. To test this hypothesis, iWAT and BAT primary cells were isolated, differentiated for 6 days and subsequently treated with CM from 24-h IL-4 (10 ng/ml)-treated BMDMs for different durations of 15 min, 1 h, 3 h or 6 h or isoproterenol for 15 min or 6 h. Isoproterenol-induced activation of the  $\beta$ -adrenergic pathway triggers phosphorylation of HSL already 15 min after administration, however IL-4 CM failed to activate HSL independent of the duration of IL-4 treatment (Fig. 11A,B). These data indicate that phosphorylation of HSL, as an indicator for lipolysis, is not regulated by IL-4 activated macrophages.

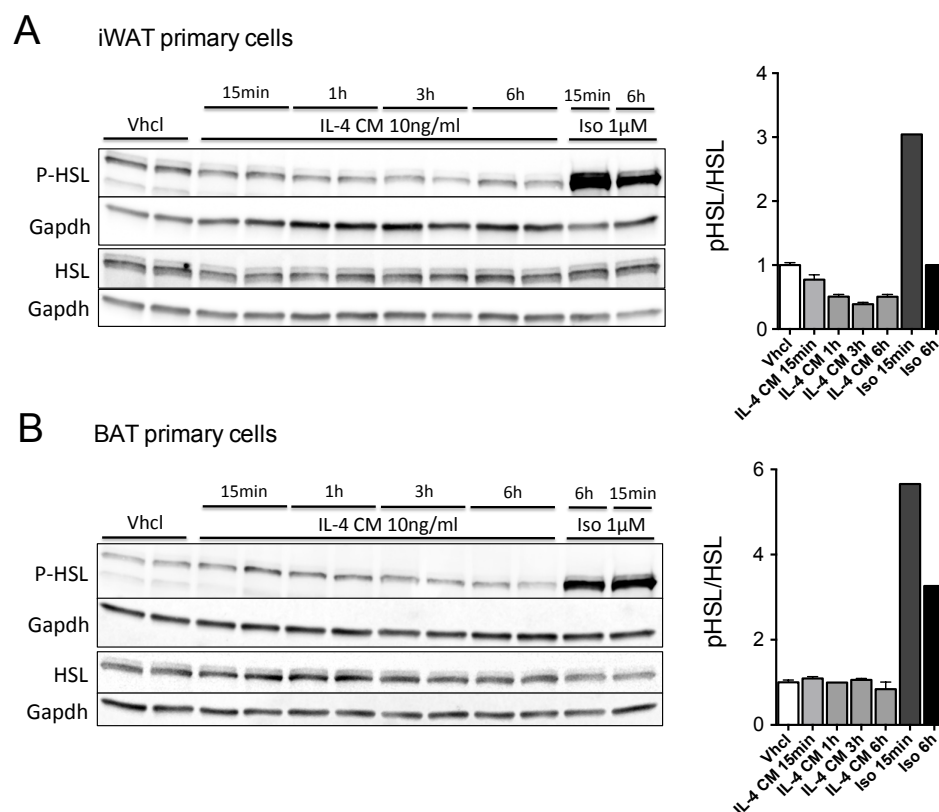


**Figure 11: Effect of alternatively activated macrophages on lipolysis in primary adipocytes.**

Bone marrow-derived macrophages (BMDM) of  $n = 3$  C57Bl/6J mice were isolated, pooled and polarized towards the M2 phenotype by 24-h stimulation with 10 ng/ml recombinant IL-4. Primary brown and white adipocytes were harvested from  $n = 3$  C57Bl/6J mice, pooled and individually differentiated for 6 d followed by varying incubation times with the conditioned medium (CM) of IL-4 treated BMDM (15 min, 30 min, 1 h, 3 h, 6 h) or isoproterenol (15 min, 6 h,  $n = 2$  technical replicates each treatment). Western blot analysis of phosphorylated and total HSL of iWAT (A) and BAT (B) primary cells. Data represent means  $\pm$  s.e.m.

### 4.1.4 Catecholamine production in alternatively activated macrophages

It has been shown that key enzymes relevant for catecholamine production, such as TH, dopa decarboxylase and dopamine  $\beta$ -hydroxylase, as well as secretion of norepinephrine, are induced in macrophages upon IL-4 treatment (Nguyen et al., 2011). Consistent with this

notion, reduced norepinephrine content in the adipose tissues in cold-exposed mice lacking IL-4 and IL-13 has been reported (Nguyen et al., 2011). Based on these findings, it is warranted to probe how catecholamine content changes in BMDMs and its supernatants upon IL-4 treatment. To directly test whether alternatively activated macrophages release catecholamines to sustain thermogenesis, absolute levels of different catecholamines were measured by HPLC-based analysis.

BMDMs were isolated from C57Bl/6J mice and stimulated with different doses of IL-4 (5 ng/ml, 10 ng/ml or 20 ng/ml) for 24 hours. HPLC analysis revealed no stimulatory effect of IL-4 at any tested dose on norepinephrine, epinephrine, 5-hydroxyindoleacetic acid, homovanillic acid, dopamine or 5-hydroxytryptamin (Fig. 12). While the amount of catecholamines is measurable by HPLC analysis, notably, the levels of catecholamines are borderline detectable and in particular IL-4 failed to induce catecholamine levels in both the supernatant (Fig. 12A-F), and within the macrophages themselves (Fig. 12G-L). These data suggest, that alternatively activated macrophages lack the ability to produce sufficient catecholamines to contribute in BAT thermogenesis.

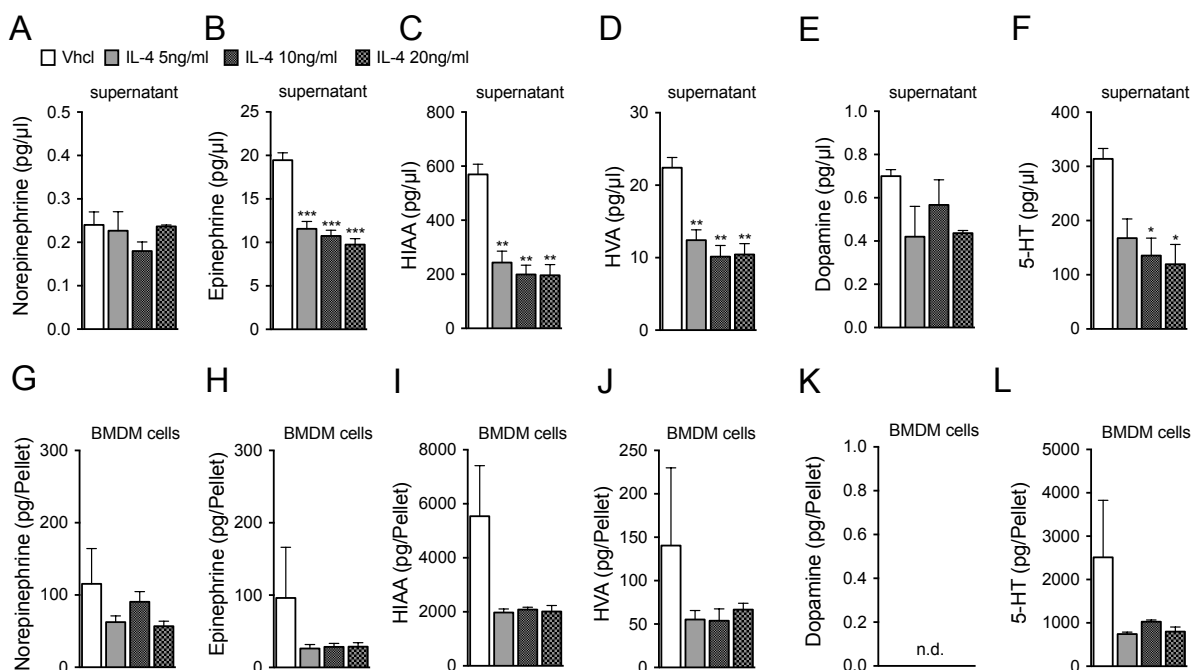


**Figure 12: Catecholamine production in bone marrow-derived macrophages.**

Bone marrow-derived macrophages (BMDM) were isolated and polarized towards the M2 phenotype by 24h stimulation with 5, 10, or 20 ng/ml recombinant IL-4. HPLC-based measurement of norepinephrine, epinephrine, 5-hydroxyindoleacetic acid (5-HIAA), homovanillic acid (HVA), dopamine and 5-hydroxytryptamin (5-HT) in supernatant (A-F) or cells (G-L) of vhcI or IL-4 treated BMDM ( $n = 3$  technical replicates per group). Data represent means  $\pm$  s.e.m. Asterisks indicate: \*,  $p < 0.05$ ; \*\*,  $p < 0.01$ ; \*\*\*,  $p < 0.001$  based on 1-way ANOVA followed by Bonferroni-multiple comparison test. Catecholamine measurement was performed by Joachim Nagler in the group of Prof. Dr. Schramm (Helmholtz Zentrum München, MEX).

#### 4.2.5 Effect of cold exposure on macrophage content in C57Bl/6J mice

Cold exposure powerfully induces beigeing/browning and thermogenic capacity of adipose tissue. Assuming that M2-type macrophages contribute to activation of BAT thermogenesis, one could argue that their content would increase upon cold exposure as previously shown by increased gene expression of *Arg1*, *Mrc1*, *Mgl2* in iWAT and BAT of cold-exposed mice (Nguyen et al., 2011). To confirm or reject these findings, C57Bl/6J WT mice were exposed to cold (4°C) for 6 hours and the BAT was dissected for subsequent tissue analysis. Cold exposure led to higher mRNA levels of *Ucp1* and *Pgc-1 $\alpha$*  as compared to room temperature (22°C) controls (Fig. 13A,B). Notably, lower expression of markers indicative of M1 and M2 polarization, such as *Nos2*, *Arg1* and *Mrc1* were found in cold-exposed BAT relative to controls (Fig. 13C,D). HPLC analysis of catecholamines revealed higher absolute levels of dopamine, 3,4-dihydroxyphenylacetic acid, 3-methoxytyramine and homovanillic acid in BAT of cold-exposed mice relative to mice held at room temperature (22°C) (Fig. 13E-H). BAT levels of NE and epinephrine were reduced in the cold-exposed mice relative to controls, likely reflecting enhanced NE turnover during cold stimulation (Fig. 13I,J). Taken together, these data demonstrate that cold exposure does not increase either M1 or M2 macrophage content within the BAT, thus rejecting the previous findings (Nguyen et al., 2011).

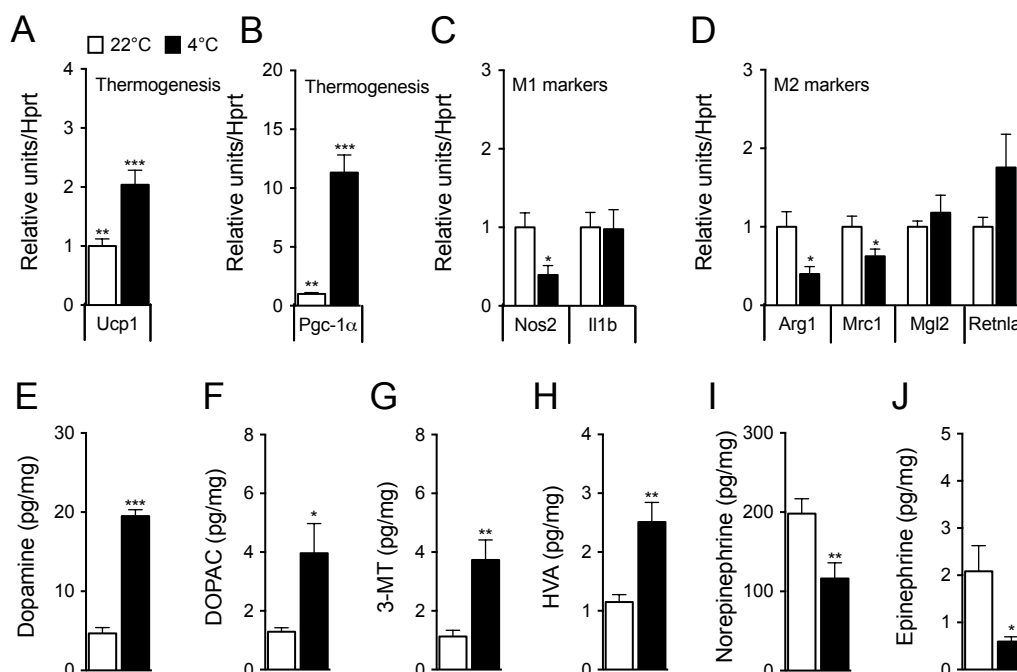


**Figure 13: Effect of 6h cold exposure on macrophage content and catecholamine turnover in brown fat.**

C57Bl/6J mice, housed at room temperature (22°C), were exposed to 4°C for 6 h ( $n = 8$ ) or kept as 22°C controls ( $n = 8$ ). Gene expression of brown fat-specific markers (*Ucp1*, *Pgc-1 $\alpha$* ) (A, B), M1 macrophage markers (*Nos2*, *Il1b*) (C) or M2 macrophage markers (*Arg1*, *Mrc1*, *Mgl2*, *Retnla*) (D) in BAT from mice housed at 22°C or 4°C. Catecholamines and metabolites, namely dopamine (E), 3,4-dihydroxyphenylacetic acid (DOPAC) (F), 3-methoxytyramine (3-MT) (G), homovanillic acid (HVA) (H), norepinephrine (I) and epinephrine (J), were measured in BAT from room temperature or cold-exposed mice. Data represent means  $\pm$  s.e.m. Asterisks indicate: \*,

p<0.05; \*\*, p<0.01; \*\*\*, p<0.001 based on student's t test. Data in panel E-J was generated by Joachim Nagler in the group of Prof. Dr. Schramm (Helmholtz Zentrum München, MEX).

#### 4.1.6 Effect of IL-4 on energy expenditure and BAT thermogenesis *in vivo*

The *in vitro* data of this thesis clearly contradict the proposed positive effect of M2 macrophages in brown fat thermogenesis as shown in multiple cellular assays. However, the possible contribution of alternatively activated macrophages to thermogenesis remains to be further evaluated in physiologically more relevant *in vivo* models. Therefore, this thesis subsequently focused on dissecting the direct effect of IL-4 administration, as well as the existence of the enzyme TH on energy expenditure and thermogenesis in several different mouse models.

##### 4.1.6.1 Temperature challenge in IL-4-treated WT and *IL4ra*<sup>-/-</sup> mice

First, to assess whether chronic IL-4 treatment affects energy expenditure in WT and mice lacking the Interleukin-4 receptor alpha (*Il4ra*<sup>-/-</sup>), energy expenditure (kcal/h) was measured in these mice at declining ambient temperatures (30°C, 20°C, 10°C or 5°C). Interestingly and in line with the *in vitro* data, daily intraperitoneal administration of IL-4 (50 µg/kg) for 12 days did not alter body weight (Fig. 14A) or energy expenditure in WT and *Il4ra*<sup>-/-</sup> mice at any temperature tested (Fig. 14B,C). Notably, despite robust induction of M2 polarization in BAT (Fig. 14D-F) after IL-4 treatment – confirming that the IL-4 was fully functional – such treatment did not increase expression of *Ucp1* or *Pgc-1α* in BAT relative to controls (Fig. 14G,H). Mice lacking *Il4ra* show no elevated expression *Arg1*, *Mrc1*, *Mgl2* after IL-4 treatment (Fig. 14D-F,I) and thus confirm their incapability to activate M2 type macrophages via *Il4ra*-mediated signaling.

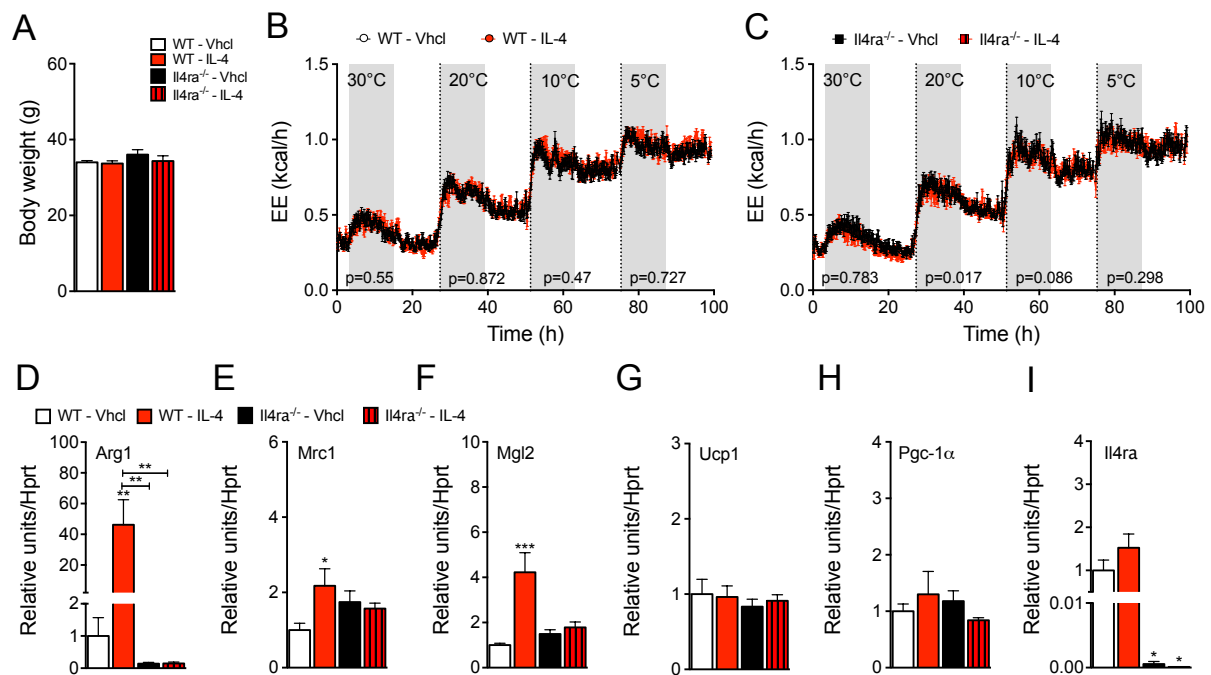


**Figure 14: Effect of IL-4 on energy expenditure and thermogenesis in C57Bl/6J and *Il4ra*<sup>-/-</sup> mice.** Body weight of saline (Vhcl) or IL-4 (50  $\mu$ g/kg)-treated WT and *Il4ra*<sup>-/-</sup> mice (A). Energy expenditure of saline (Vhcl) or IL-4 (50  $\mu$ g/kg)-treated WT (B) or *Il4ra*<sup>-/-</sup> mice (C). After 8 consecutive treatment days at 30°C, mice were placed into metabolic chambers and energy expenditure was recorded over 4 d with ambient temperature decreasing from 30°C to 20°C to 10°C to 5°C (24-h measurement for each temperature) in WT ( $n = 8$  Vhcl and  $n = 7$  IL-4) and *Il4ra*<sup>-/-</sup> mice ( $n = 7$  each treatment). Gene expression of M2 macrophage markers *Arg1* (D), *Mrc1* (E), *Mgl2* (F), brown fat-specific markers *Ucp1* (G), *Pgc-1 $\alpha$*  (H) and the Interleukin-4 receptor alpha, *Il4ra* (I) of BAT from cold-exposed WT ( $n = 8$  Vhcl and  $n = 7$  IL-4) and *Il4ra*<sup>-/-</sup> mice ( $n = 7$  each treatment). Data represent means  $\pm$  s.e.m. Asterisks indicate: \*,  $p < 0.05$ ; \*\*,  $p < 0.01$ ; \*\*\*,  $p < 0.001$  based on ANCOVA using body weight and body composition (fat and lean mass) as covariates or 1-way ANOVA followed by Bonferroni-multiple comparison test.

Consistent with the *in vitro* data demonstrating that IL-4 had no impact on phosphorylation of HSL in iWAT and BAT primary cells (Fig. 11), no difference in p-HSL was found in mice chronically treated with IL-4 as compared to vehicle control (Fig. 15A-D). Supporting these data, HPLC analysis revealed similar levels of catecholamines including NE and a series of metabolites in cold-exposed mice treated chronically with IL-4 as compared to vehicle treated control mice (Fig. 15F-J).

In contrast to the literature (Nguyen et al., 2011, Qiu et al., 2014), but in agreement with the *in vitro* findings showing no activation of BAT thermogenesis upon stimulation of M2-type macrophages, IL-4 had no impact on energy expenditure and thermogenesis *in vivo*.

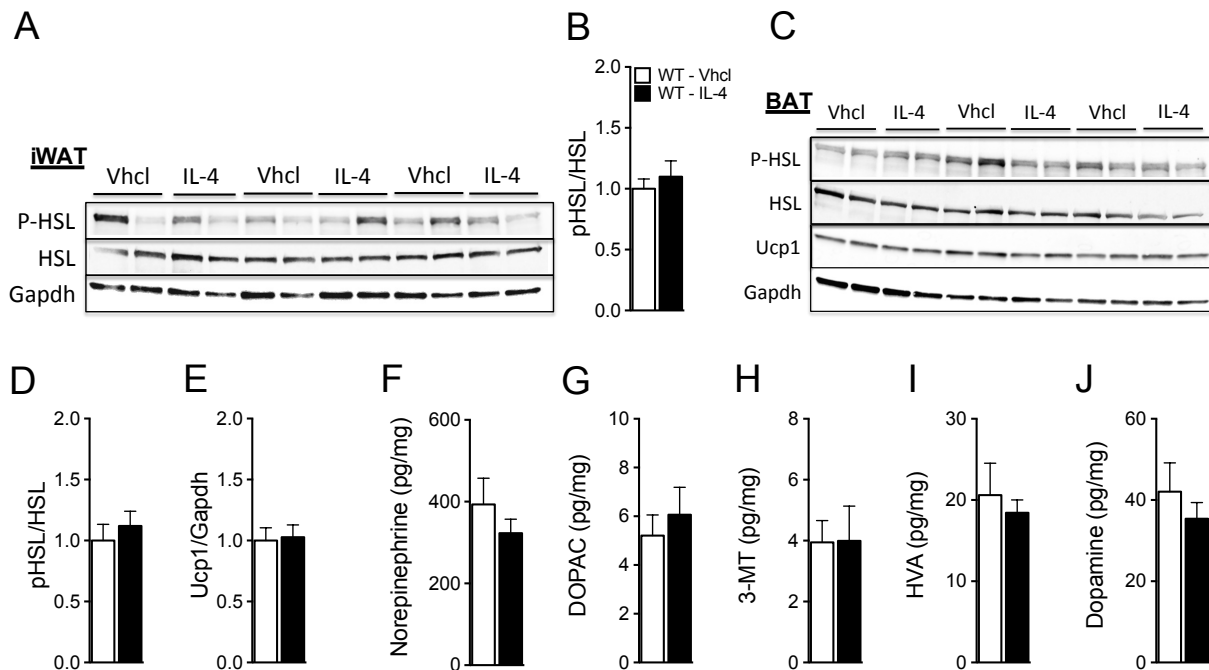


**Figure 15: Effect of IL-4 on lipolysis and catecholamine turnover in C57Bl/6J mice.**

C57Bl/6J mice (8 mo of age) were treated with saline ( $n = 7$ ) or IL-4 ( $n = 7$ ) for 12 days and exposed to ambient temperatures decreasing from 30°C to 20°C to 10°C to 4°C. Western blot and protein quantification of iWAT (A,B) and BAT (C,D,E) from cold-exposed C57Bl/6J mice treated with either vhc1 or IL-4 ( $n = 6$  each treatment). Catecholamines and metabolites (norepinephrine, 3,4-dihydroxyphenylacetic acid (DOPAC), 3-methoxytyramine (3-MT), homovanillic acid (HVA) and dopamine) were measured in BAT from cold-exposed mice treated with vehicle ( $n = 7$ ) or IL-4 ( $n = 7$ ) (F-J). Data represent means  $\pm$  s.e.m. Asterisks indicate: \*,  $p < 0.05$ ; \*\*,  $p < 0.01$  based on 2-sided student's t test. Data in panel F-J was generated by Joachim Nagler in the group of Prof. Dr. Schramm (Helmholtz Zentrum München, MEX).

#### 4.1.6.2 Tyrosine hydroxylase expression in adipose tissue macrophages

Finally, to assess the ability of macrophages to synthesis catecholamines, TH expression was studied in ATMs. TH is the essential, rate-limiting enzyme for catecholamine production, thus it was investigated whether Mac-2-expressing macrophages produce TH.

Of note, immunofluorescent staining revealed no colocalization of TH and Mac-2 signal in iWAT or BAT at either room temperature (23°C) or upon 4 hours cold exposure (5°C) (Fig. 16A,B). In general, higher TH expression was observed in BAT relative to iWAT and cold exposure increased TH expression in both iWAT and BAT, likely reflecting the increase in sympathetic innervation (Fig. 16A,B). However, in the BAT, we only detected a very low number of Mac-2-expressing macrophages (Fig. 16C).

In summary, these data demonstrate that macrophages do not express TH and thus seem to lack the capability to produce catecholamines.

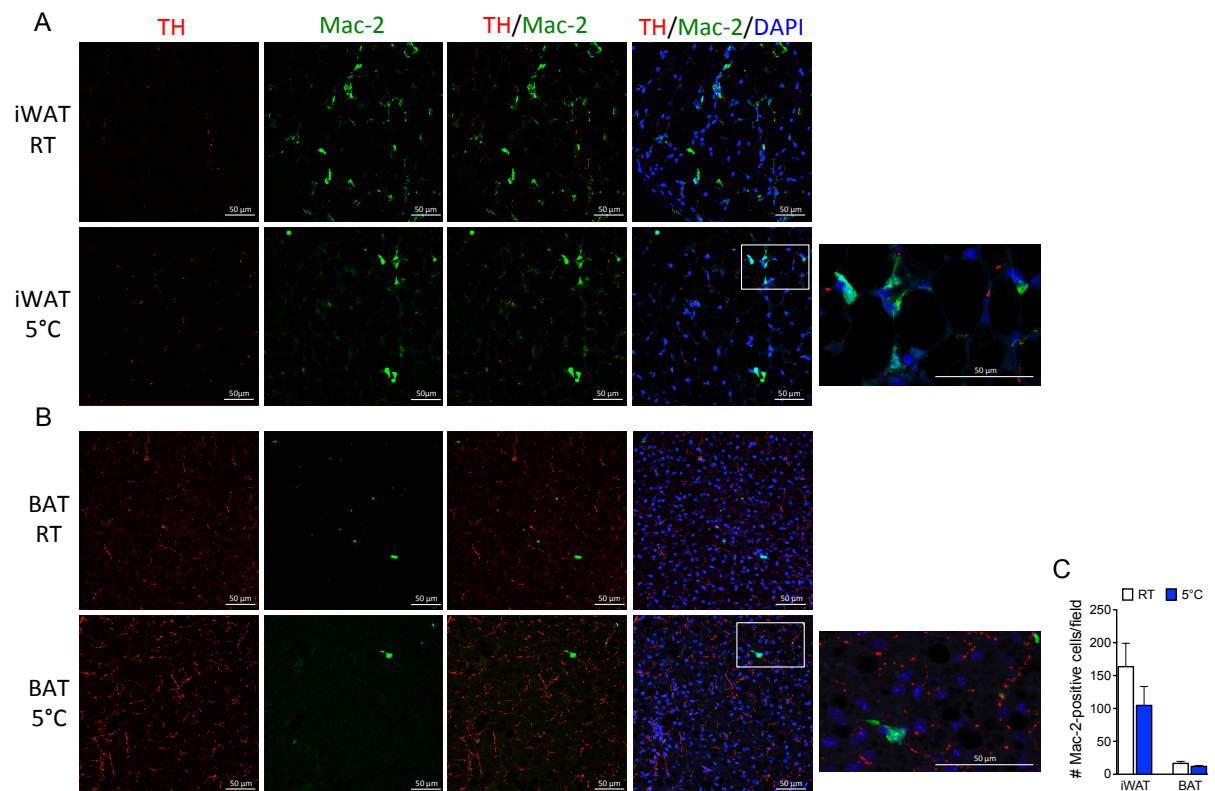


**Figure 16: Tyrosine hydroxylase and Mac-2 co-staining of cold-exposed adipose tissue.**

Immunofluorescence of TH and Mac-2 in iWAT (A) and BAT (B) of room temperature (RT) (top) or 4-h cold-exposed (5°C) (below) C57Bl/6J mice ( $n = 4$  mice each group) (scale bar: 50  $\mu\text{m}$ ). Quantification of Mac-2-positive cells (number of cells per 20x field) of RT or cold-exposed iWAT and BAT tissues (C). Displayed fluorescent images are representative images of  $n = 4$  mice per tissue and treatment. Rectangles highlight zoomed-in areas that are displayed right next to it. Data represent means  $\pm$  s.e.m.

## Part II

### 4.2 Characterization of mice lacking AA 69-251 of p62 (p62<sup>Δ69-251</sup>)

Although the obese phenotype of p62 deficient mice has been described in the literature, so far it remains elusive what functional domain of the protein is mediating the obesity pathogenesis. Based on studies signifying a role for p62 in the MAPK pathway to govern energy homeostasis (Muller et al., 2013), this thesis aims to characterize a mouse that globally lacks AA 69-251 of p62 (p62<sup>Δ69-251</sup>), enclosing the p38-binding domain of p62 (Fig. 17) (Hillmann, 2011) and thereby for the first time directly testing the implication of this pathway for the p62-linked metabolic phenotype.

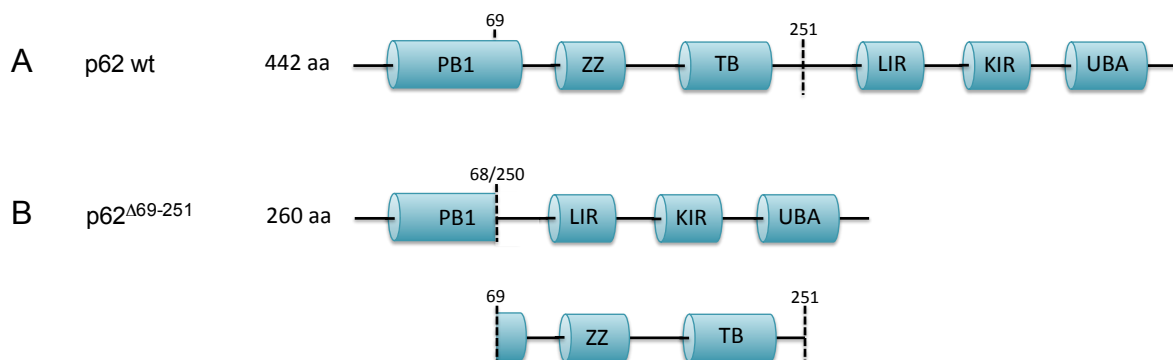


**Figure 17: Structural domain organization of p62 wt and p62<sup>Δ69-251</sup>**

Structural domains of the 442 amino acid (AA) protein p62 wt (A) and the truncated, 260 AA, p62<sup>Δ69-251</sup> (B), displaying a protein-binding domain (PB1), a zinc finger motif (ZZ), a Traf6-binding (TB) domain, a LC3-interacting region (LIR), a Keap1-interacting region (KIR) and an ubiquitin-associated domain (UBA). p62<sup>Δ69-251</sup> lacks the domains extending from amino acid 69 till 251, which represent part of the PB1 domain, the ZZ and the TB domain (see lower illustration of panel B).

#### 4.2.1 Genotype confirmation of p62<sup>Δ69-251</sup> mouse

Besides genotype confirmation by PCR analysis (data not shown), the deletion of AA 69-251 of p62 was further confirmed by quantitative RT-PCR. Therefore primers binding to the gene region encoding for AA 69-251 of p62 (WT) or primers only capable to bind p62 when this specific domain (p62<sup>Δ69-251</sup>) is deleted, were designed (primer sequences are available in Table 4). Gene expression analysis revealed that p62<sup>Δ69-251</sup> mice do not express the domain 69-251 of p62 in iWAT or BAT (Fig. 18A). Loss of AA 69-251 was further confirmed by increased gene expression of p62<sup>Δ69-251</sup> in iWAT and BAT of p62<sup>Δ69-251</sup> mice as compared to WT (Fig. 18B).

Global loss of p62 has been associated with enhanced ERK1/2 activity, which was proposed to be decisive for the development of the obese phenotype observed in p62<sup>-/-</sup> mice



(Rodriguez et al., 2006). To test whether the ERK1/2-interacting PB1 domain of p62 is still functional in p62<sup>Δ69-251</sup> mice, protein levels of phosphorylated ERK1/2 were measured in iWAT of WT and p62<sup>Δ69-251</sup> mice. Of note, no difference in protein levels of p-ERK1/2, normalized to total protein, was detected in iWAT of p62<sup>Δ69-251</sup> mice as compared to WT control (Fig. 18C,D).

These data clearly demonstrate specific loss of AA 69-251 of p62 in p62<sup>Δ69-251</sup> mice and confirm that the PB1 domain is still intact in these mice.

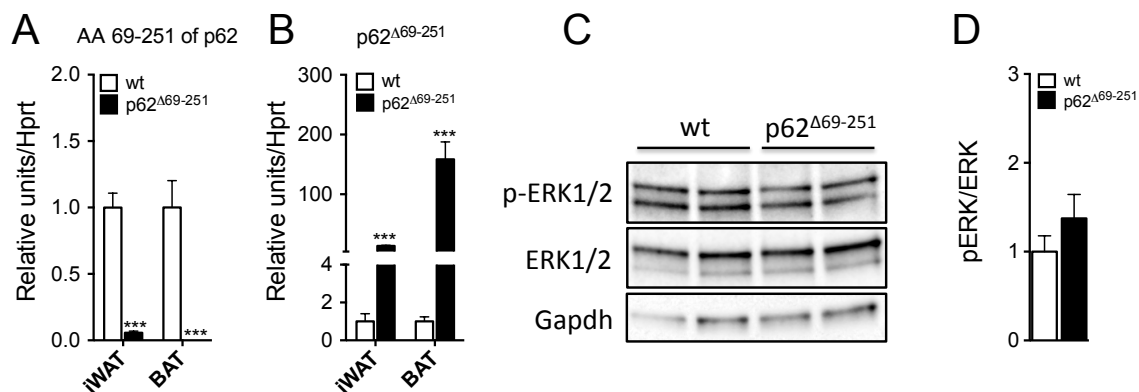


**Figure 18: Genotype of p62<sup>Δ69-251</sup> mice.**

Expression of the ablated gene region (amino acid (AA) 69-251) of p62 (p62<sup>Δ69-251</sup>) in the iWAT and BAT tissue of lean, 12-week-old, WT and p62<sup>Δ69-251</sup> mice (A). Western blot analysis (B) and protein quantification (C) of phosphorylated or total ERK1/2 in iWAT of lean, 12-week-old, p62<sup>Δ69-251</sup> or WT control mice. Data represents mean  $\pm$  s.e.m ( $n = 7-8$ ). \* $P < 0.05$ ; \*\* $P < 0.01$ ; \*\*\* $P < 0.001$  based on 2-sided student's t test.

#### 4.2.2 Metabolic phenotype of p62<sup>Δ69-251</sup> mice

Body weight and food intake of 12-week-old p62<sup>Δ69-251</sup> mice were monitored weekly for 18 weeks to determine the metabolic phenotype of these mice. From an age of 16 weeks onwards, p62<sup>Δ69-251</sup> mice gained significantly more body weight as compared to WT mice on a regular chow diet (Fig. 19A). In line with the increased body weight, primarily fat mass, but also lean mass was increased in 30-week-old p62<sup>Δ69-251</sup> mice (Fig. 19B). Notably, no difference in food intake was recorded at any time during the phenotyping procedure (Fig. 19C). 30-week-old p62<sup>Δ69-251</sup> mice develop glucose intolerance as shown by elevated blood glucose levels upon glucose administration (Fig. 19D).

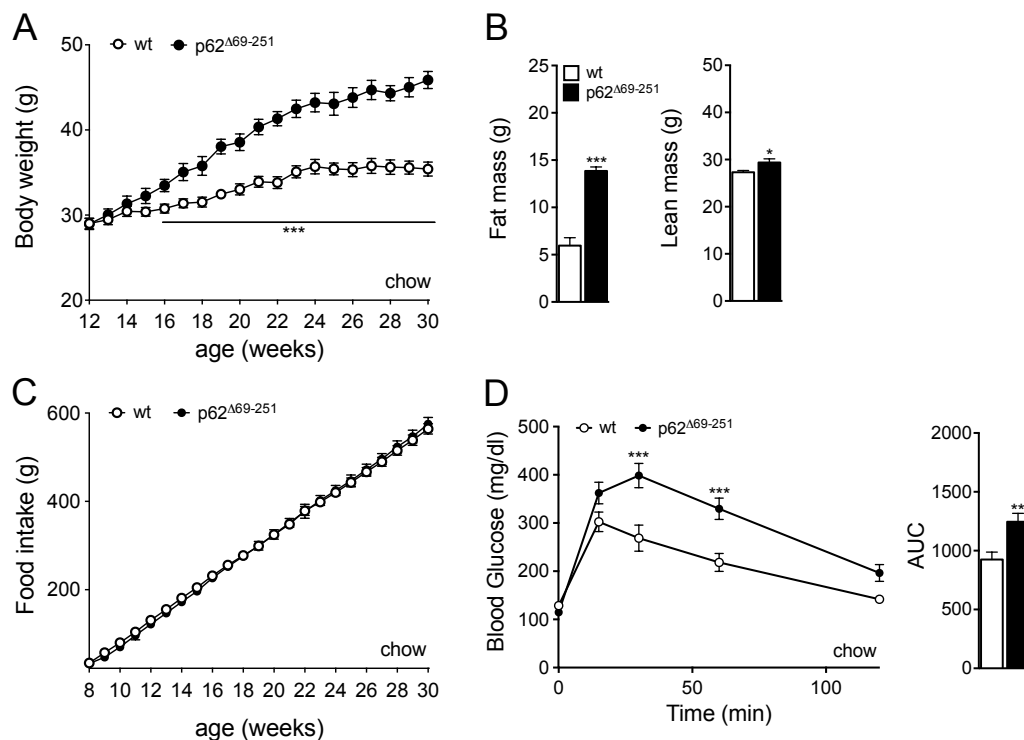


**Figure 19: Metabolic phenotype of p62<sup>Δ69-251</sup> mice on chow diet.**

Body weight (A), body composition (fat and lean tissue mass) (B) and cumulative food intake (C) of 12-30-week-old WT and p62<sup>Δ69-251</sup> on chow diet. Fat and lean mass were measured at an age of 32 weeks. Glucose tolerance (D) of 31-week-old WT and p62<sup>Δ69-251</sup> mice on chow diet. Data represents mean  $\pm$  s.e.m ( $n = 7-8$ ). \* $P < 0.05$ ; \*\* $P < 0.01$ ; \*\*\* $P < 0.001$  based on 2-way analysis of variance (ANOVA) followed by Bonferroni post-hoc comparison of the individual time-points or on 2-sided student's t test.

To compare the magnitude of body weight gain of p62<sup>Δ69-251</sup> mice with that of mice that either globally lack p62 or with mice that specifically lack p62 in the adipose tissue, all mice were side-by-side metabolically phenotyped on both regular chow and 58% high fat diet (HFD). On chow diet, p62<sup>Δ69-251</sup>, global and fat-specific (aP2<sup>cre+</sup>) p62<sup>-/-</sup> mice gained body weight to a similar degree with an average body weight of 45.9 g (p62<sup>Δ69-251</sup>), 46.8 g (p62<sup>-/-</sup>) and 45.1 g (aP2<sup>cre+</sup>;p62<sup>fllox/fllox</sup>) at an age of 30 weeks (Fig. 20A-C). On 58% HFD, all p62 KO mice exhibited a comparable increase in sensitivity to diet-induced obesity (DIO) relative to appropriate WT controls and weight gain saturated at approximately week 22 (Fig. 20D-F). This shows, that p62<sup>Δ69-251</sup> mice resemble the global and fat-specific p62<sup>-/-</sup> mice in the development of the obese phenotype and that the AA 69-251 of p62 are a part of an essential domain of p62 that is central to the obesity pathogenesis.

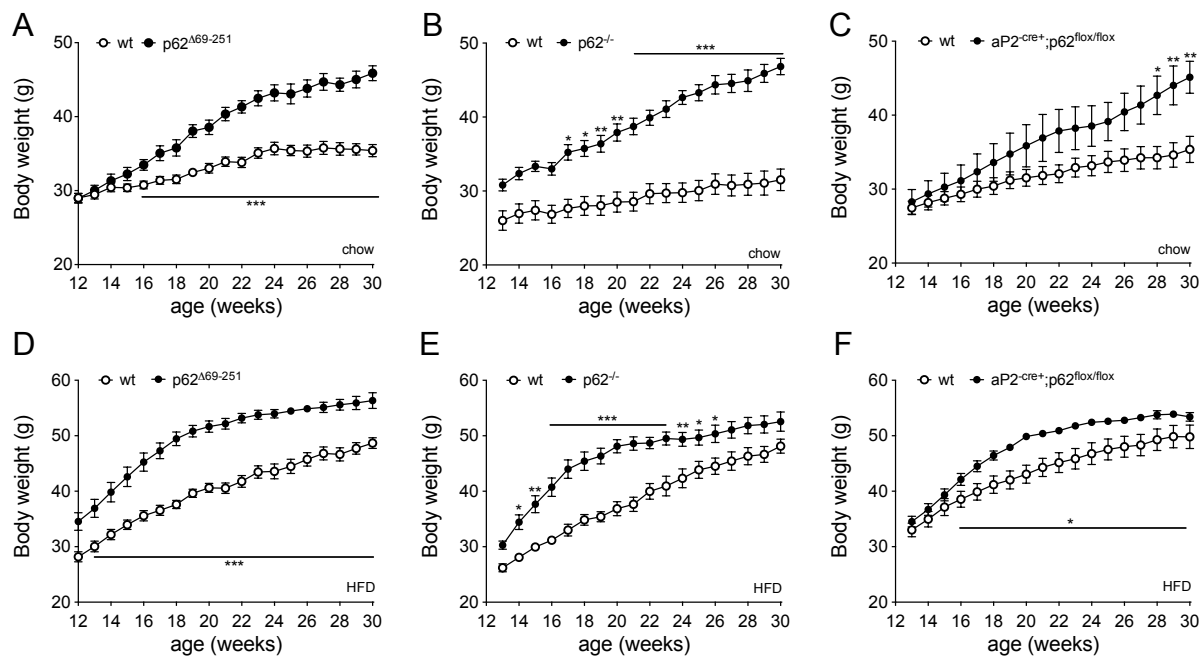


**Figure 20: Side-by-side metabolic phenotype of  $p62^{\Delta 69-251}$ , global  $p62^{-/-}$  and adipocyte-specific  $aP2^{cre+};p62^{flx/flx}$  mice on chow and 58% HFD diet.**

Body weight of male 12-30 week-old WT or  $p62^{\Delta 69-251}$  mice on chow (A) or 58% high fat diet (HFD) (D). Body weight of male 12-30 week-old WT or global  $p62^{-/-}$  mice on chow (B) or 58% HFD (E). Body weight of male 12-30 week-old WT or adipose tissue-specific  $aP2^{cre+};p62^{flx/flx}$  mice on chow (C) or 58% HFD (F). All mice cohorts were phenotyped under the same housing conditions. Data represent mean  $\pm$  s.e.m ( $n = 7-8$ ). \* $P < 0.05$ ; \*\* $P < 0.01$ ; \*\*\* $P < 0.001$  based on 2-way ANOVA followed by Bonferroni post-hoc comparison of the individual time-points.

#### 4.2.3 Energy expenditure of obese $p62^{\Delta 69-251}$ mice

To test the hypothesis that specific lack of AA 69-251 of p62 causes a defect in energy metabolism as previously seen in global and fat-specific  $p62^{-/-}$  mice (Rodriguez et al., 2006, Muller et al., 2013), energy expenditure was measured in 32-week-old, obese  $p62^{\Delta 69-251}$  mice by indirect calorimetry. Notably, although  $p62^{\Delta 69-251}$  mice had 25% enhanced body weight gain compared to WT mice,  $p62^{\Delta 69-251}$  mice displayed a similar uncorrected raw energy expenditure (kcal/h), which was, however, substantially reduced when correcting for body weight using ANCOVA (Fig. 21A,B). No difference in substrate utilization was observed as assessed by equal values for the respiratory exchange ratio (RER) during light and dark cycle between the genotypes (Fig. 21C). Average total locomotor activity as well as activity during light phase were not different between  $p62^{\Delta 69-251}$  and WT mice (Fig. 21D). However, lower physical activity was recorded in  $p62^{\Delta 69-251}$  mice during the dark phase relative to WT controls (Fig. 21D).

This data clearly demonstrate that lack of AA 69-251 of p62 is sufficient to mediate a dysfunction in regulation of energy homeostasis as obese  $p62^{\Delta 69-251}$  mice showed reduced energy expenditure without gravely affecting substrate utilization or physical activity.

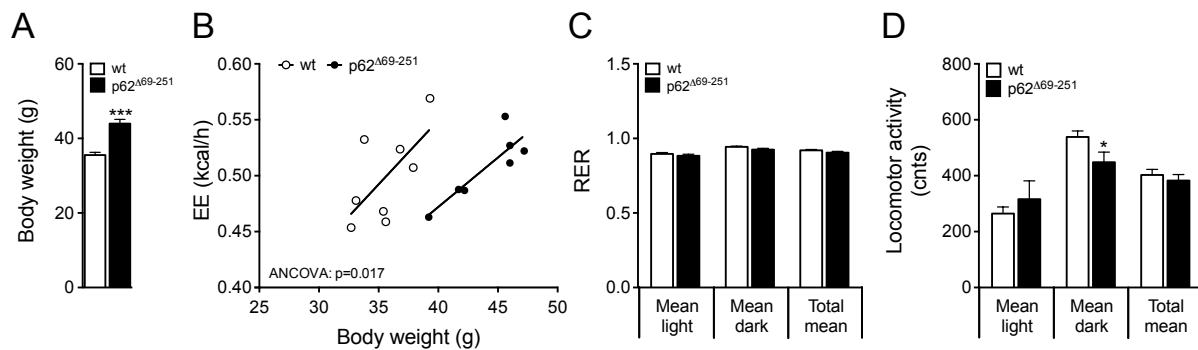


**Figure 21: Energy expenditure of obese p62<sup>Δ69-251</sup> mice on chow diet.**

Body weight (A), energy expenditure (B), respiratory exchange ratio (RER) (C) and locomotor activity (D) of male obese 32-week-old WT and p62<sup>Δ69-251</sup> mice on chow diet. Data represent mean  $\pm$  s.e.m ( $n = 7-8$ ). \* $P < 0.05$ ; \*\* $P < 0.01$ ; \*\*\* $P < 0.001$  based on 2-sided student's t test or analysis of co-variance using body weight as covariate (ANCOVA).

#### 4.2.4 Brown adipose tissue function of obese p62<sup>Δ69-251</sup> mice

To assess whether dysfunctional BAT is mediating the impaired energy metabolism of p62<sup>Δ69-251</sup> mice, BAT uncoupling and glucose utilization which has been shown to positively correlate with energy expenditure upon cold exposure (Orava et al., 2011) was examined.

First, glucose uptake was measured in WT and p62<sup>Δ69-251</sup> mice by PET-CT and magnetic resonance tomography (MRT). PET-CT/MRT imaging revealed that fluorodeoxyglucose (FDG) uptake was reduced in the BAT of p62<sup>Δ69-251</sup> mice (Fig. 22A). Total body radioactivity concentration upon <sup>18</sup>F-FDG uptake for 30 min was significantly decreased in p62<sup>Δ69-251</sup> mice as compared to WT controls (Fig. 22B). In line with that *ex vivo* biodistribution analysis of BAT tissue revealed a tendency to retarded tracer uptake in BAT of p62<sup>Δ69-251</sup> mice (Fig. 22C).

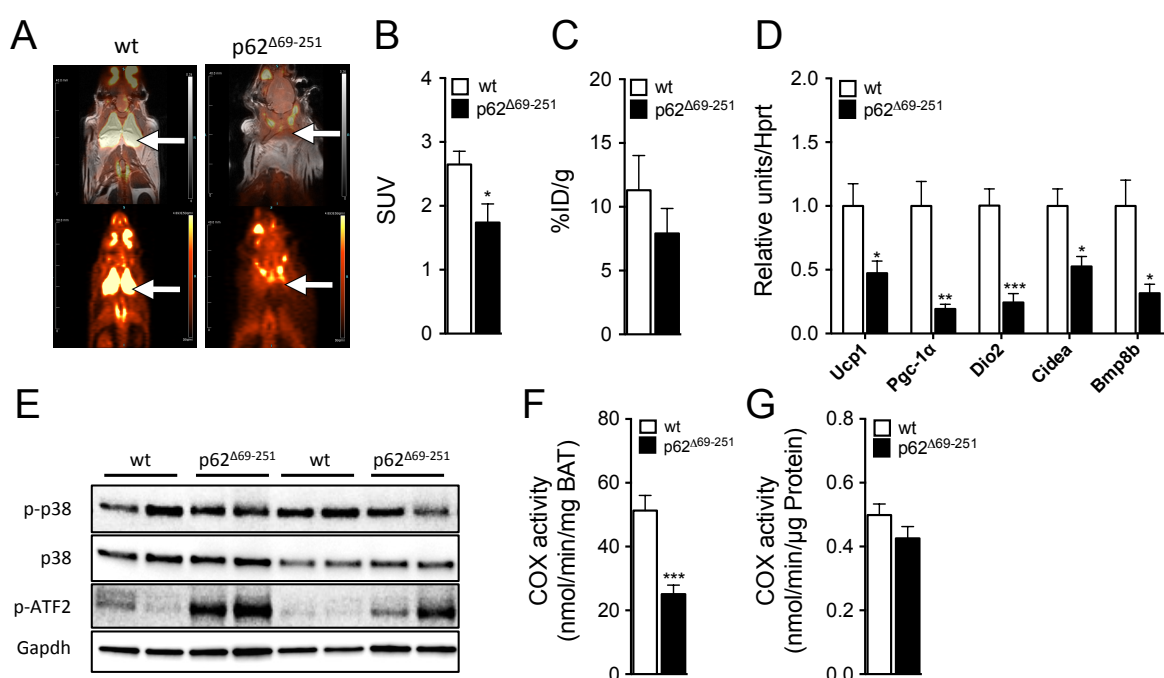


**Figure 22: Brown adipose tissue function of obese p62<sup>Δ69-251</sup> mice on chow diet.**

PET-CT/MRT imaging of male 8-months old WT or p62<sup>Δ69-251</sup> mice ( $n = 5-6$ ) (A-C). Thermogenic gene expression (D), protein levels of p-p38, p38, p-ATF2, Gapdh (E) and cytochrome C Oxidase (Cox) activity normalized to BAT tissue mass (F) or protein amount (G) of BAT from obese 33-week-old WT or p62<sup>Δ69-251</sup> mice. Data represent mean  $\pm$  s.e.m ( $n = 7-8$ ). \* $P < 0.05$ ; \*\* $P < 0.01$ ; \*\*\* $P < 0.001$  based on 2-sided student's t test. Data of panel A-C was generated by K. Fischer in collaboration with the group of Prof. Dr. Pichler (Universität Tübingen). Data of panel F,G was measured by Dr. S. Keipert in the group of Dr. Jastroch (Helmholtz Zentrum München, IDO).

Furthermore, a cluster of genes related to nonshivering thermogenesis, such as *Ucp1*, *Pgc-1 $\alpha$*  showed reduced expression in the BAT of obese, 33-week-old p62<sup>Δ69-251</sup> mice relative to WT controls (Fig. 22D). Interestingly, no difference in phosphorylation of p38 was observed in the BAT of WT and p62<sup>Δ69-251</sup> mice (Fig. 22E). However, instead higher protein levels of p-ATF2 were detected in the BAT of p62<sup>Δ69-251</sup> mice as compared to WT controls (Fig. 22E).

To further determine whether the defect in BAT thermogenesis observed in p62<sup>Δ69-251</sup> mice is accompanied by mitochondrial dysfunction, cytochrome c oxidase (COX) activity was examined in the BAT of WT and p62<sup>Δ69-251</sup> mice. Notably, COX activity was reduced in the BAT of obese, hypertrophic p62<sup>Δ69-251</sup> mice when normalizing to whole BAT tissue weight (Fig. 22F). However, a more appropriate normalization strategy, taken total protein concentration into account, instead of tissue mass, revealed no difference in COX activity between the genotypes (Fig. 22G). This data showed that complex IV, the final catalyzer of the mitochondrial electron transport chain is still functional in p62<sup>Δ69-251</sup> mice and thus indicated that the mitochondrial machinery regulating BAT thermogenesis is functional.

#### 4.2.5 Brown adipose tissue function of lean p62<sup>Δ69-251</sup> mice

To test whether the brown fat dysfunction observed in elder p62<sup>Δ69-251</sup> mice is cause or consequence of the obesity, the thermogenic characteristics of BAT from young p62<sup>Δ69-251</sup> mice were examined.

To evaluate whether p62<sup>Δ69-251</sup> mice have altered surface temperature, 7-day-old pups were recorded with an infrared thermographic camera. Thermal imaging of murine neonates has the advantage that they lack protective fur as compared to adult mice, thus thermal insulation affecting the thermal profile is avoided. P62<sup>Δ69-251</sup> neonates had a lower surface temperature in the interscapular skin region as compared to WT neonates (Fig. 23A). For quantification, the hottest spot within a defined area was determined for each mouse and the temperature was recorded for two minutes with 27 measurements each second. Finally, the average over all data points from the temperature-time diagram showed significantly reduced surface temperature in p62<sup>Δ69-251</sup> neonates as compared to controls (Fig. 23B).

To further elucidate the effect of ablated AA 69-251 of p62 prior to obesity development, the thermogenic profile in young, 12-week-old WT and p62<sup>Δ69-251</sup> mice, showing no difference in body weight (Fig. 23C), was in depth characterized. Immunohistochemistry for UCP1 in iWAT from 12-week-old mice showed lower levels of UCP1 in p62<sup>Δ69-251</sup> mice as compared to WT controls and the iWAT of p62<sup>Δ69-251</sup> mice displays hypertrophic properties (Fig. 23D).

Gene expression analysis further corroborated these observations as a lower expression of a cluster of thermogenic genes, such as *Ucp1*, *Pgc-1 $\alpha$*  in the BAT of 12-week-old  $p62^{\Delta 69-251}$  mice was detected (Fig. 23E).

Collectively these data demonstrate that  $p62^{\Delta 69-251}$  mice have a dysfunction in BAT thermogenesis before the onset of obesity, thus implying a causal defect in regulation of energy metabolism by loss of AA 69-251 of p62.

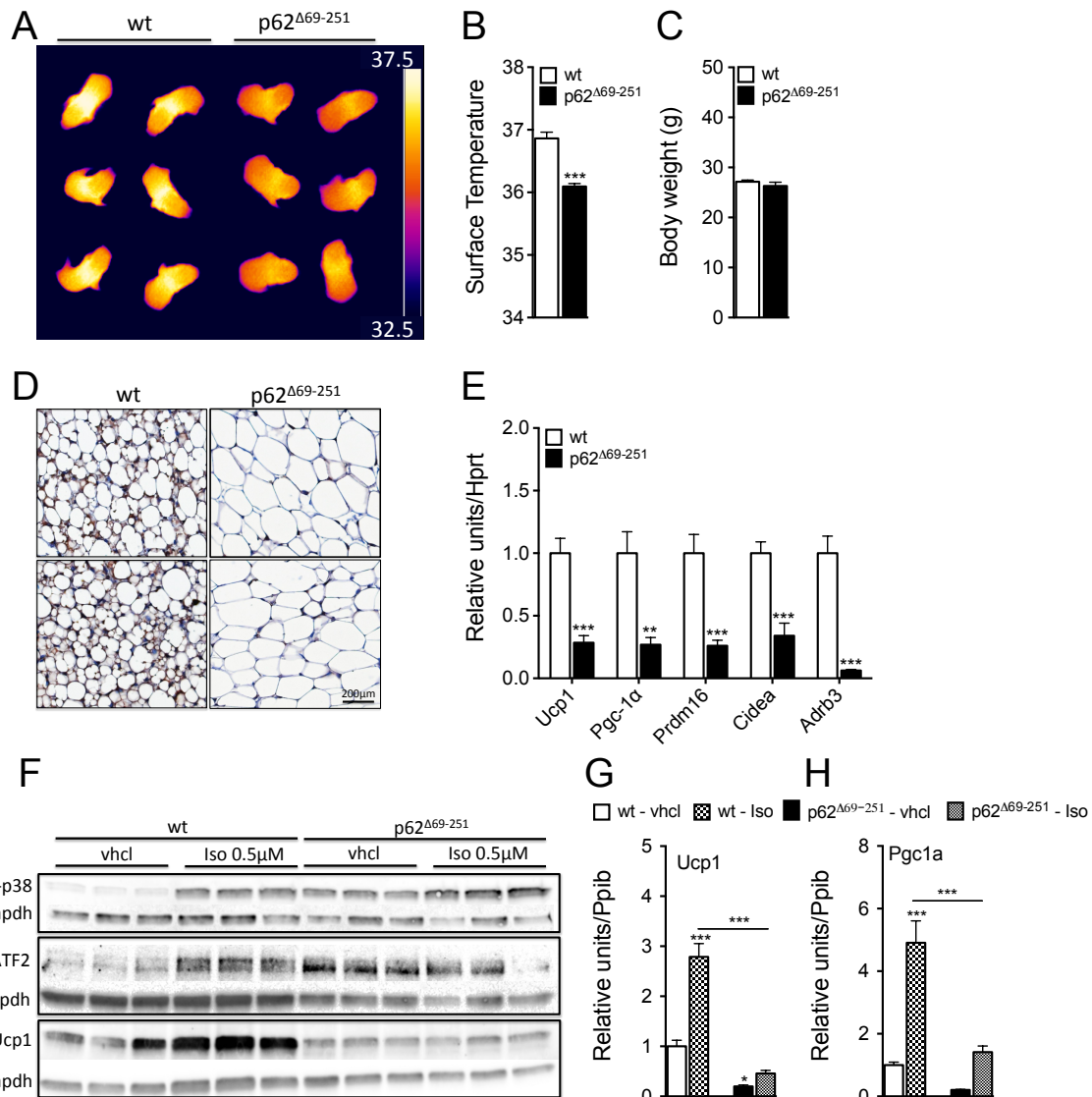


**Figure 23: Brown adipose tissue function of lean  $p62^{\Delta 69-251}$  mice on chow diet.**

Infrared thermographic imaging ( $n = 6$ ) (A) and surface temperature (B) of male 7-day old WT or  $p62^{\Delta 69-251}$  pups ( $n = 6$  mice per genotype). Body weight of 12-week-old WT or  $p62^{\Delta 69-251}$  mice ( $n = 7-8$ ) (C). Immunohistochemistry for UCP1 in iWAT from lean (12-week-old) WT or  $p62^{\Delta 69-251}$  mice ( $n = 7-8$ ) (D). Gene expression of thermogenic markers, such as *Ucp1*, *Pgc-1 $\alpha$* , *Prdm16*, *Cidea*, *Adrb3* (E) of BAT from lean WT or  $p62^{\Delta 69-251}$  mice ( $n = 7-8$ ). Western blot (F) and *Ucp1*, *Pgc-1 $\alpha$*  gene expression (G,H) of 6-day differentiated BAT primary cells from WT or  $p62^{\Delta 69-251}$  mice stimulated with saline or isoproterenol (0.5 $\mu$ M) for 6h ( $n = 3$  technical replicates). Data represent mean  $\pm$  s.e.m. \* $P < 0.05$ ; \*\* $P < 0.01$ ; \*\*\* $P < 0.001$  based on 2-sided student's t test or 1-way ANOVA followed by Bonferroni-multiple comparison test.

To gain more insight into the mechanism of how AA 69-251 of p62 affect UCP1-dependent thermogenesis, primary brown preadipocytes were isolated, cultured and differentiated *in*

*vitro* to mature brown adipocytes until day 6 of differentiation. Isoproterenol-induced activation of the  $\beta$ -adrenergic pathway increased protein levels of phosphorylated p38 (p-p38) in WT primary cells, which subsequently led to higher levels of p-ATF2 and UCP1 as compared to vehicle controls (Fig. 23F). Notably, BAT primary cells from mice lacking AA 69-251 of p62 showed elevated protein levels of p-p38 and p-ATF2 under basal conditions as compared to WT cells. Isoproterenol treatment increased p-p38 levels even more in p62 <sup>$\Delta$ 69-251</sup> primary cells relative to vehicle, whereas phosphorylation of ATF2 did not increase further upon stimulation, suggesting that maximal phosphorylation capacity of ATF2 has likely been already reached (Fig. 23F). Of note, UCP1 protein did not get activated upon isoproterenol stimulation in primary cells derived from p62 <sup>$\Delta$ 69-251</sup> mice as compared to WT controls (Fig. 23F). In line with the inability of p62 <sup>$\Delta$ 69-251</sup> cells to activate UCP1 protein, reduced gene expression of *Ucp1* and *Pgc-1 $\alpha$*  was observed in BAT primary cells stimulated with isoproterenol (Fig. 23G,H).

Taken together, loss of AA 69-251 of p62 prevents activation of the thermogenic regulators *Ucp1* and *Pgc-1 $\alpha$* , thus resulting in dysfunctional BAT thermogenesis. Hyperphosphorylation of p38 and ATF2, important mediators of the MAPK pathway, seems to be a compensatory mechanism instated to rescue the metabolic defect elicited by p62 <sup>$\Delta$ 69-251</sup> ablation.

#### 4.2.6 Metabolic phenotype of p62 <sup>$\Delta$ 69-251</sup> mice kept at thermoneutrality

The question whether the development of obesity and impaired BAT thermogenesis, observed in p62 <sup>$\Delta$ 69-251</sup> mice at room temperature, is preserved under thermoneutral conditions, was addressed by metabolic phenotyping of WT and p62 <sup>$\Delta$ 69-251</sup> mice kept at 30°C ambient temperature. The thermoneutral zone of an organism is described as the state when active thermoregulation and physical activity are lowest, thus the basal metabolic rate can be measured (Cannon and Nedergaard, 2011).

Interestingly, also at thermoneutrality p62 <sup>$\Delta$ 69-251</sup> mice gained more body weight than WT controls from an age of 22 weeks onwards at thermoneutrality (Fig. 24A). The amplified weight gain was accompanied by increased fat mass of p62 <sup>$\Delta$ 69-251</sup> mice, without any changes in lean mass (Fig. 24B). Consistently, cumulative food intake was not different between WT and p62 <sup>$\Delta$ 69-251</sup> mice during the 20 weeks of phenotyping (Fig. 24C). To test whether nutrient absorption in the gut was affected by the loss of AA 69-251 of p62, the assimilated energy was calculated by subtraction of the energy output from energy content of caloric intake, determined by bomb calorimetric analysis of collected dried food and feces. Neither assimilated energy, nor food efficiency was different in p62 <sup>$\Delta$ 69-251</sup> mice as compared to WT controls (Fig. 24D,E), demonstrating normal digestion and procession of food in mice lacking AA 69-251 of p62. At thermoneutrality, when no necessity to defend body temperature via thermogenic heat production rules (Chaffee and Roberts, 1971), indirect calorimetry

surprisingly revealed significant reduction in energy expenditure in of  $p62^{\Delta69-251}$  mice as compared to WT controls, using ANCOVA with body weight as covariate (Fig. 24F). Notably, this decrease in energy expenditure was neither a consequence of changes in resting metabolic rate (RMR) or variations in physical activity at thermoneutrality as no difference between the genotypes was observed (Fig. 24G).

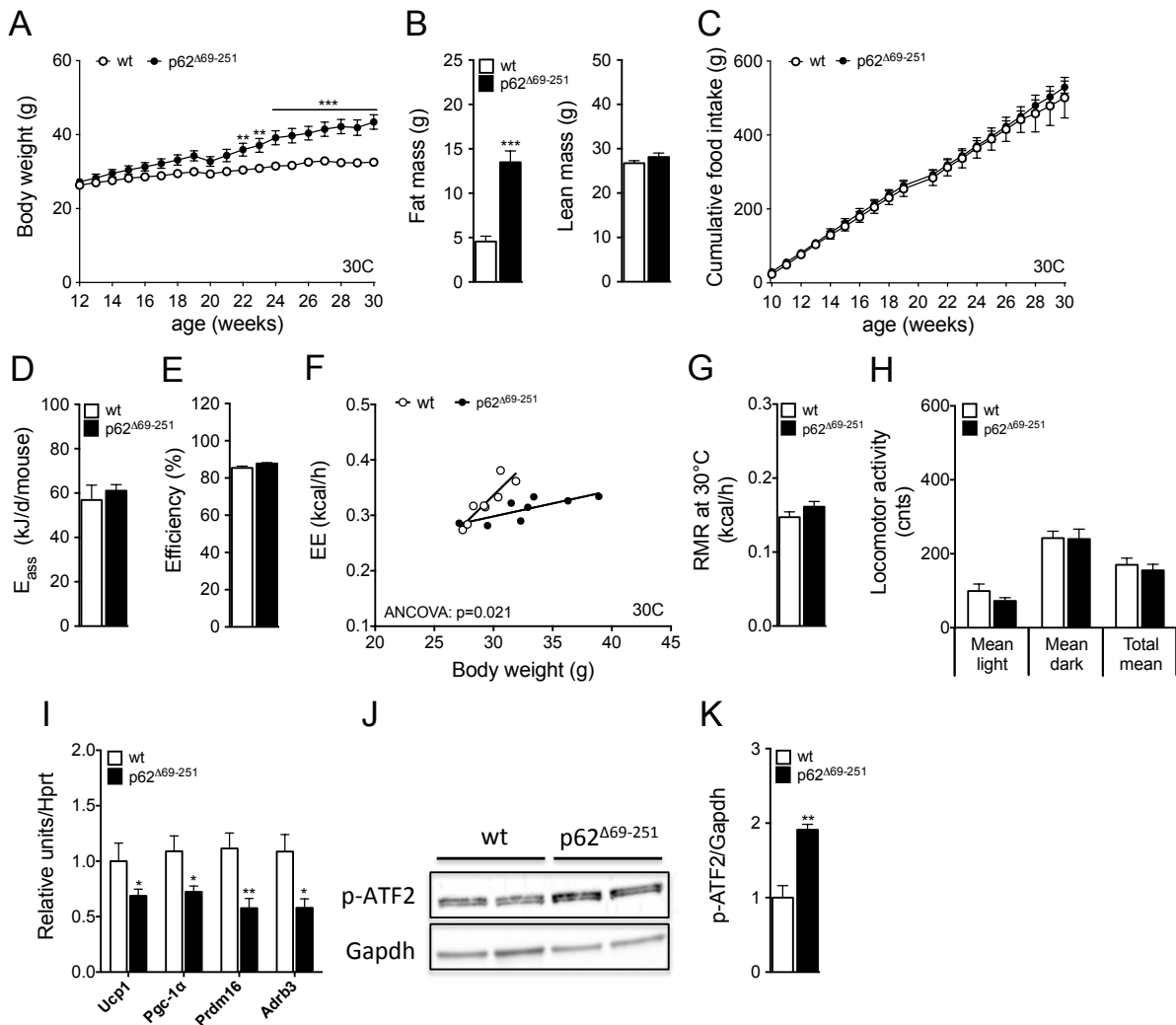


**Figure 24: Metabolic phenotype of  $p62^{\Delta69-251}$  mice at thermoneutrality (on chow diet).**

Body weight (A), body composition (fat and lean tissue mass) (B) and cumulative food intake (C) of male 12-30 week-old WT or  $p62^{\Delta69-251}$  mice on chow diet at 30°C. Assimilated energy and food efficiency calculated from feces of 30-week-old WT or  $p62^{\Delta69-251}$  mice, kept at 30°C (D,E). Energy expenditure (F), resting metabolic rate (RMR) at 30°C (G), locomotor activity (H) of WT or  $p62^{\Delta69-251}$  mice. Gene expression of *Ucp1*, *Pgc-1 $\alpha$* , *Prdm16*, *Adrb3* (I) and protein levels of phosphorylated ATF2 (J,K) in BAT of obese WT or  $p62^{\Delta69-251}$  mice at 30°C. Data represent mean  $\pm$  s.e.m ( $n = 7-8$ ). \* $P < 0.05$ ; \*\* $P < 0.01$ ; \*\*\* $P < 0.001$  based on 2-way analysis of variance (ANOVA) followed by Bonferroni post-hoc comparison of the individual time-points, 2-sided student's t test or ANCOVA. Data of panel D,E was generated by K. Fischer and S. Mocek in the group of Prof. Dr. Klingenspor (TUM).

Even at thermoneutrality, when active thermoregulation is lowest, key regulatory genes of BAT thermogenesis, such as *Ucp1*, *Pgc-1 $\alpha$* , *Prdm16* or *Adrb3* are down regulated in the BAT of  $p62^{\Delta69-251}$  mice relative to WT controls (Fig. 24I). Hyperphosphorylation of ATF2 was



observed in the BAT of p62<sup>Δ69-251</sup> mice (Fig. 24J,K), consistent with the data derived from room temperature-housed p62<sup>Δ69-251</sup> mice and primary cells (Fig. 22E and 23F).

These data underscore that the effects of AA 69-251 of p62 on energy expenditure and body weight are preserved under thermoneutral conditions, signifying the profanity of this specific domain of p62 in the regulation of energy metabolism.

#### 4.2.7 Regulation of nuclear-cytosolic transport of p-ATF2 in p62<sup>Δ69-251</sup> mice

To unravel the mechanistic underpinnings of how p62 and specifically loss of its domain of AA 69-251 regulate thermogenic processes, cytosolic and nuclear distribution of key signaling proteins of the MAPK pathway was determined. Therefore, cytosolic and nuclear protein fractions of BAT were isolated from 3-4-week-old WT and p62<sup>Δ69-251</sup> mice and protein levels of p-ATF2 and p-p38 were detected. Purity of each fraction was confirmed by detection of the nuclear protein Histon 3 (H3) or Gapdh. No cross-contaminations were detected during fractionation since the nuclear protein H3 was only detected in the nuclei, but not in the cytosol whereas the primarily cytosolic-occurring protein Gapdh was predominantly detected in the cytosol, but less in the nuclei (Fig. 25A). For quantification, cytosolic p-ATF2 levels were normalized to Gapdh, nuclear p-ATF2 levels to H3 and finally normalized nuclear p-ATF2 levels were correlated to total amount of p-ATF2 for each genotype.

Substantial decrease in p-ATF2 levels was detected in the nuclei of BAT from p62<sup>Δ69-251</sup> mice as compared to WT controls (Fig. 25A,B), suggesting that nuclear trafficking of p-ATF2 is disordered along with deletion of AA 69-251 of p62. No difference in p-p38 protein levels was detected in the nuclei of BAT from p62<sup>Δ69-251</sup> mice relative to WT controls (Fig. 25A,C). Based on the finding that less p-ATF2 enters the BAT nuclei of p62<sup>Δ69-251</sup> mice, it was evaluated whether this phenomenon could also be observed in mice globally lacking p62. Therefore, nuclear and cytosolic fractions of BAT were isolated from obese WT and p62<sup>-/-</sup> mice, revealing a strong tendency of decreased p-ATF2 levels in the nuclei of BAT from p62<sup>-/-</sup> mice as compared to WT controls, seen in three independent experiments (Fig. 25D,E). Similar to the findings in p62<sup>Δ69-251</sup> mice, no difference in nuclear protein levels of p-p38 was observed between WT and p62<sup>-/-</sup> samples (Fig. 25D,F).

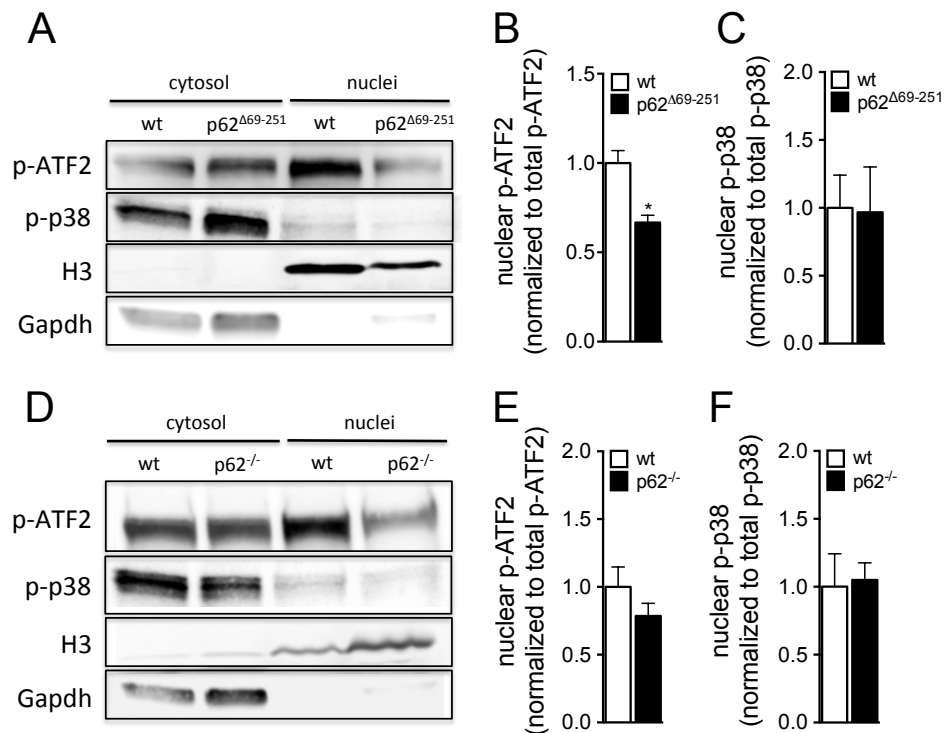


**Figure 25: Effect of p62 ablation on nuclear and cytosolic distribution of p-ATF2 and p-p38.**

Nuclear and cytosol protein fraction from BAT of 3-4 week-old WT or p62<sup>Δ69-251</sup> mice. Western blot of phosphorylated ATF2, histon 3 (H3) and Gapdh (A) or quantification of nuclear p-ATF2 (B) and p-p38 (C) normalized to total protein level in BAT of WT or p62<sup>Δ69-251</sup> nuclear/cytosol fraction. Western blot (D) and quantification (E,F) of p-ATF2, p-p38, H3, Gapdh from nuclear and cytosol fraction from BAT of obese WT and p62<sup>-/-</sup> mice. Representative western blot of panel A,D shows one out of three independently performed experiments. Data represent mean  $\pm$  s.e.m ( $n = 3$ ). \* $P < 0.05$ ; \*\* $P < 0.01$ ; \*\*\* $P < 0.001$  based on 2-sided student's t test. Western blot data displayed in panel D-F was generated by our Master student A. Fedl under supervision of K. Fischer.

To strengthen the observation that p-ATF2 levels are reduced in the nuclei of p62<sup>Δ69-251</sup> mice, a cell-based reporter system was established, which allowed measurement of transcriptional activation of proteins binding to CRE in the nucleus. The reporter contains the firefly luciferase under the control of CRE, accordingly CRE binding elements, such as CREB or ATF2 trigger a luminescent signal (Fig. 26A). The effect of p62 and ablation of its AA 69-251 on nuclear activity of CRE binding proteins was determined by cotransfection of HEK cells with several different constructs. First, single transfection of HEK cells with either p62 WT or p62<sup>Δ69-251</sup> plasmids did not alter the luminescent signal, suggesting that endogenous CREB and/or ATF2 levels might be too low to see any effect (Fig. 26B). Next, it was tested whether cotransfection of the respective p62 constructs together with ATF2 would mediate alterations in nuclear activity of CREB/ATF2, without observing any striking induction of luminescence (Fig. 26B). Further, it was tested whether it might require activation of the MAPK pathway in order to see an effect on nuclear trafficking of ATF2 in dependence of p62<sup>Δ69-251</sup>. Mitogen-activated protein kinase 6 (MKK6) induction of MAPK signaling led to a 4-fold increase in relative luminescence signal in MKK6-transfected cells as compared to controls (Fig. 26C). Similar increase in transcriptional activity of CRE binding elements was observed in cells cotransfected with MKK6 and p62 WT, however cotransfected p62<sup>Δ69-251</sup> together with MKK6

revealed impaired nuclear activity since luminescence did not increase at all (Fig. 26C). Further MKK6, ATF2 and the respective p62 WT or mutant plasmids were simultaneously incorporated to evaluate whether an augmented effect was achieved. Of note, incorporation of both MKK6 and ATF2 further increased luminescence levels as compared to single addition (Fig. 26D). Consistent with the previous observation that less CRE binding activity was found in MKK6 and p62<sup>Δ69-251</sup> cotransfected cells, less activation was revealed upon cotransfection with p62<sup>Δ69-251</sup> as compared to WT under MKK6-induced conditions along with excess levels of ATF2 (Fig. 26D). As negative control, cells were treated with SB203580, a specific p38 kinase inhibitor, leading to reduction in CRE binding activity as revealed by decreased luminescence (Fig. 26C,D).

Although this assay does not distinguish whether CREB or ATF2 are binding to CRE, yet the fact that MKK6 activation of p38 induced nuclear CRE binding activity, strongly suggest that p-ATF2 is binding to the DNA. Accordingly this supports the observation that less p-ATF2 levels are found in the BAT nuclei of p62<sup>Δ69-251</sup> mice.

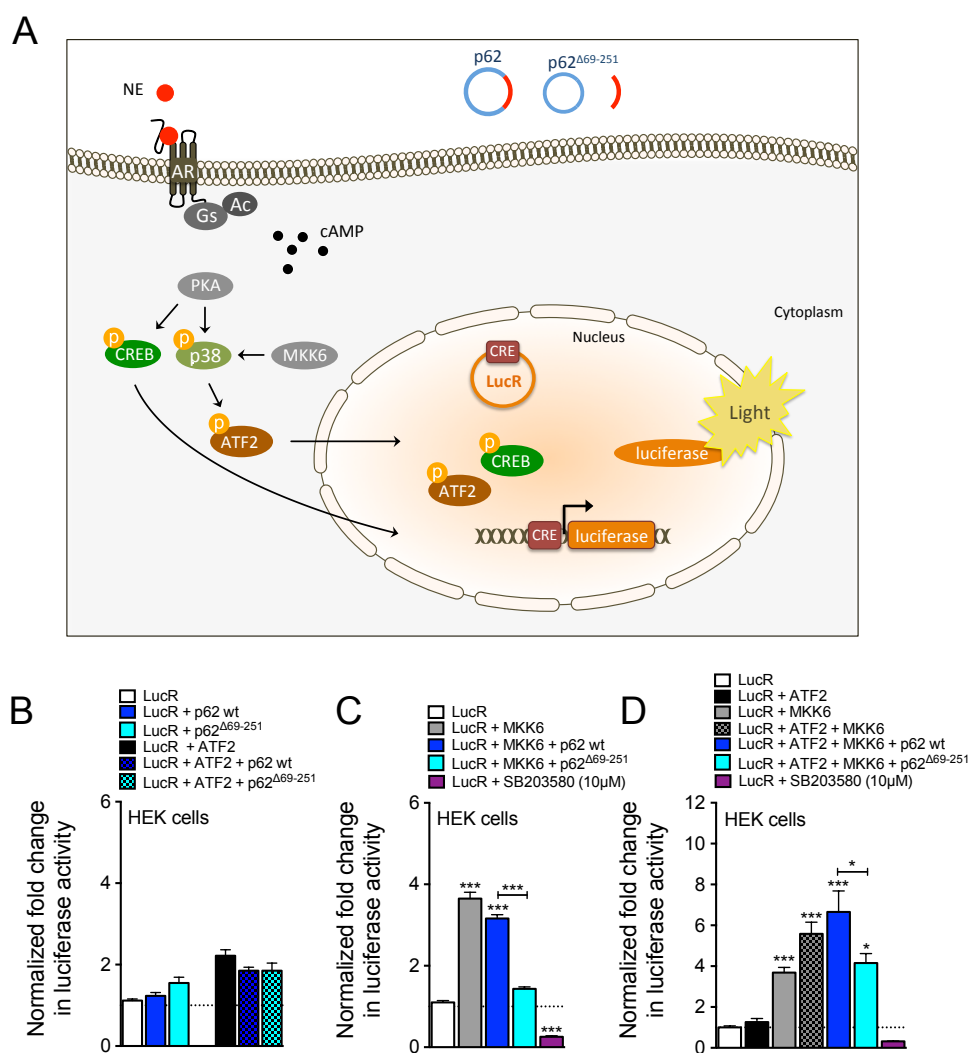


**Figure 26: Effect of MKK6 on nuclear CRE activity in p62 WT and the truncated p62<sup>Δ69-251</sup>.**

Schematic of MAPK pathway and CRE luciferase reporter assay (A). Luciferase-based CRE reporter assay in HEK cells (B,C,D) transfected with the corresponding murine constructs for firefly luciferase CRE reporter (LucR), p62 WT, p62 $\Delta^{69-251}$ , ATF2 or MKK6 (description of the backbone vector is available in the methods section) for 24 hours. DNA content was adjusted by cotransfection of corresponding amount of empty vector (MigR1) for each transfection to obtain equal transfection efficiency. For normalization, all cells were co-transfected with a renilla vector. For negative control, cells were treated with SB203580 (10 $\mu$ M) for 24 hours. Data represents one out of three independently performed experiments. Data represent mean  $\pm$  s.e.m ( $n = 3-6$  technical replicates). \* $P < 0.05$ ; \*\* $P < 0.01$ ; \*\*\* $P < 0.001$  based on 1-way ANOVA followed by Bonferroni-multiple comparison test. Data in panel B-D was generated by our Master student A. Fedl under supervision of K. Fischer.

## 5. Discussion

### 5.1 Role of alternatively activated macrophages on BAT thermogenesis

Thermoregulation processes serve to maintain of a relatively constant body temperature and are critical for the survival of the organism (Tansey and Johnson, 2015). Endotherms, such as birds and mammals, are able to produce and dissipate heat via uncoupling oxidative phosphorylation from ATP synthesis, which enables them to maintain a constant body temperature (Chaffee and Roberts, 1971, Garland, 1995, Herbert et al., 1973). In a cold environment, thermal balance is achieved by increasing the metabolic rate via either shivering or nonshivering thermogenesis in order to protect from hypothermia (Heldmaier and Ruf, 1992). Thermogenesis, the so-called process of heat production, can be induced by either physical activity, muscle shivering or via BAT nonshivering thermogenesis (Virtanen, 2014, Block, 1994, Rowland et al., 2015, Griggio, 1982). Prolonged cold adaptation considerably increases the thermogenic capacity and mainly induces nonshivering thermogenesis, whereas shivering and basal metabolic rate are barely altered (Griggio, 1982, Van Sant and Hammond, 2008).

The SNS controls BAT thermogenesis by release of NE (Cannon and Nedergaard, 2011). Although the sympathetic-driven induction of nonshivering thermogenesis is well characterized in the literature (Cannon and Nedergaard, 2004, Bartness et al., 2010), the existence of alternative mediators and pathways, able to activate BAT thermogenesis independently of the SNS, is currently being discussed (Bostrom et al., 2012, Villarroya and Vidal-Puig, 2013).

Alternatively activated macrophages were recently suggested to represent such an alternative source of catecholamines (i.e. NE) as they were proposed to synthesize catecholamines *de novo* and to locally activate  $\beta$ -adrenergic signaling in adipocytes (Nguyen et al., 2011). Similarly, it has been shown that cold exposure leads to recruitment of M2-type macrophages to the subcutaneous white adipose tissue to induce beiging/browning (Qiu et al., 2014). Adiponectin has further been suggested to induce beiging/browning of iWAT over a similar pathway through enhancing proliferation of alternatively activated macrophages (Hui et al., 2015). Meteorin-like (Metrnl), a circulating factor, expressed in muscle after exercise and in adipose tissue upon cold exposure, has been associated with beige fat thermogenesis (Rao et al., 2014). Metrnl promotes beiging/browning of iWAT through direct action on adipocytes by induction of anti-inflammatory responses, including IL-4/IL-13 signaling, in the adipose tissue (Rao et al., 2014). The authors attribute the Metrnl-induced increase in beiging/browning of iWAT to increased number or trafficking of eosinophils into

the adipose tissue, which represent the major source of IL-4 necessary to activate M2-type macrophages (Rao et al., 2014, Wu et al., 2011).

Type 2 innate lymphoid cells (ILC2s) have recently been suggested to elicit activation of M2-type macrophages via IL-4 receptor alpha (Il4ra) signaling to therefore promote beiging/browning of white adipose tissue (Brestoff et al., 2015). Notably, another study revealed that IL-33-elicited ILC2s regulate beige fat biogenesis independently of eosinophils or Il4ra signaling (Lee et al., 2015). Caloric restriction has been shown to cause beiging/browning of WAT by increasing eosinophil infiltration, type 2 cytokine signaling and recruitment of alternatively activated macrophages, however caloric restriction did not alter the amount of ILC2s in those studies (Fabbiano et al., 2016).

In sum, over the last 6 years, an increasing amount of highly profiled studies have established an alternative mechanism, in which alternatively activated macrophages autonomously produce catecholamines to induce thermogenesis. Common for these observations is the link to the Il4ra immune response to trigger activation of these M2-type macrophages. Unconventional mechanisms to induce BAT thermogenesis, besides the classical sympathetic-driven adrenergic activation, could represent a new way to target energy balance, and therefore their detailed understanding is obligatory.

The first aim of this PhD thesis was to explore whether alternatively activated macrophages in fact represent a physiologically relevant alternative source of catecholamines, sufficient to increase the thermogenic capacity of adipocytes. In this thesis, several *in vitro* systems were used to elucidate the role of adipose tissue resident macrophages and alternatively activated macrophages derived from polarization of BMDMs on adipocyte function. Absence of ATMs, achieved by depletion of CD11b-positive macrophages from the SVF of iWAT, did not affect function, differentiation and thermogenic capacity of primary adipocytes (Fig. 5-7). Notably, macrophage depletion was confirmed throughout the whole differentiation process, thus excluding macrophage reconstitution over time (Fig. 5). If M2-type macrophages produce and secrete catecholamines, then it seems reasonable to assume that this would directly induce the thermogenic program in adipocytes. However, the studies of this thesis indicate that the potential of primary adipocytes to beiging/browning and thermogenesis is not changed with activation of M2-type macrophages as treatment of iWAT or BAT primary adipocytes with conditioned media from M2-polarized BMDMs showed no alteration in *Ucp1* expression (Fig. 9,10). Polarization of BMDMs to alternatively activated macrophages by IL-4 was ensured by induction of key markers indicative of M2 macrophages, such as *Arg1*, *Mrc1* and *Mgl2* (Fig. 9,10).

Of note, in the studies of Ajay Chawla and colleagues (Qiu et al., 2014), emphasizing a role of M2 macrophages in promoting adipocyte thermogenesis, both BALB/c and C57Bl/6J

background strains were used in their experimental procedures. For example the following strains were on a BALB/c background: *Il4/13<sup>-/-</sup>*, *Il4ra<sup>-/-</sup>* and *Il4ra<sup>fl/fl</sup>Lyz2<sup>Cre</sup>*, whereas *Th<sup>fl/fl</sup>Lyz2<sup>Cre</sup>* was on a C57Bl/6J background (Qiu et al., 2014). To rule out a possible effect arising from differences in the genetic background or variability in the composition of the gut microbiome that could emerge from usage of different background strains (Ussar et al., 2016), BMDMs and SVF-derived adipocytes isolated from both BALB/c and C57Bl/6J mice were used to test the effect of M2 macrophage activation on adipocyte function and thermogenesis. Notably, secreted factors from IL-4-treated BMDMs derived from either BALB/c or C57Bl/6J mice had no impact on the thermogenic property of primary adipocytes isolated from the respective strains (Fig. 9,10). Thus, IL4-mediated activation of alternatively activated macrophages seems to have no influence on adipocyte function and specifically on its capacity to induce thermogenesis.

To directly address whether alternatively activated macrophages are able to produce catecholamines, absolute levels of NE and other metabolites in IL-4 activated BMDMs, and their supernatants, were determined. No elevated catecholamine levels were detected upon stimulation under these conditions (Fig. 12). These findings are in strong contrast to the literature finding that IL-4 treatment of peritoneal macrophages caused an approximate 30-fold increase in NE levels as compared to vehicle control (Nguyen et al., 2011). Notably, the macrophages showing this 30-fold increase in NE originate from the peritoneal cavity (Nguyen et al., 2011), whereas the macrophages investigated in this thesis stem from the bone marrow. This might explain the discrepancies in the NE measurement, as differences in morphology, proliferation or phenotype are described among macrophages from varying sources (Wang et al., 2013a). However, in the results of this thesis, the BMDMs clearly polarized towards M2-type macrophage phenotype as expression of *Arg1*, *Mgl2* is increased substantially (Fig. 9A-B, 10A-C), indicating that they are fully functional alternatively activated macrophages. Another possibility pertaining to the discrepancy in the NE data could also emerge from utilization of different analyzing methods, since either an Enzyme-linked Immunoabsorbent Assay (ELISA) (Nguyen et al., 2011) or HPLC-based technique was used. Although previous studies reported that macrophages release NE into the culture media, it is important to note that serum utilized in the cell culture also contains NE (Flierl et al., 2007). Taken together, the *in vitro* studies demonstrated that neither the absence of macrophages nor specific activation of M2-type macrophages by IL-4 affected the thermogenic potential of white or brown adipocytes. This obviously speaks against the paradigm that macrophages play a role in BAT thermogenesis. Irrespective of the potential explanations for the differences between the findings reported by Ajay Chawla and colleagues and this thesis, the *in vitro* data from this thesis accordingly challenges the proposed role of alternatively activated macrophages in the regulation of thermogenesis.

In addition to the *in vitro* studies, investigations of this thesis used several *in vivo* experiments to elucidate the role of cold exposure and IL-4 on energy expenditure and thermogenesis.

First, the effect of acute cold exposure on promoting alternative activation of ATMs was explored. Previous studies demonstrated that cold exposure for 6 hours induces activation of M2 macrophages in both iWAT and BAT (Nguyen et al., 2011). When reproducing this acute cold challenge, surprisingly no increase in gene expression of markers indicative of M2 macrophage activation was found, although 6 hours of cold exposure were sufficient to induce the thermogenic program in BAT of cold-exposed mice (Fig. 13).

If alternatively activated macrophages participate in the regulation of nonshivering thermogenesis *in vivo*, then this should alter energy expenditure accordingly. Administration of the cytokine IL-4 increases energy expenditure in a macrophage-dependent manner when mice are exposed to declining ambient temperatures, and this effect is abrogated in mice lacking the *Il4ra* in myeloid cells (Nguyen et al., 2011, Qiu et al., 2014). In this work, it was also investigated whether activation of M2 macrophages, induced by chronic administration of IL-4 affects energy metabolism at varying ambient temperatures. In fact, IL-4 treatment caused tremendous activation of M2-type macrophages in BAT of cold-exposed WT mice (Fig. 14D-F). Nonetheless, oxygen consumption remained unaffected by IL-4 treatment in WT mice at any tested temperature (Fig. 14B). Further, IL-4 treatment failed to induce NE or other intermediates or products of the catecholamine synthesis, supporting that alternatively activated macrophages are incapable of producing catecholamines via an immune-dependent mechanism (Fig. 15F-J). Essential for such literature comparison, the IL-4 study in which energy expenditure in WT and *Il4ra*<sup>-/-</sup> mice was assessed was reproduced as carefully as possible with respect to the experimental outline reported by Ajay Chawla and colleagues (Qiu et al., 2014). Despite using the same origin of mice, treatment duration, temperature challenge protocol, dose and provider of the recombinant IL-4, one noteworthy difference in the experimental details remains. In this thesis, a recombinant IL-4 was administered, whereas Ajay Chawla and colleagues injected a complex of recombinant IL-4 and anti-IL-4 monoclonal antibody (Qiu et al., 2014). It has been shown that *in vivo* administration of a mixture of the cytokine IL-4 and its neutralizing anti-IL-4 antibody enhances and prolongs the *in vivo* activity of IL-4 (Finkelman et al., 1993). Although no anti-IL-4 antibody was used as a potentiating strategy herein, administration of IL-4 alone was sufficient to increase expression of *Arg1* 40-fold as compared to vehicle, indicating that such treatment potently activated M2 macrophages (Fig. 14D). In addition, it has been shown that one acute injection of pure recombinant IL-4 is sufficient to increase oxygen consumption in WT mice at room temperature for at least 7 hours (Nguyen et al., 2011). Thus, it seems



unlikely that utilization of either IL-4 alone or in complex with the anti-IL-4 antibody could explain the controversial results in energy expenditure alteration.

In line with the current observation that energy expenditure is not affected by IL-4 treatment, a similar study in WT and *Ucp1*<sup>-/-</sup> mice to elucidate the effect of IL-4 on energy metabolism was performed in collaboration with Barbara Cannon and colleagues. Notably, chronic IL-4 treatment induced *Arg1* expression in the BAT of cold-exposed mice lacking *Ucp1*, however no difference in oxygen consumption and thermal conductance was observed during declining temperatures in IL-4-treated WT or *Ucp1*<sup>-/-</sup> mice as compared to vehicle controls (Fischer et al., 2017). These data showing no positive effect of IL-4 on energy expenditure in WT mice correlate with our finding and therefore support the assumption that M2-type macrophages have a negligible effect on energy homeostasis.

Tyrosine hydroxylase (TH), the rate-limiting enzyme in catecholamine synthesis, has been shown to be essential for mediating the previously described effects to enhance nonshivering thermogenesis by alternatively activated macrophages (Molinoff and Axelrod, 1971, Nguyen et al., 2011, Rao et al., 2014). Although IL-4 treatment was unable to induce catecholamines, such as NE, in both *in vitro* cultured BMDMs and in BAT of cold-exposed mice, another aim of this thesis was to more directly address the question whether macrophages possess the machinery to produce catecholamines. In this thesis it has been shown that Mac-2 expressing macrophages do not colocalize with TH in either room temperature or cold-exposed adipose depots (Fig. 16A,B), thus macrophages likely do not express the enzyme TH. Surprisingly only very few Mac-2 expressing macrophages were found at all in the BAT of cold-exposed mice (Fig. 16C).

In another collaborative project, Steffen Jung and colleagues, demonstrated the absence of TH signal in BAT macrophages of cold-exposed reporter mice expressing tdTomato under the control of the TH promoter (Fischer et al., 2017). RNA sequencing and FACS analysis likewise failed to detect TH expression in Cx3cr1-positive mononuclear phagocytes upon cold exposure (Fischer et al., 2017).

Consistent with the lack of TH expression and catecholamine production in macrophages, inducible deletion of *TH* in bone marrow chimeras showed no impairment in energy expenditure at either room temperature or cold as demonstrated by our collaborator Christoph Buettner and colleagues (Fischer et al., 2017). Notably, the inducible TH chimera exhibited a cold-induced increase in iWAT *Ucp1* levels comparable to that observed in WT control mice (Fischer et al., 2017).

In summary, the data of this PhD thesis indicate that alternatively activated macrophages are not involved in regulating energy metabolism. Alternatively activated macrophages are

---

unable to produce catecholamines due to the absence of requisite TH. Thus, macrophages do not contribute to adipose tissue thermogenesis. These observations contradict the paradigm that alternatively activated macrophages provide an alternative source of catecholamines to sustain thermogenesis (Nguyen et al., 2011). Conversely, the results of this PhD thesis confirm that the SNS is presumably is the key source of catecholamines driving adipose tissue thermogenesis and the associated metabolic effects.

## 5.2 Role of the scaffold protein p62 on BAT thermogenesis

Nonshivering thermogenesis is controlled by the SNS through the release of NE, which is secreted by the adrenal medulla and then binds to the  $\beta$ -adrenergic receptor located on the cell surface of the adipocytes. Binding of NE to the  $\beta_3$ -adrenergic receptor then orchestrates a coordinated set of intracellular responses. Stimulation of intracellular cAMP levels triggers activation of PKA that subsequently phosphorylates a series of proteins involved in the lipolytic and thermogenic process, such as CREB and p38 MAPK. P-p38 then activates ATF2, which, similar to CREB, translocates into the nucleus to induce expression of *Pgc-1 $\alpha$*  and *Ucp1*. At the distal end of the signaling cascade, UCP1, the key factor in the thermogenic program mediates heat generation by uncoupling oxidative phosphorylation from ATP synthesis in the mitochondria. The UCP1 enhancer region contains one PPAR-responsive element (PPRE) and two putative CREs (Cassard-Doucier et al., 1993, Kozak et al., 1994, Sears et al., 1996). Administration of PPAR $\gamma$  ligands, such as synthetic thiazolidinedione drugs has been shown to induce a thermogenic response (Foellmi-Adams et al., 1996). PPRE is conserved among different species and is essential in regulating UCP1 activity (Cao et al., 2001). In contrast, the CREs are not well conserved (Cao et al., 2001) and only one of the two CRE sequences seems to mediate NE-dependent stimulation of UCP1, while the other is only marginally significant (Kozak et al., 1994).

P38 MAPK is an important downstream mediator of the cAMP/PKA signaling pathway and recently two crucial targets of p38 have been identified to connect the  $\beta$ -adrenergic signal into UCP1 activity. The first target is ATF2, which is phosphorylated by p38 MAPK and triggers transcriptional induction of *Ucp1* and *Pgc-1 $\alpha$*  through CRE binding (Cao et al., 2004). The second target of p38 is the *Pgc-1 $\alpha$*  protein, which binds to the UCP1 promoter and activates transcription of *Ucp1* (Cao et al., 2004). Although the UCP1 promoter region, especially the PPRE sequence, has been well characterized at a molecular level, the precise mechanism how *Ucp1* expression is regulated is not completely understood.

The scaffold protein p62 regulates energy metabolism by controlling mitochondrial function and BAT thermogenesis (Rodriguez et al., 2006, Muller et al., 2013). Global and adipocyte-specific ablation of p62 cause obesity, glucose intolerance and insulin resistance. Mice lacking p62 specifically in the adipose tissue contained mitochondria with fewer cristae and had a decrease in oxidative capacity, indicating mitochondrial dysfunction in the BAT (Muller et al., 2013). The BAT of p62-deficient mice had enhanced lipid deposition and decreased expression of key thermogenic regulatory genes such as *Ucp1* and *Pgc-1 $\alpha$* , indicating that p62 regulates BAT thermogenesis (Muller et al., 2013). Isoproterenol-induced activation of p38 and its downstream target ATF2 were reduced in p62-deficient primary brown adipocytes (Muller et al., 2013). These data suggest that p62 affects BAT thermogenesis via

interfering in the MAPK pathway. However, so far it remained unknown what specific domain of p62 is causing the obesity and these alterations in the MAPK signaling. Thus, one major aim of this thesis was to identify the p62 domain that controls BAT thermogenesis and to examine the function of p62 in the MAPK pathway.

Mice that globally lack the AA 69-251 of p62 are useful for exploring the mechanistic underpinnings of how p62 regulates BAT thermogenesis, since this specific region AA 69-251 harbors the p38-binding domain (Hillmann, 2011). Side by side metabolic phenotyping demonstrated that specific lack of AA 69-251 of p62 is sufficient to recapitulate the metabolic syndrome phenotype of global p62<sup>-/-</sup> mice and mice lacking p62 in the adipose tissue (Fig. 20). P62<sup>Δ69-251</sup> mice develop severe obesity, which is primarily due to an increase in fat mass (Fig. 19A,B). Previous studies suggested that the obese phenotype of p62-deficient mice is a consequence of hyperphagia (Harada et al., 2013). However in this work, no alterations in food intake were observed between WT and p62<sup>Δ69-251</sup> mice even during thermoneutral housing conditions (Fig. 19C, 24C), indicating that the lack of p62-driven obesity is not caused by hyperphagia.

Obese p62<sup>Δ69-251</sup> mice were also glucose intolerant, likely secondary to their greater adiposity, since studies showed that glucose and insulin tolerance was normal in lean p62-deficient mice (Rodriguez et al., 2006).

Consistent with p62 ablation causing a reduction in energy expenditure (Rodriguez et al., 2006, Muller et al., 2013), p62<sup>Δ69-251</sup> mice had a comparable reduction in energy expenditure (Fig. 21B). Hence, the primary focus of this part of the thesis was to decipher the molecular defect responsible for the reduction in energy expenditure.

Since BAT not only functions to dissipate heat, but also possesses a great capacity for glucose uptake to regulate whole-body glycemia (Townsend and Tseng, 2014). Glucose utilization in BAT of p62<sup>Δ69-251</sup> mice was reduced (Fig. 22A,B). This reduction in glucose uptake was in line with the observation that ablation of p62<sup>Δ69-251</sup> caused hyperglycemia (Fig. 19D), suggesting that glucose homeostasis is unbalanced in obese p62<sup>Δ69-251</sup> mice. Since activation of BAT by cold exposure has been associated with increased glucose utilization, a reduction in glucose uptake in the BAT could indicate impairment in BAT thermogenesis. In fact, genetic programs controlling BAT thermogenesis (*Ucp1*, *Pgc-1α*, *Dio2*, *Cidea*, *Bmp8b*) were down regulated in obese p62<sup>Δ69-251</sup> mice (Fig. 22D), clearly demonstrating that UCP1, the key regulator of the thermogenesis cannot be activated. Instead, p-ATF2, the transcriptional activator of *Ucp1* was hyperphosphorylated in the BAT of obese p62<sup>Δ69-251</sup> mice (Fig. 22E), which suggests that the system strives to compensate for the defect in UCP1 activation by increasing phosphorylation of ATF2. Even before the onset of obesity,

p62<sup>Δ69-251</sup> mice show reduced expression of key markers indicative of thermogenesis, such as *Ucp1*, *Pgc-1α*, *Prdm16*, *Cidea* in the BAT as well as lower protein levels of UCP1 in the iWAT (Fig. 23D,E), indicating that loss of AA 69-251 of p62 has a causal effect on thermogenesis. In line with that observation, p62<sup>Δ69-251</sup> pups as young as 7 days display a lower surface temperature in the interscapular region (Fig. 23A,B), which further supports the fundamental role of this specific domain of p62 in the regulation of thermogenesis. Primary cell experiments showed that lack of AA 69-251 of p62 is detrimental to activation of UCP1 and in particular this constitutes a cell-autonomous effect by the differentiated brown adipocytes derived from p62<sup>Δ69-251</sup> mice. This is consistent with previous findings that reported that p62 controls the mitochondrial function of brown adipocytes in a direct and cell-autonomous manner (Muller et al., 2013). Notably, in primary brown adipocytes lacking AA 69-251 of p62 neither UCP1 mRNA nor protein levels were increased by β-adrenergic activation (Fig. 23F,G). P38 and ATF2, however, were highly activated in primary brown adipocytes from p62<sup>Δ69-251</sup> mice under both basal and β-adrenergically stimulated conditions (Fig. 23F). This reinforces the conclusion that impaired UCP1 activity observed in p62<sup>Δ69-251</sup> mice triggers a feedback mechanism that tries to rescue the cell's impairment in BAT thermogenesis through over activation of the MAPK signaling pathway.

Based on previous reports showing that mitochondrial function is affected by the loss of full-length p62, COX activity, a key component of the electron transport chain, was determined in mice lacking AA 69-251 of p62. Surprisingly, no difference in COX activity was observed (Fig. 22G), indicating that this essential complex IV of the respiratory chain is fully functional in the BAT of p62<sup>Δ69-251</sup> mice. This also indicates that the AA 69-251 domain of p62 is not involved in regulation of the electron transport chain that catalyzes the reduction of oxygen, which conflicts with previous findings showing reduced COX activity in BAT of adipocyte-specific p62<sup>-/-</sup> mice (Muller et al., 2013). In this previous study, however, COX activity was normalized to wet tissue weight, which presents some caveats. The p62 KO mice become severely obese, causing hyperplasia of several tissues, including the retroperitoneal fat, spleen or liver (Rodriguez et al., 2006). Progression of this obesity phenotype has the consequence that the BAT is “whitening”. This is driven by a loss of mitochondria due to the accumulation of large lipid droplets, which effectively dilute the number of mitochondria in the BAT. Thus normalization by tissue weight could skew the results. A better strategy may be the normalization of COX activity to protein content. Notably, when normalizing to tissue weight, COX activity in the BAT of p62<sup>Δ69-251</sup> mice measured in this current study is reduced (Fig. 22F). In contrast, after correcting for protein concentration this difference disappeared (Fig. 22G), suggesting that the complex IV is functional in the BAT of these mice.

Ablation of AA 69-251 of p62 has now been solidly demonstrated to cause reduced energy expenditure and impairment in BAT thermogenic function at room temperature (Fig. 21B, Fig. 22). Mice that are housed at 20-23°C are routinely under mild to moderate cold stress. Consequently they have to increase their metabolism to 50-60% above basal in order to defend their body temperature (Golozoubova et al., 2004). The thermoneutral zone of mice is around 30°C, which is best to determine their basal metabolic rate. Metabolic characteristics strongly vary depending on the ambient housing temperature, as best described in mice lacking UCP1 (*Ucp1*<sup>-/-</sup> mice). Although *Ucp1*<sup>-/-</sup> mice are more susceptible to cold and lack the ability to induce adrenergic thermogenesis during cold, they surprisingly do not develop obesity at room temperature (Enerback et al., 1997, Liu et al., 2003). However, under thermoneutral conditions, *Ucp1*<sup>-/-</sup> mice become obese when fed an obesogenic diet or even a regular chow diet (Feldmann et al., 2009).

The impact of the ambient temperature on metabolic behavior and the fact that humans normally also live at thermoneutral temperatures, sparked the interest in examining the role of AA 69-251 of p62 in energy metabolism control at thermoneutrality. Surprisingly, this current study demonstrated that p62<sup>Δ69-251</sup> mice gained fat mass and became severely obese even when housed at 30°C (Fig. 24A,B). Energy expenditure was significantly reduced in p62<sup>Δ69-251</sup> mice when body weight was considered as covariate for ANCOVA (Fig. 24F). To determine the component responsible for the impairment in energy expenditure, the sections of total daily energy expenditure (TDEE) were examined in these mice. Food intake, food efficiency, resting metabolic rate (RMR) and locomotor activity were not affected by the loss of AA 69-251 of p62 (Fig. 24C,G,H). This indicates that the contribution to the reduced energy phenotype likely results from alterations in thermogenesis. A component of TDEE, not yet discussed, is the thermic effect of food (TEF), which is the increase in metabolic rate after ingestion of a meal. The TEF is determined by indirect calorimetry measurement at 30°C through serving a single meal after a fasting period. The TEF can only be distinguished from the RMR if single diet is delivered, as *ad libitum* access to food will hamper measurement of TEF (van Klinken et al., 2013). In the scope of this thesis, TEF could not be measured in p62<sup>Δ69-251</sup> mice and therefore TEF as possible contributor to the low energy expenditure observed in p62<sup>Δ69-251</sup> mice cannot be excluded. The current work, however, examined the thermogenic profile in BAT of p62<sup>Δ69-251</sup> mice that have been housed at 30°C for 18 weeks. Even at thermoneutral conditions, p62<sup>Δ69-251</sup> mice had lower expression of *Ucp1*, *Pgc-1α*, *Prdm16* and *Adrb3* in the BAT (Fig. 24I). In line with previous findings in BAT of room temperature-housed p62<sup>Δ69-251</sup> mice and primary brown adipocytes, hyperphosphorylation of ATF2 was also detected in BAT of p62<sup>Δ69-251</sup> mice kept at 30°C (Fig. 24J,K). This suggests that p62<sup>Δ69-251</sup> mice exhibit impaired BAT thermogenesis even when held at an ambient temperature that is characteristic for minimal active thermoregulation.

This emphasizes the importance of p62 and especially its AA 69-251 in the regulation of energy metabolism and its conserved effect on thermogenesis within the thermoneutral zone.

This thesis unraveled the p62 domain that is controlling BAT thermogenesis and identified the AA 69 to 251 of p62 as an essential region for the control of obesity and energy metabolism. In addition, this work demonstrates that translocation of p-ATF2 into the nucleus is impaired in BAT of p62<sup>Δ69-251</sup> mice (Fig. 25A,B). This likely explains the decreased *Ucp1* mRNA expression in the BAT of p62<sup>Δ69-251</sup> mice (Fig. 22D, 23E, 24I). In contrast, nuclear and cytosolic p-p38 distribution was normal in the BAT of p62<sup>Δ69-251</sup> mice (Fig. 25A,C), suggesting that AA 69-251 of p62 more selectively affect p-ATF2 signaling or transport. Furthermore, using a reporter assay for CRE binding activity in the nucleus, it was shown that the AA 69-251 of p62 are necessary for full CRE binding activity (Fig. 26C,D). One caveat in this approach is that HEK cells still possess endogenous levels of p62. Thus, future studies should focus on p62 knockdown experiments to further investigate the mechanistic details of p62's role in nuclear shuttling of p-ATF2.

The ATF2 protein contains a basal leucine zipper domain that contains nuclear localization and export sequences to facilitate trafficking of ATF2 to and from the nucleus, which is controlled by exportin-1 (Liu et al., 2006, Lau and Ronai, 2012). These small peptide motifs are required by other enzymes, such as β-karyopherins to mediate the active, energy-dependent nuclear transport of proteins via the nuclear pore complex (Freitas and Cunha, 2009). Although AA 69-251 of p62 seems to play an important role in this complex process of nuclear shuttling of p-ATF2, its precise function remains elusive. So far, one could only speculate whether p62 recruits a relevant mediator necessary for nuclear transport of p-ATF2 to enable nuclear shuttling, which is abrogated when the AA 69-251 domain is omitted, or whether p62 exerts a direct interaction with ATF2. Future investigations with respect to the interaction of p62 and ATF2 are urgently required to decipher this conundrum.

Low sympathetic activity has been associated with decreased nonshivering thermogenesis and obesity (Jung et al., 1979). The data of this study evidently demonstrated that the impairment in BAT thermogenesis is relevantly contributing to the progression of obesity in p62<sup>Δ69-251</sup> mice. The conclusion why nonshivering thermogenesis is impaired in these mice is prospectively that ATF2-UCP1 signaling is compromised. This is in line with the observation, that *Ucp1*<sup>-/-</sup> mice become obesogenic under distinct conditions, e.g. when thermal stress is eliminated, in combination with HFD or with age (Liu et al., 2003, Kontani et al., 2005, Feldmann et al., 2009). Contrary to all expectations, *Ucp1*<sup>-/-</sup> mice do not develop obesity when exposed to thermal stress at room temperature housing conditions (Enerback et al., 1997, Liu et al., 2003). Until today, the paradoxical resistance to diet-induced obesity in

Ucp1-ablated mice has not been clarified. However, *Ucp1*<sup>-/-</sup> mice represent a whole-body KO model, whose properties should not be directly compared to those of p62<sup>Δ69-251</sup> mice that mediate an adipose tissue-directed down-regulation of UCP1.

In summary, the work of this thesis identified AA 69-251 of p62 as the region that is regulating BAT thermogenesis. Ablation of this region of p62 causes severe obesity and impaired energy expenditure through interfering in the MAPK pathway, in particular preventing the nuclear transport of p-ATF2.



## 6. Outlook and Perspectives

The relevance and therapeutic potential of targeting BAT thermogenesis to improve metabolic diseases increased with the discovery of active BAT depots in adult humans (Cypess et al., 2009, van Marken Lichtenbelt et al., 2009, Virtanen et al., 2009, Saito, 2013). Understanding the detailed mechanisms of how BAT thermogenesis is activated and what molecular signaling pathways are contributing to modulate thermogenesis is important to develop potential new therapeutics that increase energy expenditure to induce a negative balance and lower body weight.

In this PhD thesis two potential – but distinct – key modulators of BAT thermogenesis were investigated with the overarching objective to gain additional insight into the regulation of nonshivering thermogenesis.

A major finding of this thesis was that alternatively activated macrophages do not play a role in promoting BAT thermogenesis. The data presented in this thesis aligns with similar findings generated by several collaborators (Fischer et al., 2017) and all together refute the proposed alternative pathway in regulating energy metabolism implicating macrophages (Nguyen et al., 2011). The source of these contradictory results remains elusive. Future studies aiming to illuminate this could focus on whether macrophages are capable of taking up and releasing catecholamines, similar to differentiated osteoblasts that exhibit NE uptake activity via the norepinephrine transporter (NET) and can catabolize, but not generate, NE (Ma et al., 2013). If macrophages are capable of taking up NE this could represent a potential mechanism for NE-linked crosstalk between macrophages and adipocytes not involving *de novo* synthesis of catecholamines. Shuttle of NE across the cell membrane is enabled by the transmembrane protein NET. This process can be blocked by administration of tricyclic antidepressants (e.g. desipramine) – a drug class frequently used for treating depression (Gillman, 2007, Bonisch and Bruss, 2006). If the macrophages might express NET, this would be an interesting phenomenon to explore. Thinking ahead, this could perhaps serve as a potential target for pharmaceutical approaches to develop selective NET activating drugs to increase NE uptake. A subsequent recruitment of such NE-loaded macrophages to the adipose depots, allowing them to release NE, might substantially induce the thermogenic program in the adipocytes. For example, macrophage-specific delivery of compounds affecting NET activity could present one such pharmaceutical approach that may be applied for future investigations in case macrophages are in fact capable of taking up catecholamines. The institute in which I did my PhD thesis has championed the field of targeted drug-delivery over the past decade (Tschop et al., 2016) and continuing along these lines could be an interesting new research avenue.

The data obtained from the herein described work demonstrating that macrophages do not affect thermogenesis point to the SNS control still being the main player in BAT thermogenesis. In this context the second major aim of this thesis seems appropriately relevant, i.e. the focus was to obtain mechanistic insights into how p62 functions as a key mediator of UCP1-linked BAT thermogenesis.

In this PhD thesis, the specific domain of the protein p62 that modulates BAT thermogenesis has been identified. This domain, constituting AA 69-251 of p62, was found to affect nuclear transport of p-ATF2 to ultimately regulate UCP1 activity. These findings add new insights into the cellular pathway in which p62 affects UCP1 activation. However, future analyses are required to fully understand the sequential molecular nodes connecting these cellular components. It is still unclear if p62, specifically its AA 69-251, directly interacts with ATF2 and thus affect UCP1 activation, or whether accessory modulators are integrated in this signaling. Co-immunoprecipitation or chromatin immunoprecipitation (ChIP) sequencing studies to analyze protein-protein or protein-DNA interactions could resolve this uncertainty. The multifunctional physiology of the scaffold protein p62 makes determination of its diverse roles challenging. Many crucial interacting proteins of p62 have been identified and assigned to specific regions of p62 that mediate different cellular functions involved in adipogenesis, inflammation, cancer and autophagy (Moscat et al., 2007). For example, p62 activates mTOR, a central regulator of cell growth and autophagy that is activated in many types of cancer (Duran et al., 2011). Notably, the adapter molecule of p62, that triggers activation of mTOR, binds within the p62 region, AA 69-251, that was herein identified to control energy metabolism. Notably, inhibition of raptor, and therefore mTORC1, increases energy expenditure and reverses obesity demonstrating that mTORC1 positively regulates lipogenesis and adiposity (Moscat and Diaz-Meco, 2011). If mTORC1 causes lower energy expenditure while simultaneously preventing autophagy, this could trigger a negative feedback mechanism that increases p62 expression to possibly reduce energy expenditure. High levels of p62 in turn could potentially counteract to increase energy expenditure. The complexities of the interplay of many p62 adaptor proteins in regulation of several cell-signaling cascades are evident and represent a large challenge for future work dealing with the biological actions of p62.

Complete understanding of these key mechanisms of p62's broad signaling network is essential to unravel the diverse functions of p62 in autophagy, inflammation and cancer. Connection of the various functions of p62 and its adaptor proteins could enable the development of new therapeutics by targeting p62-regulated functions in the future.

## Abstract

Brown adipose tissue (BAT) is the major site of nonshivering thermogenesis. In this cold-induced process energy is converted into heat through the uncoupling of oxidative phosphorylation from mitochondrial ATP production. Norepinephrine represents the main driver of sympathetic nervous system (SNS)-mediated activation of nonshivering thermogenesis. However, recent studies suggested that cold-induced activation of alternatively activated macrophages induces local catecholamine production to stimulate nonshivering thermogenesis (Nguyen et al., 2011, Qiu et al., 2014).

**Aim 1: Evaluate and corroborate the role of macrophages in mitochondrial function and nonshivering thermogenesis.** Unexpectedly, the results of this thesis showed that depletion of macrophages from inguinal white adipose tissue (iWAT) and BAT preadipocytes (primary cells) had, upon *in vitro* differentiation, no effect on the thermogenic capacity of these cells. Treatment of iWAT and BAT primary cells with conditioned media from interleukin 4 (IL-4) stimulated bone marrow-derived macrophages (BMDMs) likewise had no impact on thermogenic pathways and for example the expression of the uncoupling protein 1 (*Ucp1*) and the Peroxisome proliferator-activated receptor gamma coactivator 1-alpha (*Pgc-1 $\alpha$* ) was unaffected. In agreement, IL-4 treatment of mice at various environmental temperatures ranging from thermoneutrality to cold exposure had no additional effect on energy expenditure. Similarly, no difference in energy expenditure was observed between *Il4ra*<sup>-/-</sup> mice and their wild-type (WT) controls. In addition, no colocalization of tyrosine hydroxylase (TH) and galectin 3 (Mac-2) signal was observed in iWAT or BAT of mice kept at either room temperature or 4°C, indicating that macrophages do not express TH, the key enzyme for catecholamine synthesis. Collectively, these data suggest that alternatively activated macrophages do not play a major role in the regulation of nonshivering thermogenesis. This instead reconfirms that the SNS is the key source of catecholamines relevant for adipose tissue biology and energy homeostasis.

**Aim 2: Identify the molecular mechanisms underlying energy metabolism control by the scaffold protein p62.**

The scaffold protein p62 was recently shown to regulate energy metabolism via modulation of mitochondrial function and BAT thermogenesis (Rodriguez et al., 2006, Muller et al., 2013). The aim of this work was therefore to unravel the mechanistic underpinnings underlying energy metabolism control by p62. To identify the p62 domain responsible for impaired BAT thermogenesis, mice that globally lack AA (AA) 69-251 of p62 (p62 <sup>$\Delta$ 69-251</sup>) were metabolically characterized. Thorough metabolic characterization demonstrated that obesity of the p62 <sup>$\Delta$ 69-251</sup> mice is exclusively a result of increased body fat mass and is not related to differences in food intake. Instead, energy expenditure is impaired in p62 <sup>$\Delta$ 69-251</sup> mice, notably, even before the onset of obesity. In line with the lower energy expenditure, key regulatory

pathways of BAT function (*Ucp1*, *Pgc-1 $\alpha$* ) were decreased in BAT of p62 <sup>$\Delta$ 69-251</sup> mice. In addition, protein levels of UCP1 were decreased in BAT primary cells of the p62 <sup>$\Delta$ 69-251</sup> mice and were resistant to  $\beta$ -adrenergic receptor stimulation. Of note, the activating transcription factor 2 (ATF2), regulator of *Ucp1*, cannot enter the nucleus in the BAT of p62 <sup>$\Delta$ 69-251</sup> mice, thus preventing activation of *Ucp1*. Together, the data of this thesis identify AA 69-251 of p62 as the key functional domain exclusively mediating the obese phenotype and suggest a role of this specific domain of p62 in nuclear shuttling of ATF2 to control BAT thermogenesis.

## Zusammenfassung

Braunes Fettgewebe ist in der Lage durch zitterfreie Thermogenese überschüssige Energiereserven in Wärme umzuwandeln um so vor Kälte zu schützen. Zitterfreie Thermogenese wird durch das sympathische Nervensystem (SNS) stimuliert, wobei primär das Hormon Noradrenalin zur Wärmeproduktion beiträgt. Kürzlich wurde jedoch gezeigt, dass alternativ aktivierte Makrophagen (Typ 2) in der Lage sind lokal im braunen Fettgewebe Katecholamine wie Noradrenalin zu produzieren, um den Prozess der zitterfreien Thermogenese zu induzieren (Nguyen et al., 2011, Qiu et al., 2014).

***Das erste Ziel dieser Dissertation war die Rolle von Typ 2 aktivierten Makrophagen auf die Funktion der zitterfreien Thermogenese zu untersuchen.***

Es wurde gezeigt, dass die Eliminierung von Makrophagen in Preadipozyten (Primärzellen), isoliert aus weißem oder braunem Fettgewebe und *in vitro* differenziert zu gereiften Adipozyten, keinen Einfluss auf die Fähigkeit dieser Zellen zur Thermogenese hat. Wenn Knochenmark isolierte Makrophagen mit Interleukine 4 (IL-4) behandelt werden führt dies zur Aktivierung der naiven Makrophagen zu einem Typ 2 Phänotyp. Behandelt man primäre Adipozyten mit jenem Zellüberstand, führt dies zu keiner Verbesserung der zitterfreien Thermogenese. Mäuse die chronisch mit IL-4 behandelt wurden, zeigten zudem keinen Unterschied im Energiestoffwechsel im Vergleich zu unbehandelten Mäusen. Außerdem haben Kolokalisations-Studien gezeigt, dass Makrophagen nicht fähig sind das für die Katecholamine Synthese essentielle Enzym Tyrosine Hydroxylase (TH) zu synthetisieren. Im Gegensatz zu zahlreichen veröffentlichten Studien deuten die Daten dieser Arbeit darauf hin dass Typ 2 Makrophagen keine relevante Rolle in der Regulierung der zitterfreien Thermogenese im Energiestoffwechsel spielen. Stattdessen verdeutlicht dies die fundamentale Rolle des SNS als Katecholaminlieferant zur Initiierung der zitterfreien Thermogenese.

***Das zweite Ziel dieser Dissertation bestand darin den molekularen Mechanismus, wie das Gerüstprotein p62 den Energiestoffwechsel reguliert zu identifizieren.***

Dem Gerüstprotein p62 wurde kürzlich eine wichtige Rolle im Energiestoffwechsel genauer gesagt der Modulation in der Funktion von Mitochondrien und der zitterfreien Thermogenese zugeschrieben (Rodriguez et al., 2006, Muller et al., 2013).

Zur Identifizierung der Domäne von p62 die verantwortlich ist für die Regulierung der zitterfreien Thermogenese wurde eine genetisch veränderte Maus metabolisch phänotypisiert der die Aminosäuren 69 bis 251 von p62 fehlen (p62<sup>Δ69-251</sup>). Es wurde beobachtet, dass p62<sup>Δ69-251</sup> Mäuse einen ähnlichen adipösen Phänotyp mit erhöhter Fettmasse, jedoch unveränderter Futteraufnahme, zu Mäusen mit Deletion des gesamten p62 aufweisen. Des Weiteren ist der Energiestoffwechsel in p62<sup>Δ69-251</sup> Mäusen, bereits vor Ausbruch der Adipositas, verschlechtert, und die Expression von Schlüsselgenen der

zitterfreien Thermogenese, wie das „uncoupling protein 1“ (*Ucp1*) im braunen Fett ist reduziert. Primäre braune Adipozyten, isoliert aus dem braunen Fett von  $p62^{\Delta 69-251}$  Mäusen, sind resistent zu  $\beta$ -adrenerger Stimulierung, da das Protein UCP1 nicht mehr aktiviert werden kann. Zusätzlich wurde gezeigt, dass der „activating transcription factor 2“ (ATF2), ein Transkriptionsfaktor von UCP1, im braunen Fett von  $p62^{\Delta 69-251}$  Mäusen nicht mehr in den Nukleus transportiert werden kann. Hiermit wurde die funktionelle Domäne von p62 identifiziert, die verantwortlich ist für den adipösen Phänotyp. Außerdem deuten die Daten darauf hin, dass die Aminosäuren 69 bis 251 von p62 eine essentielle Rolle im Transport von ATF2 in den Nukleus spielen um somit die zitterfreie Thermogenese im braunen Fett zu regulieren.

## References

2000. Obesity: preventing and managing the global epidemic. Report of a WHO consultation. *World Health Organ Tech Rep Ser*, 894, i-xii, 1-253.
- BAO, Q., NEWPORT, D., CHEN, M., STOUT, D. B. & CHATZIOANNOU, A. F. 2009. Performance evaluation of the inveon dedicated PET preclinical tomograph based on the NEMA NU-4 standards. *J Nucl Med*, 50, 401-8.
- BARGMANN, W., VON HEHN, G. & LINDNER, E. 1968. [On the cells of the brown fatty tissue and their innervation]. *Z Zellforsch Mikrosk Anat*, 85, 601-13.
- BARTNESS, T. J., VAUGHAN, C. H. & SONG, C. K. 2010. Sympathetic and sensory innervation of brown adipose tissue. *Int J Obes (Lond)*, 34 Suppl 1, S36-42.
- BAUER, U. E., BRISS, P. A., GOODMAN, R. A. & BOWMAN, B. A. 2014. Prevention of chronic disease in the 21st century: elimination of the leading preventable causes of premature death and disability in the USA. *Lancet*, 384, 45-52.
- BAYS, H. E., TOTH, P. P., KRIS-ETHERTON, P. M., ABATE, N., ARONNE, L. J., BROWN, W. V., GONZALEZ-CAMPOY, J. M., JONES, S. R., KUMAR, R., LA FORGE, R. & SAMUEL, V. T. 2013. Obesity, adiposity, and dyslipidemia: a consensus statement from the National Lipid Association. *J Clin Lipidol*, 7, 304-83.
- BERGER, N. A. 2014. Obesity and cancer pathogenesis. *Ann N Y Acad Sci*, 1311, 57-76.
- BLOCK, B. A. 1994. Thermogenesis in muscle. *Annu Rev Physiol*, 56, 535-77.
- BONISCH, H. & BRUSS, M. 2006. The norepinephrine transporter in physiology and disease. *Handb Exp Pharmacol*, 485-524.
- BOSTROM, P., WU, J., JEDRYCHOWSKI, M. P., KORDE, A., YE, L., LO, J. C., RASBACH, K. A., BOSTROM, E. A., CHOI, J. H., LONG, J. Z., KAJIMURA, S., ZINGARETTI, M. C., VIND, B. F., TU, H., CINTI, S., HOJLUND, K., GYGI, S. P. & SPIEGELMAN, B. M. 2012. A PGC1-alpha-dependent myokine that drives brown-fat-like development of white fat and thermogenesis. *Nature*, 481, 463-8.
- BRESTOFF, J. R., KIM, B. S., SAENZ, S. A., STINE, R. R., MONTICELLI, L. A., SONNENBERG, G. F., THOME, J. J., FARBER, D. L., LUTFY, K., SEALE, P. & ARTIS, D. 2015. Group 2 innate lymphoid cells promote beiging of white adipose tissue and limit obesity. *Nature*, 519, 242-6.
- BÜRGIS, S. 2006. *Interleukin-4 Receptor Signal Transduction: Involvement of p62*. University Erlangen-Nürnberg.
- CALLE, E. E., RODRIGUEZ, C., WALKER-THURMOND, K. & THUN, M. J. 2003. Overweight, obesity, and mortality from cancer in a prospectively studied cohort of U.S. adults. *N Engl J Med*, 348, 1625-38.
- CALLE, E. E. & THUN, M. J. 2004. Obesity and cancer. *Oncogene*, 23, 6365-78.
- CANNON, B. & NEDERGAARD, J. 2004. Brown adipose tissue: function and physiological significance. *Physiol Rev*, 84, 277-359.
- CANNON, B. & NEDERGAARD, J. 2011. Nonshivering thermogenesis and its adequate measurement in metabolic studies. *J Exp Biol*, 214, 242-53.
- CAO, W., DANIEL, K. W., ROBIDOUX, J., PUIGSERVER, P., MEDVEDEV, A. V., BAI, X., FLOERING, L. M., SPIEGELMAN, B. M. & COLLINS, S. 2004. p38 mitogen-activated protein

- kinase is the central regulator of cyclic AMP-dependent transcription of the brown fat uncoupling protein 1 gene. *Mol Cell Biol*, 24, 3057-67.
- CAO, W., MEDVEDEV, A. V., DANIEL, K. W. & COLLINS, S. 2001. beta-Adrenergic activation of p38 MAP kinase in adipocytes: cAMP induction of the uncoupling protein 1 (UCP1) gene requires p38 MAP kinase. *J Biol Chem*, 276, 27077-82.
- CASSARD-DOULCIER, A. M., GELLY, C., FOX, N., SCHREMENTI, J., RAIMBAULT, S., KLAUS, S., FOREST, C., BOUILLAUD, F. & RICQUIER, D. 1993. Tissue-specific and beta-adrenergic regulation of the mitochondrial uncoupling protein gene: control by cis-acting elements in the 5'-flanking region. *Mol Endocrinol*, 7, 497-506.
- CHAFFEE, R. R. & ROBERTS, J. C. 1971. Temperature acclimation in birds and mammals. *Annu Rev Physiol*, 33, 155-202.
- CHEN, J., GUAN, Z., WANG, L., SONG, G., MA, B. & WANG, Y. 2014. Meta-analysis: overweight, obesity, and Parkinson's disease. *Int J Endocrinol*, 2014, 203930.
- CHEN, Z. J., BHOJ, V. & SETH, R. B. 2006. Ubiquitin, TAK1 and IKK: is there a connection? *Cell Death Differ*, 13, 687-92.
- CINTI, S. 2002. Adipocyte differentiation and transdifferentiation: plasticity of the adipose organ. *J Endocrinol Invest*, 25, 823-35.
- CINTI, S. 2009. Transdifferentiation properties of adipocytes in the adipose organ. *Am J Physiol Endocrinol Metab*, 297, E977-86.
- CINTI, S. 2012. The adipose organ at a glance. *Dis Model Mech*, 5, 588-94.
- COHEN, P. & SPIEGELMAN, B. M. 2015. Brown and Beige Fat: Molecular Parts of a Thermogenic Machine. *Diabetes*, 64, 2346-51.
- CYPRESS, A. M. & KAHN, C. R. 2010. The role and importance of brown adipose tissue in energy homeostasis. *Curr Opin Pediatr*, 22, 478-84.
- CYPRESS, A. M., LEHMAN, S., WILLIAMS, G., TAL, I., RODMAN, D., GOLDFINE, A. B., KUO, F. C., PALMER, E. L., TSENG, Y. H., DORIA, A., KOLODNY, G. M. & KAHN, C. R. 2009. Identification and importance of brown adipose tissue in adult humans. *N Engl J Med*, 360, 1509-17.
- DANSINGER, M. L., GLEASON, J. A., GRIFFITH, J. L., SELKER, H. P. & SCHAEFER, E. J. 2005. Comparison of the Atkins, Ornish, Weight Watchers, and Zone diets for weight loss and heart disease risk reduction: a randomized trial. *JAMA*, 293, 43-53.
- DIVAKARUNI, A. S. & BRAND, M. D. 2011. The regulation and physiology of mitochondrial proton leak. *Physiology (Bethesda)*, 26, 192-205.
- DURAN, A., AMANCHY, R., LINARES, J. F., JOSHI, J., ABU-BAKER, S., POROLLO, A., HANSEN, M., MOSCAT, J. & DIAZ-MECO, M. T. 2011. p62 is a key regulator of nutrient sensing in the mTORC1 pathway. *Mol Cell*, 44, 134-46.
- DURAN, A., LINARES, J. F., GALVEZ, A. S., WIKENHEISER, K., FLORES, J. M., DIAZ-MECO, M. T. & MOSCAT, J. 2008. The signaling adaptor p62 is an important NF-kappaB mediator in tumorigenesis. *Cancer Cell*, 13, 343-54.
- DURAN, A., SERRANO, M., LEITGES, M., FLORES, J. M., PICARD, S., BROWN, J. P., MOSCAT, J. & DIAZ-MECO, M. T. 2004. The atypical PKC-interacting protein p62 is an important mediator of RANK-activated osteoclastogenesis. *Dev Cell*, 6, 303-9.



- EMORINE, L. J., MARULLO, S., BRIEND-SUTREN, M. M., PATEY, G., TATE, K., DELAVIER-KLUTCHKO, C. & STROSBERG, A. D. 1989. Molecular characterization of the human beta 3-adrenergic receptor. *Science*, 245, 1118-21.
- ENERBACK, S., JACOBSSON, A., SIMPSON, E. M., GUERRA, C., YAMASHITA, H., HARPER, M. E. & KOZAK, L. P. 1997. Mice lacking mitochondrial uncoupling protein are cold-sensitive but not obese. *Nature*, 387, 90-4.
- FABBIANO, S., SUAREZ-ZAMORANO, N., RIGO, D., VEYRAT-DUREBEX, C., STEVANOVIC DOKIC, A., COLIN, D. J. & TRAJKOVSKI, M. 2016. Caloric Restriction Leads to Browning of White Adipose Tissue through Type 2 Immune Signaling. *Cell Metab*, 24, 434-46.
- FARMER, S. R. 2006. Transcriptional control of adipocyte formation. *Cell Metab*, 4, 263-73.
- FELDMANN, H. M., GOLOZOUBOVA, V., CANNON, B. & NEDERGAARD, J. 2009. UCP1 ablation induces obesity and abolishes diet-induced thermogenesis in mice exempt from thermal stress by living at thermoneutrality. *Cell Metab*, 9, 203-9.
- FERRANTE, A. W., JR. 2013. The immune cells in adipose tissue. *Diabetes Obes Metab*, 15 Suppl 3, 34-8.
- FILOMENI, G., DE ZIO, D. & CECCONI, F. 2015. Oxidative stress and autophagy: the clash between damage and metabolic needs. *Cell Death Differ*, 22, 377-88.
- FINKELMAN, F. D., MADDEN, K. B., MORRIS, S. C., HOLMES, J. M., BOIANI, N., KATONA, I. M. & MALISZEWSKI, C. R. 1993. Anti-cytokine antibodies as carrier proteins. Prolongation of in vivo effects of exogenous cytokines by injection of cytokine-anti-cytokine antibody complexes. *J Immunol*, 151, 1235-44.
- FISCHER, K., RUIZ, H., H., JHUN, K., FINAN, B., OBERLIN, D., J., HEIDE, V., KALINOVICH, A., V., PETROVIC, N., WOLF, Y., CLEMMENSEN, C., SHIN, A. C., DIVANOVIC, S., BROMBACHER, F., GLASMACHER, E., KEIPERT, S., JASTROCH, M., NAGLER, J., SCHRAMM, K.-W., MEDRIKOVA, D., COLLDEN, G., WOODS, S., C., HERZIG, S., HOMANN, D., JUNG, S., NEDERGAARD, J., CANNON, B., TSCHÖP, M., H., MÜLLER, T., D. & BUETTNER, C. 2017. Alternatively activated macrophages do not synthesize catecholamines or contribute to adipose tissue adaptive thermogenesis. *Nat Med*, in press.
- FLIERL, M. A., RITTIRSCH, D., NADEAU, B. A., CHEN, A. J., SARMA, J. V., ZETOUNE, F. S., MCGUIRE, S. R., LIST, R. P., DAY, D. E., HOESEL, L. M., GAO, H., VAN ROOIJEN, N., HUBER-LANG, M. S., NEUBIG, R. R. & WARD, P. A. 2007. Phagocyte-derived catecholamines enhance acute inflammatory injury. *Nature*, 449, 721-5.
- FOELLM-ADAMS, L. A., WYSE, B. M., HERRON, D., NEDERGAARD, J. & KLETZIEN, R. F. 1996. Induction of uncoupling protein in brown adipose tissue. Synergy between norepinephrine and pioglitazone, an insulin-sensitizing agent. *Biochem Pharmacol*, 52, 693-701.
- FOSTER, D. O. & FRYDMAN, M. L. 1979. Tissue distribution of cold-induced thermogenesis in conscious warm- or cold-acclimated rats reevaluated from changes in tissue blood flow: the dominant role of brown adipose tissue in the replacement of shivering by nonshivering thermogenesis. *Can J Physiol Pharmacol*, 57, 257-70.
- FREDRIKSSON, J. M., THONBERG, H., OHLSON, K. B., OHBA, K., CANNON, B. & NEDERGAARD, J. 2001. Analysis of inhibition by H89 of UCP1 gene expression and thermogenesis indicates protein kinase A mediation of beta(3)-adrenergic signalling rather than beta(3)-adrenoceptor antagonism by H89. *Biochim Biophys Acta*, 1538, 206-17.
- FREITAS, N. & CUNHA, C. 2009. Mechanisms and signals for the nuclear import of proteins. *Curr Genomics*, 10, 550-7.
- FRONTINI, A. & CINTI, S. 2010. Distribution and development of brown adipocytes in the murine and human adipose organ. *Cell Metab*, 11, 253-6.

- GARBETT, D. & BRETSCHER, A. 2014. The surprising dynamics of scaffolding proteins. *Mol Biol Cell*, 25, 2315-9.
- GARLAND, H. 1995. *The Evolution of Endothermy: Testing the Aerobic Capacity Model*.
- GARLAND, T., JR., SCHUTZ, H., CHAPPELL, M. A., KEENEY, B. K., MEEK, T. H., COPES, L. E., ACOSTA, W., DRENOWATZ, C., MACIEL, R. C., VAN DIJK, G., KOTZ, C. M. & EISENMANN, J. C. 2011. The biological control of voluntary exercise, spontaneous physical activity and daily energy expenditure in relation to obesity: human and rodent perspectives. *J Exp Biol*, 214, 206-29.
- GARLID, K. D., JABUREK, M. & JEZEK, P. 1998. The mechanism of proton transport mediated by mitochondrial uncoupling proteins. *FEBS Lett*, 438, 10-4.
- GEISLER, J. G. 2011. Targeting energy expenditure via fuel switching and beyond. *Diabetologia*, 54, 237-44.
- GESTA, S., TSENG, Y. H. & KAHN, C. R. 2007. Developmental origin of fat: tracking obesity to its source. *Cell*, 131, 242-56.
- GILLMAN, P. K. 2007. Tricyclic antidepressant pharmacology and therapeutic drug interactions updated. *Br J Pharmacol*, 151, 737-48.
- GINHOUX, F., GRETER, M., LEBOEUF, M., NANDI, S., SEE, P., GOKHAN, S., MEHLER, M. F., CONWAY, S. J., NG, L. G., STANLEY, E. R., SAMOKHVALOV, I. M. & MERAD, M. 2010. Fate mapping analysis reveals that adult microglia derive from primitive macrophages. *Science*, 330, 841-5.
- GLICK, D., BARTH, S. & MACLEOD, K. F. 2010. Autophagy: cellular and molecular mechanisms. *J Pathol*, 221, 3-12.
- GOLOZOUBOVA, V., GULLBERG, H., MATTHIAS, A., CANNON, B., VENNSTROM, B. & NEDERGAARD, J. 2004. Depressed thermogenesis but competent brown adipose tissue recruitment in mice devoid of all hormone-binding thyroid hormone receptors. *Mol Endocrinol*, 18, 384-401.
- GORDON, S., PLUDDMANN, A. & MARTINEZ ESTRADA, F. 2014. Macrophage heterogeneity in tissues: phenotypic diversity and functions. *Immunol Rev*, 262, 36-55.
- GREENBERG, A. S., EGAN, J. J., WEK, S. A., GARTY, N. B., BLANCHETTE-MACKIE, E. J. & LONDOS, C. 1991. Perilipin, a major hormonally regulated adipocyte-specific phosphoprotein associated with the periphery of lipid storage droplets. *J Biol Chem*, 266, 11341-6.
- GRIGGIO, M. A. 1982. The participation of shivering and nonshivering thermogenesis in warm and cold-acclimated rats. *Comp Biochem Physiol A Comp Physiol*, 73, 481-4.
- GUO, F. & GARVEY, W. T. 2016. Trends in Cardiovascular Health Metrics in Obese Adults: National Health and Nutrition Examination Survey (NHANES), 1988-2014. *J Am Heart Assoc*, 5.
- HALL, K. D., HEYMSFIELD, S. B., KEMNITZ, J. W., KLEIN, S., SCHOELLER, D. A. & SPEAKMAN, J. R. 2012. Energy balance and its components: implications for body weight regulation. *Am J Clin Nutr*, 95, 989-94.
- HAMACHER, K., COENEN, H. H. & STOCKLIN, G. 1986. Efficient stereospecific synthesis of no-carrier-added 2-[<sup>18</sup>F]-fluoro-2-deoxy-D-glucose using aminopolyether supported nucleophilic substitution. *J Nucl Med*, 27, 235-8.
- HAMILTON, J. M., BARTNESS, T. J. & WADE, G. N. 1989. Effects of norepinephrine and denervation on brown adipose tissue in Syrian hamsters. *Am J Physiol*, 257, R396-404.

- HARADA, H., WARABI, E., MATSUKI, T., YANAGAWA, T., OKADA, K., UWAYAMA, J., IKEDA, A., NAKASO, K., KIRII, K., NOGUCHI, N., BUKAWA, H., SIOW, R. C., MANN, G. E., SHODA, J., ISHII, T. & SAKURAI, T. 2013. Deficiency of p62/Sequestosome 1 causes hyperphagia due to leptin resistance in the brain. *J Neurosci*, 33, 14767-77.
- HARMS, M. & SEALE, P. 2013. Brown and beige fat: development, function and therapeutic potential. *Nat Med*, 19, 1252-63.
- HASHIMOTO, D., CHOW, A., NOIZAT, C., TEO, P., BEASLEY, M. B., LEBOEUF, M., BECKER, C. D., SEE, P., PRICE, J., LUCAS, D., GRETER, M., MORTHA, A., BOYER, S. W., FORSBERG, E. C., TANAKA, M., VAN ROOIJEN, N., GARCIA-SASTRE, A., STANLEY, E. R., GINHOUX, F., FRENETTE, P. S. & MERAD, M. 2013. Tissue-resident macrophages self-maintain locally throughout adult life with minimal contribution from circulating monocytes. *Immunity*, 38, 792-804.
- HELDMAIER, G. & RUF, T. 1992. Body temperature and metabolic rate during natural hypothermia in endotherms. *J Comp Physiol B*, 162, 696-706.
- HERBERT, H., BRÜCK, K. & RATHS, P. 1973. *Homeothermic Organisms*, Springer-Verlag.
- HILLMANN, A. 2011. *Der Verlust des Signaltransduktionsmoduls des Protein p62 führt zu einem adipösen Phänotyp bei Mäusen*. University Münster.
- HIMMS-HAGEN, J., CUI, J., DANFORTH, E., JR., TAATJES, D. J., LANG, S. S., WATERS, B. L. & CLAUS, T. H. 1994. Effect of CL-316,243, a thermogenic beta 3-agonist, on energy balance and brown and white adipose tissues in rats. *Am J Physiol*, 266, R1371-82.
- HIMMS-HAGEN, J., MELNYK, A., ZINGARETTI, M. C., CERESI, E., BARBATELLI, G. & CINTI, S. 2000. Multilocular fat cells in WAT of CL-316243-treated rats derive directly from white adipocytes. *Am J Physiol Cell Physiol*, 279, C670-81.
- HONDARES, E., ROSELL, M., DIAZ-DELFIN, J., OLMOS, Y., MONSALVE, M., IGLESIAS, R., VILLARROYA, F. & GIRALT, M. 2011. Peroxisome proliferator-activated receptor alpha (PPARalpha) induces PPARgamma coactivator 1alpha (PGC-1alpha) gene expression and contributes to thermogenic activation of brown fat: involvement of PRDM16. *J Biol Chem*, 286, 43112-22.
- HUANG, J. T., WELCH, J. S., RICOTE, M., BINDER, C. J., WILLSON, T. M., KELLY, C., WITZTUM, J. L., FUNK, C. D., CONRAD, D. & GLASS, C. K. 1999. Interleukin-4-dependent production of PPAR-gamma ligands in macrophages by 12/15-lipoxygenase. *Nature*, 400, 378-82.
- HUI, X., GU, P., ZHANG, J., NIE, T., PAN, Y., WU, D., FENG, T., ZHONG, C., WANG, Y., LAM, K. S. & XU, A. 2015. Adiponectin Enhances Cold-Induced Browning of Subcutaneous Adipose Tissue via Promoting M2 Macrophage Proliferation. *Cell Metab*, 22, 279-90.
- JESPERSEN, N. Z., LARSEN, T. J., PEIJS, L., DAUGAARD, S., HOMOE, P., LOFT, A., DE JONG, J., MATHUR, N., CANNON, B., NEDERGAARD, J., PEDERSEN, B. K., MOLLER, K. & SCHEELE, C. 2013. A classical brown adipose tissue mRNA signature partly overlaps with brite in the supraclavicular region of adult humans. *Cell Metab*, 17, 798-805.
- JUNG, R. T., SHETTY, P. S., JAMES, W. P., BARRAND, M. A. & CALLINGHAM, B. A. 1979. Reduced thermogenesis in obesity. *Nature*, 279, 322-3.
- KAJIMURA, S., SEALE, P., KUBOTA, K., LUNSFORD, E., FRANGIONI, J. V., GYGI, S. P. & SPIEGELMAN, B. M. 2009. Initiation of myoblast to brown fat switch by a PRDM16-C/EBP-beta transcriptional complex. *Nature*, 460, 1154-8.
- KAJIMURA, S., SPIEGELMAN, B. M. & SEALE, P. 2015. Brown and Beige Fat: Physiological Roles beyond Heat Generation. *Cell Metab*, 22, 546-59.

- KAWAI, K., SAITO, A., SUDO, T. & OSADA, H. 2008. Specific regulation of cytokine-dependent p38 MAP kinase activation by p62/SQSTM1. *J Biochem*, 143, 765-72.
- KLINGENBERG, M. & HUANG, S. G. 1999. Structure and function of the uncoupling protein from brown adipose tissue. *Biochim Biophys Acta*, 1415, 271-96.
- KLINGENBERG, M. & WINKLER, E. 1985. The reconstituted isolated uncoupling protein is a membrane potential driven H<sup>+</sup> translocator. *EMBO J*, 4, 3087-92.
- KOBAYASHI, N., KADONO, Y., NAITO, A., MATSUMOTO, K., YAMAMOTO, T., TANAKA, S. & INOUE, J. 2001. Segregation of TRAF6-mediated signaling pathways clarifies its role in osteoclastogenesis. *EMBO J*, 20, 1271-80.
- KOMATSU, M., KUROKAWA, H., WAGURI, S., TAGUCHI, K., KOBAYASHI, A., ICHIMURA, Y., SOU, Y. S., UENO, I., SAKAMOTO, A., TONG, K. I., KIM, M., NISHITO, Y., IEMURA, S., NATSUME, T., UENO, T., KOMINAMI, E., MOTOHASHI, H., TANAKA, K. & YAMAMOTO, M. 2010. The selective autophagy substrate p62 activates the stress responsive transcription factor Nrf2 through inactivation of Keap1. *Nat Cell Biol*, 12, 213-23.
- KOMATSU, M., WAGURI, S., KOIKE, M., SOU, Y. S., UENO, T., HARA, T., MIZUSHIMA, N., IWATA, J., EZAKI, J., MURATA, S., HAMAZAKI, J., NISHITO, Y., IEMURA, S., NATSUME, T., YANAGAWA, T., UWAYAMA, J., WARABI, E., YOSHIDA, H., ISHII, T., KOBAYASHI, A., YAMAMOTO, M., YUE, Z., UCHIYAMA, Y., KOMINAMI, E. & TANAKA, K. 2007. Homeostatic levels of p62 control cytoplasmic inclusion body formation in autophagy-deficient mice. *Cell*, 131, 1149-63.
- KONIGE, M., WANG, H. & SZTALRYD, C. 2014. Role of adipose specific lipid droplet proteins in maintaining whole body energy homeostasis. *Biochim Biophys Acta*, 1842, 393-401.
- KONTANI, Y., WANG, Y., KIMURA, K., INOKUMA, K. I., SAITO, M., SUZUKI-MIURA, T., WANG, Z., SATO, Y., MORI, N. & YAMASHITA, H. 2005. UCP1 deficiency increases susceptibility to diet-induced obesity with age. *Aging Cell*, 4, 147-55.
- KOPPE, S. W. 2014. Obesity and the liver: nonalcoholic fatty liver disease. *Transl Res*, 164, 312-22.
- KOSTELI, A., SUGARU, E., HAEMMERLE, G., MARTIN, J. F., LEI, J., ZECHNER, R. & FERRANTE, A. W., JR. 2010. Weight loss and lipolysis promote a dynamic immune response in murine adipose tissue. *J Clin Invest*, 120, 3466-79.
- KOZAK, L. P. & KOZA, R. A. 2010. The genetics of brown adipose tissue. *Prog Mol Biol Transl Sci*, 94, 75-123.
- KOZAK, U. C., KOPECKY, J., TEISINGER, J., ENERBACK, S., BOYER, B. & KOZAK, L. P. 1994. An upstream enhancer regulating brown-fat-specific expression of the mitochondrial uncoupling protein gene. *Mol Cell Biol*, 14, 59-67.
- LAU, E. & RONAI, Z. A. 2012. ATF2 - at the crossroad of nuclear and cytosolic functions. *J Cell Sci*, 125, 2815-24.
- LAUTERBACH, M. A. & WUNDERLICH, F. T. 2017. Macrophage function in obesity-induced inflammation and insulin resistance. *Pflugers Arch*.
- LEE, M. W., ODEGAARD, J. I., MUKUNDAN, L., QIU, Y., MOLOFSKY, A. B., NUSSBAUM, J. C., YUN, K., LOCKSLEY, R. M. & CHAWLA, A. 2015. Activated type 2 innate lymphoid cells regulate beige fat biogenesis. *Cell*, 160, 74-87.
- LEE, S. J., PFLUGER, P. T., KIM, J. Y., NOGUEIRAS, R., DURAN, A., PAGES, G., POUYSSEGUR, J., TSCHOP, M. H., DIAZ-MECO, M. T. & MOSCAT, J. 2010. A functional role for the p62-ERK1 axis in the control of energy homeostasis and adipogenesis. *EMBO Rep*, 11, 226-32.

- LIDELL, M. E., BETZ, M. J., DAHLQVIST LEINHARD, O., HEGLIND, M., ELANDER, L., SLAWIK, M., MUSSACK, T., NILSSON, D., ROMU, T., NUUTILA, P., VIRTANEN, K. A., BEUSCHLEIN, F., PERSSON, A., BORGA, M. & ENERBACK, S. 2013. Evidence for two types of brown adipose tissue in humans. *Nat Med*, 19, 631-4.
- LIU, H., DENG, X., SHYU, Y. J., LI, J. J., TAPAROWSKY, E. J. & HU, C. D. 2006. Mutual regulation of c-Jun and ATF2 by transcriptional activation and subcellular localization. *EMBO J*, 25, 1058-69.
- LIU, P. S., LIN, Y. W., BURTON, F. H. & WEI, L. N. 2015. Injecting engineered anti-inflammatory macrophages therapeutically induces white adipose tissue browning and improves diet-induced insulin resistance. *Adipocyte*, 4, 123-8.
- LIU, X., ROSSMEISL, M., MCCLAIN, J., RIACHI, M., HARPER, M. E. & KOZAK, L. P. 2003. Paradoxical resistance to diet-induced obesity in UCP1-deficient mice. *J Clin Invest*, 111, 399-407.
- LOCKE, R. M., RIAL, E. & NICHOLLS, D. G. 1982. The acute regulation of mitochondrial proton conductance in cells and mitochondria from the brown fat of cold-adapted and warm-adapted guinea pigs. *Eur J Biochem*, 129, 381-7.
- LUMENG, C. N., BODZIN, J. L. & SALTIEL, A. R. 2007a. Obesity induces a phenotypic switch in adipose tissue macrophage polarization. *J Clin Invest*, 117, 175-84.
- LUMENG, C. N., DELPROPOSTO, J. B., WESTCOTT, D. J. & SALTIEL, A. R. 2008. Phenotypic switching of adipose tissue macrophages with obesity is generated by spatiotemporal differences in macrophage subtypes. *Diabetes*, 57, 3239-46.
- LUMENG, C. N., DEYOUNG, S. M., BODZIN, J. L. & SALTIEL, A. R. 2007b. Increased inflammatory properties of adipose tissue macrophages recruited during diet-induced obesity. *Diabetes*, 56, 16-23.
- LUSTIG, R. H. 2006. Childhood obesity: behavioral aberration or biochemical drive? Reinterpreting the First Law of Thermodynamics. *Nat Clin Pract Endocrinol Metab*, 2, 447-58.
- MA, Y., KRUEGER, J. J., REDMON, S. N., UPPUGANTI, S., NYMAN, J. S., HAHN, M. K. & ELEFTERIOU, F. 2013. Extracellular norepinephrine clearance by the norepinephrine transporter is required for skeletal homeostasis. *J Biol Chem*, 288, 30105-13.
- MANTOVANI, A., SICA, A., SOZZANI, S., ALLAVENA, P., VECCHI, A. & LOCATI, M. 2004. The chemokine system in diverse forms of macrophage activation and polarization. *Trends Immunol*, 25, 677-86.
- MARTINEZ, F. O. & GORDON, S. 2014. The M1 and M2 paradigm of macrophage activation: time for reassessment. *F1000Prime Rep*, 6, 13.
- MARTINEZ, F. O., GORDON, S., LOCATI, M. & MANTOVANI, A. 2006. Transcriptional profiling of the human monocyte-to-macrophage differentiation and polarization: new molecules and patterns of gene expression. *J Immunol*, 177, 7303-11.
- MARTINEZ, F. O., SICA, A., MANTOVANI, A. & LOCATI, M. 2008. Macrophage activation and polarization. *Front Biosci*, 13, 453-61.
- MARTINEZ-BOTAS, J., ANDERSON, J. B., TESSIER, D., LAPILLONNE, A., CHANG, B. H., QUAST, M. J., GORENSTEIN, D., CHEN, K. H. & CHAN, L. 2000. Absence of perilipin results in leanness and reverses obesity in *Lepr*(db/db) mice. *Nat Genet*, 26, 474-9.
- MOHRS, M., LEDERMANN, B., KOHLER, G., DORFMULLER, A., GESSNER, A. & BROMBACHER, F. 1999. Differences between IL-4- and IL-4 receptor alpha-deficient mice in chronic leishmaniasis reveal a protective role for IL-13 receptor signaling. *J Immunol*, 162, 7302-8.

- MOLINOFF, P. B. & AXELROD, J. 1971. Biochemistry of catecholamines. *Annu Rev Biochem*, 40, 465-500.
- MORIMOTO, C., KAMEDA, K., TSUJITA, T. & OKUDA, H. 2001. Relationships between lipolysis induced by various lipolytic agents and hormone-sensitive lipase in rat fat cells. *J Lipid Res*, 42, 120-7.
- MORRIS, D. L., SINGER, K. & LUMENG, C. N. 2011. Adipose tissue macrophages: phenotypic plasticity and diversity in lean and obese states. *Curr Opin Clin Nutr Metab Care*, 14, 341-6.
- MOSCAT, J. & DIAZ-MECO, M. T. 2009. p62 at the crossroads of autophagy, apoptosis, and cancer. *Cell*, 137, 1001-4.
- MOSCAT, J. & DIAZ-MECO, M. T. 2011. Feedback on fat: p62-mTORC1-autophagy connections. *Cell*, 147, 724-7.
- MOSCAT, J., DIAZ-MECO, M. T. & WOOTEN, M. W. 2007. Signal integration and diversification through the p62 scaffold protein. *Trends Biochem Sci*, 32, 95-100.
- MULLER, T. D., LEE, S. J., JASTROCH, M., KABRA, D., STEMMER, K., AICHLER, M., ABPLANALP, B., ANANTHAKRISHNAN, G., BHARDWAJ, N., COLLINS, S., DIVANOVIC, S., ENDELE, M., FINAN, B., GAO, Y., HABEGGER, K. M., HEMBREE, J., HEPPNER, K. M., HOFMANN, S., HOLLAND, J., KUCHLER, D., KUTSCHKE, M., KRISHNA, R., LEHTI, M., OELKRUG, R., OTTAWAY, N., PEREZ-TILVE, D., RAVER, C., WALCH, A. K., SCHRIEVER, S. C., SPEAKMAN, J., TSENG, Y. H., DIAZ-MECO, M., PFLUGER, P. T., MOSCAT, J. & TSCHOP, M. H. 2013. p62 links beta-adrenergic input to mitochondrial function and thermogenesis. *J Clin Invest*, 123, 469-78.
- MURRAY, P. J., ALLEN, J. E., BISWAS, S. K., FISHER, E. A., GILROY, D. W., GOERDT, S., GORDON, S., HAMILTON, J. A., IVASHKIV, L. B., LAWRENCE, T., LOCATI, M., MANTOVANI, A., MARTINEZ, F. O., MEGE, J. L., MOSSER, D. M., NATOLI, G., SAEIJ, J. P., SCHULTZE, J. L., SHIREY, K. A., SICA, A., SUTTLES, J., UDALOVA, I., VAN GINDERACHTER, J. A., VOGEL, S. N. & WYNN, T. A. 2014. Macrophage activation and polarization: nomenclature and experimental guidelines. *Immunity*, 41, 14-20.
- NADERALI, E. K., RATCLIFFE, S. H. & DALE, M. C. 2009. Obesity and Alzheimer's disease: a link between body weight and cognitive function in old age. *Am J Alzheimers Dis Other Demen*, 24, 445-9.
- NAHMIAS, C., BLIN, N., ELALOUF, J. M., MATTEI, M. G., STROSBERG, A. D. & EMORINE, L. J. 1991. Molecular characterization of the mouse beta 3-adrenergic receptor: relationship with the atypical receptor of adipocytes. *EMBO J*, 10, 3721-7.
- NGUYEN, K. D., QIU, Y., CUI, X., GOH, Y. P., MWANGI, J., DAVID, T., MUKUNDAN, L., BROMBACHER, F., LOCKSLEY, R. M. & CHAWLA, A. 2011. Alternatively activated macrophages produce catecholamines to sustain adaptive thermogenesis. *Nature*, 480, 104-8.
- NICHOLLS, D. G. & LOCKE, R. M. 1984. Thermogenic mechanisms in brown fat. *Physiol Rev*, 64, 1-64.
- ODEGAARD, J. I., LEE, M. W., SOGAWA, Y., BERTHOLET, A. M., LOCKSLEY, R. M., WEINBERG, D. E., KIRICHOK, Y., DEO, R. C. & CHAWLA, A. 2016. Perinatal Licensing of Thermogenesis by IL-33 and ST2. *Cell*, 166, 841-54.
- ODEGAARD, J. I., RICARDO-GONZALEZ, R. R., GOFORTH, M. H., MOREL, C. R., SUBRAMANIAN, V., MUKUNDAN, L., RED EAGLE, A., VATS, D., BROMBACHER, F., FERRANTE, A. W. & CHAWLA, A. 2007. Macrophage-specific PPARgamma controls alternative activation and improves insulin resistance. *Nature*, 447, 1116-20.

- OELKRUG, R., POLYMEROPOULOS, E. T. & JASTROCH, M. 2015. Brown adipose tissue: physiological function and evolutionary significance. *J Comp Physiol B*, 185, 587-606.
- OLEFSKY, J. M. & GLASS, C. K. 2010. Macrophages, inflammation, and insulin resistance. *Annu Rev Physiol*, 72, 219-46.
- ORAVA, J., NUUTILA, P., LIDELL, M. E., OIKONEN, V., NOPONEN, T., VILJANEN, T., SCHEININ, M., TAITTONEN, M., NIEMI, T., ENERBACK, S. & VIRTANEN, K. A. 2011. Different metabolic responses of human brown adipose tissue to activation by cold and insulin. *Cell Metab*, 14, 272-9.
- ORTMANN, S. & HELDMAIER, G. 2000. Regulation of body temperature and energy requirements of hibernating alpine marmots (*Marmota marmota*). *Am J Physiol Regul Integr Comp Physiol*, 278, R698-704.
- PETROVIC, N., WALDEN, T. B., SHABALINA, I. G., TIMMONS, J. A., CANNON, B. & NEDERGAARD, J. 2010. Chronic peroxisome proliferator-activated receptor gamma (PPARgamma) activation of epididymally derived white adipocyte cultures reveals a population of thermogenically competent, UCP1-containing adipocytes molecularly distinct from classic brown adipocytes. *J Biol Chem*, 285, 7153-64.
- POLAK, P., CYBULSKI, N., FEIGE, J. N., AUWERX, J., RUEGG, M. A. & HALL, M. N. 2008. Adipose-specific knockout of raptor results in lean mice with enhanced mitochondrial respiration. *Cell Metab*, 8, 399-410.
- PUIGSERVER, P., WU, Z., PARK, C. W., GRAVES, R., WRIGHT, M. & SPIEGELMAN, B. M. 1998. A cold-inducible coactivator of nuclear receptors linked to adaptive thermogenesis. *Cell*, 92, 829-39.
- QIU, Y., NGUYEN, K. D., ODEGAARD, J. I., CUI, X., TIAN, X., LOCKSLEY, R. M., PALMITER, R. D. & CHAWLA, A. 2014. Eosinophils and type 2 cytokine signaling in macrophages orchestrate development of functional beige fat. *Cell*, 157, 1292-308.
- RAO, R. R., LONG, J. Z., WHITE, J. P., SVENSSON, K. J., LOU, J., LOKURKAR, I., JEDRYCHOWSKI, M. P., RUAS, J. L., WRANN, C. D., LO, J. C., CAMERA, D. M., LACHEY, J., GYGI, S., SEEHRA, J., HAWLEY, J. A. & SPIEGELMAN, B. M. 2014. Meteorin-like is a hormone that regulates immune-adipose interactions to increase beige fat thermogenesis. *Cell*, 157, 1279-91.
- ROCHE, S. L. & SILVERSIDES, C. K. 2013. Hypertension, obesity, and coronary artery disease in the survivors of congenital heart disease. *Can J Cardiol*, 29, 841-8.
- RODGERS, R. J., TSCHOP, M. H. & WILDING, J. P. 2012. Anti-obesity drugs: past, present and future. *Dis Model Mech*, 5, 621-6.
- RODRIGUEZ, A., DURAN, A., SELLOUM, M., CHAMPY, M. F., DIEZ-GUERRA, F. J., FLORES, J. M., SERRANO, M., AUWERX, J., DIAZ-MECO, M. T. & MOSCAT, J. 2006. Mature-onset obesity and insulin resistance in mice deficient in the signaling adapter p62. *Cell Metab*, 3, 211-22.
- ROSENWALD, M., PERDIKARI, A., RULICKE, T. & WOLFRUM, C. 2013. Bi-directional interconversion of brite and white adipocytes. *Nat Cell Biol*, 15, 659-67.
- ROWLAND, L. A., BAL, N. C. & PERIASAMY, M. 2015. The role of skeletal-muscle-based thermogenic mechanisms in vertebrate endothermy. *Biol Rev Camb Philos Soc*, 90, 1279-97.
- SABATINI, D. M. 2006. mTOR and cancer: insights into a complex relationship. *Nat Rev Cancer*, 6, 729-34.
- SAITO, M. 2013. Brown adipose tissue as a therapeutic target for human obesity. *Obes Res Clin Pract*, 7, e432-8.

- SANCHEZ-GURMACHES, J. & GUERTIN, D. A. 2014. Adipocyte lineages: tracing back the origins of fat. *Biochim Biophys Acta*, 1842, 340-51.
- SANZ, L., DIAZ-MECO, M. T., NAKANO, H. & MOSCAT, J. 2000. The atypical PKC-interacting protein p62 channels NF-kappaB activation by the IL-1-TRAF6 pathway. *EMBO J*, 19, 1576-86.
- SCHENK, S., SABERI, M. & OLEFSKY, J. M. 2008. Insulin sensitivity: modulation by nutrients and inflammation. *J Clin Invest*, 118, 2992-3002.
- SCHULZ, C., GOMEZ PERDIGUERO, E., CHORRO, L., SZABO-ROGERS, H., CAGNARD, N., KIERDORF, K., PRINZ, M., WU, B., JACOBSEN, S. E., POLLARD, J. W., FRAMPTON, J., LIU, K. J. & GEISSMANN, F. 2012. A lineage of myeloid cells independent of Myb and hematopoietic stem cells. *Science*, 336, 86-90.
- SEALE, P., BJORK, B., YANG, W., KAJIMURA, S., CHIN, S., KUANG, S., SCIME, A., DEVARAKONDA, S., CONROE, H. M., ERDJUMENT-BROMAGE, H., TEMPST, P., RUDNICKI, M. A., BEIER, D. R. & SPIEGELMAN, B. M. 2008. PRDM16 controls a brown fat/skeletal muscle switch. *Nature*, 454, 961-7.
- SEALE, P., KAJIMURA, S., YANG, W., CHIN, S., ROHAS, L. M., ULDRY, M., TAVERNIER, G., LANGIN, D. & SPIEGELMAN, B. M. 2007. Transcriptional control of brown fat determination by PRDM16. *Cell Metab*, 6, 38-54.
- SEARS, I. B., MACGINNITIE, M. A., KOVACS, L. G. & GRAVES, R. A. 1996. Differentiation-dependent expression of the brown adipocyte uncoupling protein gene: regulation by peroxisome proliferator-activated receptor gamma. *Mol Cell Biol*, 16, 3410-9.
- SHABALINA, I. G., JACOBSSON, A., CANNON, B. & NEDERGAARD, J. 2004. Native UCP1 displays simple competitive kinetics between the regulators purine nucleotides and fatty acids. *J Biol Chem*, 279, 38236-48.
- SHARP, L. Z., SHINODA, K., OHNO, H., SCHEEL, D. W., TOMODA, E., RUIZ, L., HU, H., WANG, L., PAVLOVA, Z., GILSANZ, V. & KAJIMURA, S. 2012. Human BAT possesses molecular signatures that resemble beige/brite cells. *PLoS One*, 7, e49452.
- SILVA, J. E. & LARSEN, P. R. 1983. Adrenergic activation of triiodothyronine production in brown adipose tissue. *Nature*, 305, 712-3.
- SPEAKMAN, J. R. 2013. Measuring energy metabolism in the mouse - theoretical, practical, and analytical considerations. *Front Physiol*, 4, 34.
- SUDO, T., MARUYAMA, M. & OSADA, H. 2000. p62 functions as a p38 MAP kinase regulator. *Biochem Biophys Res Commun*, 269, 521-5.
- TANG, Q. Q. & LANE, M. D. 2012. Adipogenesis: from stem cell to adipocyte. *Annu Rev Biochem*, 81, 715-36.
- TANSEY, E. A. & JOHNSON, C. D. 2015. Recent advances in thermoregulation. *Adv Physiol Educ*, 39, 139-48.
- TIMMONS, J. A., WENNMALM, K., LARSSON, O., WALDEN, T. B., LASSMANN, T., PETROVIC, N., HAMILTON, D. L., GIMENO, R. E., WAHLESTEDT, C., BAAR, K., NEDERGAARD, J. & CANNON, B. 2007. Myogenic gene expression signature establishes that brown and white adipocytes originate from distinct cell lineages. *Proc Natl Acad Sci U S A*, 104, 4401-6.
- TOWNSEND, K. L. & TSENG, Y. H. 2014. Brown fat fuel utilization and thermogenesis. *Trends Endocrinol Metab*, 25, 168-77.
- TRAYHURN, P. & BEATTIE, J. H. 2001. Physiological role of adipose tissue: white adipose tissue as an endocrine and secretory organ. *Proc Nutr Soc*, 60, 329-39.



- TSCHOP, M. H., FINAN, B., CLEMMENSEN, C., GELFANOV, V., PEREZ-TILVE, D., MULLER, T. D. & DIMARCHI, R. D. 2016. Unimolecular Polypharmacy for Treatment of Diabetes and Obesity. *Cell Metab*, 24, 51-62.
- TSCHOP, M. H., SPEAKMAN, J. R., ARCH, J. R., AUWERX, J., BRUNING, J. C., CHAN, L., ECKEL, R. H., FARESE, R. V., JR., GALGANI, J. E., HAMBLY, C., HERMAN, M. A., HORVATH, T. L., KAHN, B. B., KOZMA, S. C., MARATOS-FLIER, E., MULLER, T. D., MUNZBERG, H., PFLUGER, P. T., PLUM, L., REITMAN, M. L., RAHMOUNI, K., SHULMAN, G. I., THOMAS, G., KAHN, C. R. & RAVUSSIN, E. 2011. A guide to analysis of mouse energy metabolism. *Nat Methods*, 9, 57-63.
- TSENG, Y. H., KOKKOTOU, E., SCHULZ, T. J., HUANG, T. L., WINNAY, J. N., TANIGUCHI, C. M., TRAN, T. T., SUZUKI, R., ESPINOZA, D. O., YAMAMOTO, Y., AHRENS, M. J., DUDLEY, A. T., NORRIS, A. W., KULKARNI, R. N. & KAHN, C. R. 2008. New role of bone morphogenetic protein 7 in brown adipogenesis and energy expenditure. *Nature*, 454, 1000-4.
- USSAR, S., FUJISAKA, S. & KAHN, C. R. 2016. Interactions between host genetics and gut microbiome in diabetes and metabolic syndrome. *Mol Metab*, 5, 795-803.
- VAN DYKEN, S. J. & LOCKSLEY, R. M. 2013. Interleukin-4- and interleukin-13-mediated alternatively activated macrophages: roles in homeostasis and disease. *Annu Rev Immunol*, 31, 317-43.
- VAN FURTH, R. & COHN, Z. A. 1968. The origin and kinetics of mononuclear phagocytes. *J Exp Med*, 128, 415-35.
- VAN KLINKEN, J. B., VAN DEN BERG, S. A. & VAN DIJK, K. W. 2013. Practical aspects of estimating energy components in rodents. *Front Physiol*, 4, 94.
- VAN MARKEN LICHTENBELT, W. D., VANHOMMERIG, J. W., SMULDERS, N. M., DROSSAERTS, J. M., KEMERINK, G. J., BOUVY, N. D., SCHRAUWEN, P. & TEULE, G. J. 2009. Cold-activated brown adipose tissue in healthy men. *N Engl J Med*, 360, 1500-8.
- VAN SANT, M. J. & HAMMOND, K. A. 2008. Contribution of shivering and nonshivering thermogenesis to thermogenic capacity for the deer mouse (*Peromyscus maniculatus*). *Physiol Biochem Zool*, 81, 605-11.
- VIELAND, V. J. 2014. Evidence, temperature, and the laws of thermodynamics. *Hum Hered*, 78, 153-63.
- VILLARROYA, F. & VIDAL-PUIG, A. 2013. Beyond the sympathetic tone: the new brown fat activators. *Cell Metab*, 17, 638-43.
- VIRTANEN, K. A. 2014. BAT thermogenesis: Linking shivering to exercise. *Cell Metab*, 19, 352-4.
- VIRTANEN, K. A., LIDELL, M. E., ORAVA, J., HEGLIND, M., WESTERGRÉN, R., NIEMI, T., TAITTONEN, M., LAINE, J., SAVISTO, N. J., ENERBACK, S. & NUUTILA, P. 2009. Functional brown adipose tissue in healthy adults. *N Engl J Med*, 360, 1518-25.
- WALDEN, T. B., HANSEN, I. R., TIMMONS, J. A., CANNON, B. & NEDERGAARD, J. 2012. Recruited vs. nonrecruited molecular signatures of brown, "brite," and white adipose tissues. *Am J Physiol Endocrinol Metab*, 302, E19-31.
- WANG, C., YU, X., CAO, Q., WANG, Y., ZHENG, G., TAN, T. K., ZHAO, H., ZHAO, Y., WANG, Y. & HARRIS, D. 2013a. Characterization of murine macrophages from bone marrow, spleen and peritoneum. *BMC Immunol*, 14, 6.
- WANG, Q. A., TAO, C., GUPTA, R. K. & SCHERER, P. E. 2013b. Tracking adipogenesis during white adipose tissue development, expansion and regeneration. *Nat Med*, 19, 1338-44.

- WEISBERG, S. P., MCCANN, D., DESAI, M., ROSENBAUM, M., LEIBEL, R. L. & FERRANTE, A. W., JR. 2003. Obesity is associated with macrophage accumulation in adipose tissue. *J Clin Invest*, 112, 1796-808.
- WILDING, J. P. 2014. The importance of weight management in type 2 diabetes mellitus. *Int J Clin Pract*, 68, 682-91.
- WIRSÉN, C. 2011. *Distribution of adrenergic nerve fibers in brown and white adipose tissue*, Wiley Online Library.
- WU, D., MOLOFSKY, A. B., LIANG, H. E., RICARDO-GONZALEZ, R. R., JOUIHAN, H. A., BANDO, J. K., CHAWLA, A. & LOCKSLEY, R. M. 2011. Eosinophils sustain adipose alternatively activated macrophages associated with glucose homeostasis. *Science*, 332, 243-7.
- WU, J., BOSTROM, P., SPARKS, L. M., YE, L., CHOI, J. H., GIANG, A. H., KHANDEKAR, M., VIRTANEN, K. A., NUUTILA, P., SCHAART, G., HUANG, K., TU, H., VAN MARKEN LICHTENBELT, W. D., HOEKS, J., ENERBACK, S., SCHRAUWEN, P. & SPIEGELMAN, B. M. 2012. Beige adipocytes are a distinct type of thermogenic fat cell in mouse and human. *Cell*, 150, 366-76.
- WU, J., COHEN, P. & SPIEGELMAN, B. M. 2013. Adaptive thermogenesis in adipocytes: is beige the new brown? *Genes Dev*, 27, 234-50.
- WU, Z., PUIGSERVER, P., ANDERSSON, U., ZHANG, C., ADELMANT, G., MOOTHA, V., TROY, A., CINTI, S., LOWELL, B., SCARPULLA, R. C. & SPIEGELMAN, B. M. 1999. Mechanisms controlling mitochondrial biogenesis and respiration through the thermogenic coactivator PGC-1. *Cell*, 98, 115-24.
- XU, H., BARNES, G. T., YANG, Q., TAN, G., YANG, D., CHOU, C. J., SOLE, J., NICHOLS, A., ROSS, J. S., TARTAGLIA, L. A. & CHEN, H. 2003. Chronic inflammation in fat plays a crucial role in the development of obesity-related insulin resistance. *J Clin Invest*, 112, 1821-30.
- ZHAO, J., CANNON, B. & NEDERGAARD, J. 1997. alpha1-Adrenergic stimulation potentiates the thermogenic action of beta3-adrenoreceptor-generated cAMP in brown fat cells. *J Biol Chem*, 272, 32847-56.

## Acknowledgments

At this point, I would like to express my gratitude to all the people who made this work possible. First, I want to thank Prof. Dr. Matthias Tschöp for providing an outstanding research environment and for giving me the opportunity to do my PhD thesis at the IDO. Beyond, I want to thank Matthias for sharing his immense insight in science and for integrating me in a research environment of world-class scientists.

A very special thanks goes to my supervisor and mentor Dr. Timo Müller who supported me during the whole time as graduate student. I especially want to thank Timo for taking me under his wings, sharing his enormous knowledge and pushing my project to a high impact gate. Timo has been an excellent supervisor and always had an open door for me.

I would also like to thank my second supervisor Prof. Dr. Martin Klingenspor for many fruitful scientific discussions that advanced the progress of my thesis.

I also want to thank Dr. Christoffer Clemmensen and Dr. Brian Finan who guided me through the PhD and had always been a great scientific and mental support.

Besides, I want to thank Dr. Maximilian Kleinert and Dr. Sara Brandt for numerous fruitful discussions and their expert insights. A special thanks also goes to the whole pharmacology team, especially to the lab girls, for sharing their knowledge and providing a joyful and sociable work environment.

I would also like to acknowledge all collaboration partners who substantially contributed to publishing the work of this thesis: Prof. Dr. Christoph Buettner, Prof. Dr. Barbara Cannon, Prof. Dr. Jan Nedergaard, Dr. Senad Divanovic, Prof. Dr. Steffen Jung, Prof. Dr. Stephan Herzig. It was a great pleasure to experience collaborating with so many world-class scientists. Especially I want to thank Senad & his team for temporally hosting me at the Children's Hospital and for making my stay in Cincinnati a pleasant life experience.

Finally, the biggest thanks goes to my friends and family for their never-ending support and encouragement to finalize the PhD thesis.

## Curriculum Vitae

### Katrin Fischer

---

Date of birth: 15/04/1986  
 Place of birth: Heppenheim  
 Nationality: German  
 Family status: Single

### Education

---

01/2016 – 03/2016 Collaboration with the group of Dr. S. Divanovic at the Cincinnati Children's Hospital, USA to study energy expenditure in *Il4ra*<sup>-/-</sup> mice.

Since 05/2013 PhD thesis "*Novel regulators of energy metabolism: From alternatively activated macrophages to the role of the scaffold protein p62 in BAT thermogenesis*" at the Helmholtz Zentrum München, Institute for Diabetes and Obesity (IDO), Division of Molecular Pharmacology (Dr. T.D. Müller)

04/2012 – 01/2013 Diploma Thesis „*Biological and immunological studies of Human Endogenous Retrovirus K (HERV-K)*” at the Paul-Ehrlich Institute, in Langen (Research group: HIV vaccines and AIDS – Prof. Dr. Schnierle) 1.0

01/2012 – 04/2012 Final examinations in microbiology, genetics and biochemistry (final grade: 1.5)

08/2010 – 03/2013 Continuing studies of Diploma Biology, Technische Universität Darmstadt (Specialization: microbiology, genetics, biochemistry)

09/2009 – 06/2010 Erasmus exchange program at the “Université Bordeaux 2”, France (Master Biochemistry; Genetics)

10/2006 – 09/2009 Technische Universität Darmstadt, Germany, Diploma Biology

08/1996 - 06/2006 High school, Goethe Gymnasium, Bensheim

08/1992 – 06/1996 Elementary school, Kirchbergschule, Bensheim

## List of publications

- [1] Alternatively activated macrophages do not synthesize catecholamines or contribute to adipose tissue adaptive thermogenesis. Fischer et al., *Nature Medicine* 2017 (in press)
- [2] Loss of amino acid 69-251 of p62 drives obesity by controlling energy metabolism through brown fat thermogenesis. Fischer et al., 2017 (in preparation)
- [3] Smart delivery of glucocorticoids safely reverses hypothalamic inflammation and obesity. Quarta et al., *Cell Metabolism* 2017 (in revision)
- [4] Chemical hybridization of glucagon and thyroid hormone optimizes therapeutic impact for metabolic disease. Finan et al., *Cell* 2016
- [5] Adipocyte glucocorticoid receptor deficiency attenuates aging- and HFD-induced obesity and impairs the feeding-fasting transition. Mueller et al., *Diabetes* 2016
- [6] A rationally designed monomeric peptide triagonist corrects obesity and diabetes in rodents. Finan et al. *Nature Medicine* 2015
- [7] Dual melanocortin-4-receptor and GLP-1 receptor agonism amplifies metabolic benefits in diet-induced obese mice. Clemmensen et al. *EMBO Molecular Medicine* 2015
- [8] The pentapeptide RM-131 promotes food intake and adiposity in wildtype mice but not in mice lacking the Ghrelin receptor. Fischer et al., *Frontiers in Nutrition* 2015
- [9] Relationship status update for PTP1B and LepR: It's complicated. Fischer et al., *Molecular Metabolism* 2014
- [10] GLP-1/glucagon coagonism restores leptin responsiveness in obese mice chronically maintained on an obesogenic diet. Clemmensen et al. *Diabetes* 2014

## Conference presentations

- [1] Macrophage depletion does not alter differentiation and browning capacity of inguinal white adipocytes. Fischer et al. CNIC Madrid 2014
- [2] The weight-lowering efficacy of GLP-1/GIP/Glucagon triple agonism is not dependent on functional brown adipose tissue thermogenesis. Fischer et al. Keystone Symposia 2015
- [3] Macrophage depletion does not alter differentiation and browning capacity of inguinal white adipocytes. Fischer et al. EYES meeting Modena 2016

## Eidesstattliche Erklärung

Ich erkläre an Eides statt, dass ich die bei der Fakultät für Medizin zur Promotionsprüfung vorgelegte Arbeit mit dem Titel:

***„Novel regulators of energy metabolism: From alternatively activated macrophages to the role of the scaffold protein p62 in BAT thermogenesis“***

am Institut für Diabetes und Adipositas (Helmholtz Zentrum München) unter der Anleitung und Betreuung durch Prof. Dr. Tschöp ohne sonstige Hilfsmittel erstellt und bei der Abfassung nur die gemäß § 6 Abs. 6 und 7 Satz 2 angegebenen Hilfsmittel benutzt habe.

Ich habe keine Organisation eingeschaltet, die gegen Entgelt Betreuerinnen und Betreuer für die Anfertigung von Dissertationen sucht, oder die mir obliegenden Pflichten hinsichtlich der Prüfungsleistungen für mich ganz oder teilweise erledigt.

Ich habe die Dissertation in dieser oder ähnlicher Form in keinem anderen Prüfungsverfahren als Prüfungsleistung vorgelegt.

Die vollständige Dissertation wurde noch nicht veröffentlicht.

Ich habe den angestrebten Doktorgrad noch nicht erworben und bin nicht in einem früheren Promotionsverfahren für den angestrebten Doktorgrad endgültig gescheitert.

Die öffentlich zugängliche Promotionsordnung der TUM ist mir bekannt, insbesondere habe ich die Bedeutung von § 28 (Nichtigkeit der Promotion) und § 29 (Entzug des Doktorgrades) zur Kenntnis genommen. Ich bin mir der Konsequenzen einer falschen Eidesstattlichen Erklärung bewusst.

Mit der Aufnahme meiner personenbezogenen Daten in die Alumni-Datei bei der TUM bin ich einverstanden.

München, den

Katrin Fischer